

# Lactate uptake into mouse cardiomyocytes is coupled to CO<sub>2</sub>-dependent acid/base regulation

vom Fachbereich Biologie der Universität Kaiserslautern zur Verleihung des akademischen  
Grades  
„Doktor der Naturwissenschaften“  
genehmigte Dissertation

vorgelegt von

Jan Peetz

Chairman: Prof. Dr. E. Friauf

First reviewer: Jun. Prof. H. Becker

Second reviewer: Prof. Dr. S. Kins

Defence of Ph.D. thesis: June, 6 Kaiserslautern 2014

D386

I assure that I wrote this Ph.D. thesis according to my best knowledge without the help of plagiarism or illegal manipulation. This work has not been submitted in this or any other similar form to any university before.

Jan Peetz

-----

# Content

<b>Figures</b>	<b>4</b>
<b>Tables</b>	<b>6</b>
<b>Abbreviations</b>	<b>7</b>
<b>Acknowledgements</b>	<b>9</b>
<b>Abstract</b>	<b>11</b>
<b>1. INTRODUCTION</b>	<b>12</b>
1.1 general introduction	12
1.2 H <sup>+</sup> buffering and pH regulation	13
1.3 Carbonic anhydrase	14
1.4 Lactate transport	16
1.5 Acid/Base regulation and lactate transport	18
1.6 Motivation	23
<b>2. MATERIALS &amp; METHODS</b>	<b>24</b>
2.1 Cardiomyocyte isolation and cultivation	24
2.2 Imaging	32
2.3 Western blot	46
<b>3. RESULTS</b>	<b>58</b>
3.1 Buffer capacity and buffer ratio in ventricular mouse cardiomyocytes	58
3.2 pH regulating proteins and lactate transporter present in mouse cardiomyocytes	61
3.3 Lactate flux and physiological implementation	85
<b>4. DISCUSSION</b>	<b>96</b>
4.1 Discussion - Proteins (CAs, MCTs, NBC and NHE in mouse cardiomyocytes)	96
4.3 Lactate transport and physiological implementation	105
4.4 Final conclusion, model & further speculations	114
<b>5. LITERATURE</b>	<b>123</b>
<b>CURRICULUM VITAE</b>	<b>134</b>

# Figures

Figure 1 Scheme of potential non-catalytic interaction of MCT1 and extracellular CAs in mouse .....	19
Figure 2 Acid/base regulation potentially involved in cardiomyocytes' lactate uptake .....	22
Figure 3 Scheme of myocardial perfusion.....	28
Figure 4 Test for cell viability after isolation .....	29
Figure 5 Scheme of the imaging setup used at the LSM 700.....	32
Figure 6 Fluorescence properties of SNARF-5F .....	35
Figure 7 Chemical structure of SNARF.....	36
Figure 8 SNARF recordings.....	37
Figure 9 Calibration of the SNARF-imaging setup .....	39
Figure 10 Chemical structure of Fluorescein DHPE (modified from Invitrogen).....	42
Figure 11 Expression of <i>Laconic</i> in mouse cardiomyocytes.....	44
Figure 12 Example recording of lactate imaging in cardiomyocytes with <i>Laconic</i> .....	45
Figure 13 Genotype determination of CAII <sup>+/-</sup> , CAII <sup>+/+</sup> and CAII <sup>-/-</sup> mice.....	53
Figure 14 Genotype determination of CAIX <sup>+/-</sup> , CAIX <sup>+/+</sup> and CAIX <sup>-/-</sup> mice.....	54
Figure 15 Genotype determination of CAXIV <sup>+/-</sup> , CAXIV <sup>+/+</sup> and CAXIV <sup>-/-</sup> mice.....	55
Figure 16 Determination of $\beta$ and $\rho$ in mouse cardiomyocytes .....	58
Figure 17 Buffer capacity ( $\beta$ ) and fixed buffer ratio ( $\rho_{\text{fixed}}$ ) in mouse cardiomyocytes .....	59
Figure 18 Impact of basal pH on buffer ratio and buffer capacity .....	60
Figure 19 Test for cytosolic CA activity .....	62
Figure 20 Cytosolic CA activity in WT and CAII <sup>-/-</sup> cardiomyocytes .....	63
Figure 21 Detection of CAII in WT and CAII <sup>-/-</sup> cardiomyocytes .....	64
Figure 22 CAII detection in mouse heart with western blot .....	64
Figure 23 CAII antibody detects CAIII.....	65
Figure 24 CAIII in skeletal and heart muscle. ....	65
Figure 25 Activity of extracellular CA on mouse cardiomyocytes .....	67
Figure 26 CAIV in mouse heart .....	68
Figure 27 CAIV detection in dissociated heart sample.....	69
Figure 28 CAIX in mouse heart and stomach .....	70
Figure 29 The presence of MCT1, MCT2 and MCT 4 in mouse cardiomyocytes .....	72
Figure 30 The $K_m$ for lactate influx into cardiomyocytes.....	73
Figure 31 $K_m$ of lactate induced $J_{A/B}$ .....	74
Figure 32 Acid extruding mechanisms in mouse cardiomyocytes .....	76
Figure 33 Dissection of $\Delta[H^+]_i / \Delta t$ mediating mechanisms after acid load.....	77
Figure 34 Dissection of $J_{A/B}$ mediating mechanisms after acid load.....	79
Figure 35 Mouse cardiomyocytes contain a S0859 sensitive and an insensitive NBC isoform.....	80
Figure 36 Western blot with NBCe1 detection .....	81
Figure 37 Na <sup>+</sup> -independent, HCO <sub>3</sub> <sup>-</sup> -dependent acid extrusion .....	82
Figure 38 Threshold of CO <sub>2</sub> /HCO <sub>3</sub> <sup>-</sup> -independent acid extrusion.....	83
Figure 39 Effect of EZA on HCO <sub>3</sub> <sup>-</sup> -dependent acid extrusion .....	84
Figure 40 Measurement of lactate-induced acidification in different buffers .....	86
Figure 41 Lactate (3 mM) induced $J_{A/B}$ according to $\beta$ , $\rho_{\text{fixed}}$ and $\rho_{\text{adap}}$ . ....	87
Figure 42 Lactate uptake measured with <i>Laconic</i> .....	88
Figure 43 Non-catalytic interaction of MCT1 and CAIX.....	89
Figure 44 Non-catalytic interaction of MCT1 and CAXIV .....	90



Figure 45 Effect of cellular respiration on lactate uptake.....	91
Figure 46 Effect of NHE on lactate influx .....	92
Figure 47 S0859 inhibits lactate induced $\Delta[H^+]/\Delta t$ .....	93
Figure 48 Lactate metabolism in mouse cardiomyocytes.....	94
Figure 49 Cytosolic conversion of lactate to pyruvate.....	95
Figure 50 Model of potential catalytic interaction of MCT and intracellular CA.....	106
Figure 51 Model of potential catalytic interaction of MCT and extracellular CA.....	107
Figure 52 Scheme of S0859 effect on lactate-induced acidification .....	108
Figure 53 Model of NBC, CA and MCT interaction .....	110
Figure 54 Potential interaction of respiration and lactate uptake.....	111
Figure 55 Final model of CA, NBC, MCT and mitochondrion interaction.....	116
Figure 56 Potential stimulation of pentose phosphate pathway by lactate and ROS.....	119
Figure 57 Final model with hypothetical ROS protection by lactate .....	120

## Tables

Table 1 Medium for cardiomyocytes isolation (Yog-Mod) .....	30
Table 2 Medium for cultivation of cardiomyocytes (ITS-Medium) .....	30
Table 3 Further materials used for cardiomyocytes cultivation.....	31
Table 4 Dyes used for pH imaging.....	33
Table 5 Inhibitors used in imaging experiments .....	33
Table 6 Recipe of HEPES-buffered imaging solution.....	34
Table 7 Recipe of TBST .....	49
Table 8 Recipe of western blot blocking solution .....	49
Table 9 Antibodies used for western blot .....	49
Table 10 Recipe of blocking solution for immunohistochemistry. ....	50
Table 11 Antibodies used for immunohistochemistry. ....	50
Table 12 TE-Buffer .....	55
Table 13 Lysis buffer 1x MGB (Modified Gitschier Buffer) .....	56
Table 14 Further materials used for genotyping.....	56
Table 15 Buffer capacity ( $\beta$ ) and fixed buffer ratio ( $\rho_{\text{fixed}}$ ) in mouse cardiomyocytes.....	59
Table 16 $\Delta[\text{H}^+]_i / \Delta t$ after $\text{NH}_4\text{Cl}$ pre-pulse .....	78
Table 17 Dissection of $\Delta[\text{H}^+]_i / \Delta t$ contributors after acid load.....	78
Table 18 $J_{\text{A/B}}$ after $\text{NH}_4\text{Cl}$ pre-pulse .....	79
Table 19 Dissection of $J_{\text{A/B}}$ contributors after acid load .....	79
Table 20 Effect of EZA on $\text{HCO}_3^-$ -dependent acid extrusion .....	84
Table 21 Lactate (3 mM) induced $J_{\text{A/B}}$ according to $\beta$ , $\rho_{\text{fixed}}$ and $\rho_{\text{adap}}$ .....	87
Table 22 Effect of buffering condition on $J_{\text{A/B}}$ according to $\beta$ , $\rho_{\text{fixed}}$ and $\rho_{\text{adap}}$ .....	87
Table 23 Lactate influx during extracellular application (3 mM).....	88
Table 24 Effect of buffering system on lactate influx during extracellular application (3 mM) .....	89

## Abbreviations

AE: anion exchanger (membrane transporter)

a.u.: arbitrary units

$\beta$ : buffer capacity

BDM: 2,3-Butanedione monoxime (inhibits muscle contraction)

bp: base pairs

BSA: bovine serum albumin

CA: carbonic anhydrase (catalyses conversion of  $\text{CO}_2 + \text{H}_2\text{O}$  to  $\text{HCO}_3^-$  and  $\text{H}^+$ )

CBE: chloride / bicarbonate exchanger (membrane transporter)

CFP: cyan fluorescent protein

CHE: chloride / hydroxyl exchanger (membrane transporter)

DMEM: Dulbecco's Modified Eagle's Medium (cell culture medium)

DMF: dimethylformamide (organic solvent)

DMSO: dimethyl sulfoxide (solvent)

DHPE: dihexadecanoyl-sn-glycero-3-phosphoethanolamine (artificial lipophilic membrane anchor)

DIDS: 4,4'-diisothiocyanostilbene-2,2'-disulfonic acid (NBC/MCT inhibitor)

EDTA: ethylenediaminetetraacetic acid ( $\text{Ca}^{2+}$  buffer)

EZA: 6-Ethoxy-2-benzothiazolesulfonamide (CA inhibitor)

FCS: foetal calf serum

GPI: glyco-phosphatidylinositol (membrane anchor for certain proteins like CAIV)

HRP: horse radish peroxidase

ITS: Insulin transferrin selenium (cell culture supplement)

$J_{A/B}$ : acid/base flux

kDa: kilo Dalton

$K_i$ : dissociation constant for enzyme inhibitor

KO: knock out

LSM: laser scanning microscope

MCT: mono carboxylate transporter (membrane transporter)

mM: milli molar

nl: nano litre

nM: nano molar

nm: nano meter

mTFP: monomeric teal fluorescent protein (CFP variant)

NBC:  $\text{Na}^+/\text{HCO}_3^-$  co-transporter (membrane transporter)

NHE:  $\text{Na}^+/\text{H}^+$  exchanger (membrane transporter)

p.: page

PBS: phosphate-buffered saline

PFU: plaque forming unit (unit used to express virus concentration)

$\rho$ : buffer ratio

SDS: sodium dodecyl sulfate (detergent, provides negative charge to proteins)

SNARF: Seminaaphthorhodafluor (pH sensitive fluorescent dye)

SR: sarcoplasmic reticulum

TBST: TrisHCl-buffered solvent + Tween20 (solution used for western blot)

WT: wild type

YFP: yellow fluorescent protein

Yog-mod: Yogananda's recipe, modified (medium used for myocardial dissociation)

$\mu\text{M}$ : micro molar

$\mu\text{m}$ : micro meter

## **Acknowledgements**

First of all I want to thank my wife and family for their moral and scientific support. Second, thanks to my dear colleagues who shared, corrected or inspired my work. Special thanks to Linda Forero-Quintero, Somayeh Jamali, Shefееq Theparambil and Dr. Ivan Ruminot who spend several hours with the review of my thesis. Next I want to thank Sandra Bergstein, who taught me all I know and even more about cell culture. Thanks to jun. Prof. Dr. Holger M. Becker, who provided this Ph.D. position, helped me to sharpen my thesis and allowed me the freedom to test most of my ideas. Thanks to Prof. Kins for being my second reviewer. Thanks to Prof. Friauf for being chairman of my doctoral examination.

Finally, I want to thank all the small and tall obstacles that accompanied me during the last three and a half years. Without you it would have been much less frustrating, disappointing, unfruitful and annoying; but also much less beneficial.

不管白猫、黑猫，逮住老鼠就是好猫。

“It doesn't matter whether it's a white cat or a black; a cat that catches mice is a good cat.”

*Deng Xiaoping*

## Abstract

The heart is reported to show a net consumption of lactate. This may contribute up to 15% to the total body lactate disposal. In this work, the consumption of lactate was shown for the first time on the single cell level with the new FRET-based lactate sensor *Laconic*.

Research published until today, almost exclusively reports the monocarboxylate transporter 1 (MCT1) as the transporter responsible for myocardial lactate uptake. As this membrane transporter transports lactate together with H<sup>+</sup> in a stoichiometry of 1:1, lactate transport is coupled to pH regulation. Consequently, interactions of MCT1 and acid/base regulating proteins (carbonic anhydrases (CAs and sodium bicarbonate co-transporters (NBCs)) are described in the oocyte expression system, skeletal muscle and cancer cells.

In this work it is shown that activity of extracellular CA increases lactate uptake into mouse cardiomyocytes by 27% and lactate induced  $J_{A/B}$  by 42.8% to 46.2%. This effect is most likely mediated via NBC/CA interaction because inhibition of extracellular CA reduces HCO<sub>3</sub><sup>-</sup>-dependent acid extruding  $J_{A/B}$  by 53.3% to 78.4%. This may link lactate uptake to cellular respiration. When lactate was applied in medium gassed with 100% N<sub>2</sub>, lactate induced acidification was 12.6% faster than in medium gassed with 100% O<sub>2</sub>. Thus, CO<sub>2</sub> produced on the pathway transferring redox energy from substrates like glucose and lactate to ADP and phosphate via oxidative phosphorylation, may support further lactate uptake. The findings of this work suggest an auto regulation of lactate uptake via CO<sub>2</sub> release in ventricular mouse cardiomyocytes.

# 1. INTRODUCTION

---

## 1.1 General introduction

Cardiomyocytes provide a simple activity to the heart: contraction and relaxation. Beside this, cardiomyocytes possess several processes from energy metabolism to signal processing at the same time. As they are the basic elements of the heart, the blood circulation and finally our life depend on their accurate function. Therefore they must, other than skeletal muscle cells, remain the whole life long constantly active. The biggest part of the redox energy, trapped in glucose is transferred to ADP + phosphate via oxidative phosphorylation (Pfeiffer et al., 2001). Accordingly, cardiomyocytes meet their energy needs on the oxidative pathway (Ventura-Clapier et al., 2003). Several authors have reported that cardiomyocytes consume glucose and fatty acids but also lactate (Baker et al., 1998; Bergman et al., 2009; Gertz et al., 1988; Gladden, 2007 review; Johannson et al., 2001; Kempainen et al., 2002; Wahl et al., 2009 review). Mitochondrial activity is potentially involved in the formation of toxic reactive oxygen species (ROS) (Ghosh et al., 2005). This is important in view of cardiomyocytes' low regenerative capacities (Poolman et al., 1998). Even though more recent research revealed much higher regenerative properties of the heart than previously expected, (Beltrami et al., 2001; Matsuyama and Kawahara, 2008) cardiomyocytes must be robust and enduring. Especially under the hyperglycemic conditions that are associated with diabetes, mitochondrial ROS formation may cause myocardial damage (Fiordaliso et al., 2004, Ghosh et al., 2005 and Ye et al., 2003). Thus, the handling of myocardial ROS is essential.

However, lactate consumption in the human heart may increase from 35  $\mu\text{mol}/\text{min}$  at resting conditions to 120  $\mu\text{mol}/\text{min}$  during exercise (Gertz et al., 1988). Myocardial lactate consumption is supported by the properties of the LDH (lactate dehydrogenase) isoform present in the heart. The myocardial LDH is being inhibited by excess pyruvate (10 mM, *in vitro*, Dawson et al., 1964). Thus, strong glycolytic activity and the resulting cytosolic pyruvate would rather inhibit the enzyme, whereas cells with strong respiratory activity should be able to keep the pyruvate level low and therefore allow the enzyme to produce pyruvate out of lactate.



Since the processes in the citric acid cycle and the previous formation of acetyl-CoA from pyruvate are accompanied by CO<sub>2</sub> production, the respiratory consumption of lactate is connected to CO<sub>2</sub> release (Gertz et al., 1988).

## **1.2 H<sup>+</sup> buffering and pH regulation**

CO<sub>2</sub> will always be equilibrated with HCO<sub>3</sub><sup>-</sup> + H<sup>+</sup> as it is present in an aqueous environment. As consequence, altered CO<sub>2</sub> concentrations go along with altered H<sup>+</sup> concentrations. Beside this CO<sub>2</sub> caused “respiratory acidosis”, further metabolic processes potentially generate H<sup>+</sup> (Gevers et al. 1977). In the heart, the major H<sup>+</sup> generating processes beside CO<sub>2</sub> formation might be triglyceride synthesis and its degeneration as well as glycolysis, but not lactate formation (Gevers et al. 1977). A general reason for cytosolic H<sup>+</sup> load might be the inward directed electrochemical gradient for H<sup>+</sup> whose reversal potential lies between 0 and -30 mV (Deitmer and Chesler, 2009). In muscle cells, a raise in cytosolic H<sup>+</sup> can reduce contractility (Chin and Allen, 1998) and may even cause arrhythmia (Vaughan-Jones et al., 2009). Such effects on cell physiology are avoided or reduced by H<sup>+</sup> buffering. In general, cells provide two different H<sup>+</sup> buffering systems. On the one hand, amino acids of cytosolic proteins may bind or release H<sup>+</sup>. Especially the amino acid histidine contributes to this intrinsic H<sup>+</sup> buffering (Roos and Boron, 1981). The intrinsic buffer may be further divided into mobile and immobile buffer (Vaughan-Jones et al., 2002). The immobile fraction of intrinsic buffering is thought to be mediated by proteins that are either fixed to intracellular structures or so big that their diffusion coefficients are bigger than 10<sup>-8</sup> cm<sup>2</sup>/s and are therefore considered to be immobile in relation to the speed of pH regulation (Zamboni et al. 2003). The mobile fraction of intrinsic buffering in cardiomyocytes provides a diffusion coefficient of 8-12 x 10<sup>-7</sup> cm<sup>2</sup>/s (Zamboni et al. 2003) and is suggested to be mainly mediated by homocarnosine and phosphate (Vaughan-Jones et al., 2002). On the other hand, the reversible hydration of CO<sub>2</sub> (H<sub>2</sub>O + CO<sub>2</sub> ↔ HCO<sub>3</sub><sup>-</sup> + H<sup>+</sup>) provides a strong and dynamic system for H<sup>+</sup> buffering (Casey et al., 2010). The strength of the buffering system is described by the buffer capacity. The buffer capacity describes the amount of H<sup>+</sup> that has to be added to or removed from the cytosol to change the pH by one unit. The CO<sub>2</sub>/HCO<sub>3</sub><sup>-</sup>-independent buffer capacity is the so called intrinsic buffer capacity (β<sub>i</sub>). In rabbit cardiomyocytes, a β<sub>i</sub> of 26.4 mM was described by Vaughan-Jones et al. (2002). Zamboni et al. (2003) report a β<sub>i</sub> of approximately 30 mM at pH 7.0 that declines to 10 mM at approximately

pH 7.5 in guinea-pig, rat and rabbit cardiomyocytes. The  $\text{CO}_2/\text{HCO}_3^-$ -dependent buffer capacity ( $\beta_{\text{CO}_2}$ ) was determined by Leem et al. (1999) in ventricular cardiomyocytes from guinea-pig to be approximately 20 mM at pH 7.0 and approximately 45 mM at pH 7.35. The sum of intrinsic and  $\text{CO}_2/\text{HCO}_3^-$ -dependent buffering system provide the total  $\text{H}^+$  buffer capacity ( $\beta_{\text{tot}}$ ), which is at the basal pH of 7.2 approximately 50 mM in guinea-pig cardiomyocytes (Leem et al., 1999).

Beside this cellular buffering capacity, tissues provide additional mechanisms for pH regulation. In cardiomyocytes, acid extrusion is reported to be mainly mediated by the sodium/ $\text{H}^+$  exchanger (NHE) and by the sodium/bicarbonate co-transporter (NBC). The main acid loaders are chloride/hydroxyl exchanger (CHE) and chloride/bicarbonate exchanger (CBE) (Vaughan-Jones et al., 2009). This pH regulation has been suggested to be called  $\text{H}^+$  muffling to distinguish it from the  $\text{H}^+$  buffering (Deitmer, 1991; Thomas et al. 1991). Recent results by Theparambil et al. (2014) suggest that  $\text{H}^+$  muffling may not just be a slow regulator that brings the pH back to the baseline after a severe deflection, but may even dominate  $\beta_{\text{tot}}$ . Thus, a cell's ability to compensate net  $\text{H}^+$  in- or efflux depends on the three systems: intrinsic buffering,  $\text{CO}_2/\text{HCO}_3^-$ -dependent buffering and  $\text{H}^+$  muffling.

### **1.3 Carbonic anhydrase**

The dynamics of the  $\text{CO}_2/\text{HCO}_3^-$ -dependent buffering system depend on the activity of carbonic anhydrase (CA), an enzyme that speeds up the conversion of  $\text{CO}_2$  to  $\text{HCO}_3^- + \text{H}^+$  and vice versa. The CA isoforms I, II, III, VII and XIII are found to be cytosolic, the CAV is found in the mitochondrial matrix and the isoforms IV, IX, XII, XIV and XV are found to be membrane bound (Supuran, 2008). Every mammalian tissue contains CA, just the composition of its isoforms differs (Gilmour, 2010; Spicer et al., 1979; Sly and Hu, 1995; Spicer et al., 1993; Hilvo et al., 2005). This broad variety indicates the physiological importance and as consequence the CA provides adaption to various requirements.

As broad the CA's varieties, as diverse are its roles in physiology. Especially the physiological role of CAIII is puzzling. This isoform is reported to contribute up to 50% of the total cytosolic enzyme in red skeletal muscle from rat (Shiels et al., 1983; Shiels et al., 1984). However, the purified enzyme does not contribute to the conversion of  $\text{CO}_2$  to  $\text{HCO}_3^- + \text{H}^+$  (Schüler et al., 2011), even though in *Xenopus* oocytes, heterologously expressing CAIII, activity was

observed (Schüler et al., 2011). This may indicate an activating factor present in intact cells. Some authors found a potential involvement of CAIII in reactive oxygen species (ROS) handling (Räisänen et al., 1999; Roy et al., 2009) and its high presence in adipocytes (Kim and Levine, 2005; Spicer et al., 1990) may suggest an involvement in fatty acid handling. In any case, CAIII knockout mice do not show any phenotype (Kim et al., 2004) so that the question remains what this protein shall be good for at all. In general, the broad variety of CA isoforms makes it likely that the KO of a particular CA isoform can be compensated by other CAs (Sly and Hu, 1995; Pan et al., 2006). In contrast to the loss of CAIII, the loss of other CA isoforms may have severe consequences for the organism. Knock out animals show phenotypes that may reach from osteoporosis (CAII-KO; Margolis et al., 2008) to impaired fertility (CAIV-KO; Wandernoth et al., 2010) or infertility (CAIV/CAXIV double KO; Shah et al., 2005).

Older *in vitro* studies on the catalytic activity of the purified enzyme determined a CAII-dependent speed up of several thousand times and declared the CAII as the fastest CA isoform (Forster and Crandell, 1975; Silverman and Lindskog, 1988). More recent studies on *Xenopus laevis* oocytes, heterologously expressing CAII (Schüler et al., 2011) or on brain tissue sections (Stridh et al., 2012) revealed a CAII-dependent speed up of 2 to 7 fold under physiological conditions. In addition, Schüler et al. (2011) found that the CAI was almost as fast as CAII when present in *Xenopus* oocytes. In that study, the enzyme concentration was not determined so that differences in the measured kinetics might be due to different enzyme concentrations. But considered together with the finding that purified CAIII is almost inactive but active when present in intact cells, one might conclude that enzyme kinetics determined *in vitro*, might not reflect its physiological activity. However, erythrocytes contain large amounts of CAI and CAII, so these isoforms participate in respiration (Poole and Halestrap, 1994; Roughton, 1935; Sly and Hu, 1995).

The presence of a cytosolic CA in cardiomyocytes is controversial. Alvarez et al. (2013) detected the CAII in human and mouse heart on the RNA and protein level. Alvarez et al. (2007) detected the CAII on RNA and protein level the rat and mouse heart. Schroeder et al. (2013) reported CA-catalysed CO<sub>2</sub> hydration in rat cardiomyocytes and could detect the CAII on the protein level. Villafuerte et al. (2014) reported intracellular and extracellular catalytic CA activity. Geers et al. (1992) could not observe CA activity in the cytosolic fraction of lysed rabbit hearts. Vuillemin and Pexieder (1997) detected the CAII on the protein level in the ventricle of the

embryonic mouse heart at the age of 13-16 embryonic days, but at later developmental stages the CAII signal disappeared from the ventricle and was observed in endothelial tissues instead. In contrast, different membrane bound CA isoforms were found in the heart. Scheibe et al. (2006) detected the isoforms CAIV, CAIX and CAXIV on the protein level in mouse cardiomyocytes. Alvarez et al. (2013) detected the CAIV and CAXIV in the human and mouse heart. Geers et al. (1992) could detect CA activity in the membrane fraction of lysed rabbit hearts and Vandenberg et al. (1996) could observe CA activity only at the sarcolemma of cardiomyocytes from the ferret heart. Thus, strong evidence suggests membrane bound CA activity in mammalian cardiomyocytes, whereas cytosolic CA activity needs to be confirmed.

## **1.4 Lactate transport**

Lactate transport across mammalian cell membranes is mainly mediated by MCTs (monocarboxylate transporters) (Pierre and Pellerin, 2005; Yanase et al., 2008; Bonen et al., 2001; Vinnakota et al., 2011). The MCT isoforms 1-4 couple the transport of monocarboxylates, such as lactate, to H<sup>+</sup> transport at a stoichiometry of 1:1 (Halestrap and Meredith, 2004). The characteristic difference between the isoforms is their affinity towards substrates. This is described by the Michaelis-constant ( $K_m$ ), which is the substrate concentration at which the enzyme shows its half-maximal kinetic. For lactate,  $K_m$  values of 0.75 mM, 3.5 mM and 28 mM are reported for MCT2, MCT1 and MCT4, respectively (Bröer et al., 1998; Fox et al., 2000). Therefore, the MCT2 and MCT4 are widely considered as the high affinity and the high capacity specialist, respectively. According to the neuron-astrocyte lactate shuttle hypothesis, astrocytes release lactate into the extracellular space from where it will be imported to neurons, which utilise lactate for ATP production via oxidative phosphorylation (Chih and Roberts, 2003). As the released lactate gets diluted in the extracellular space, in the brain the MCT2 is mainly associated with lactate uptake into Neurons due to its high affinity (Pierre and Pellerin, 2005). The low affinity but high capacity of the MCT4 let this transporter suit lactate producing and consequently releasing cells, like astrocytes (Pierre and Pellerin, 2005). A high capacity for lactate export becomes essential in cells whose rate of ATP production via glycolysis largely exceeds their rate of ATP production via oxidative phosphorylation, like in cancer cells or in white skeletal muscle (Kroemer and Pouyssegur, 2008; Pilegaard et al., 1999). In those cells, glycolysis ending with pyruvate would cause a NAD<sup>+</sup> deficit and consequently ATP generation would get impaired. The reaction  $NADH + H^+ + Pyruvate \rightarrow NAD^+ + Lactate$  allows the

continuous ATP production via glycolysis. This reaction gets further supported by a special feature of the MCT4. While MCT1 and MCT2 show higher affinity towards pyruvate in comparison to lactate, the  $K_m$  for pyruvate transport via MCT4 is reported to be more than four times higher than for lactate ( $K_m$  MCT4: lactate 28 mM, pyruvate 153 mM; Fox et al., 2000). This would rather trap pyruvate inside the cell and allow its conversion to lactate. The MCT1 may be considered as all-rounder that suits the biggest part of metabolic needs, which might explain its almost ubiquitous distribution (Pierre and Pellerin, 2005; Poole and Halestrap, 1994). The MCT3 is a lactate transporter, restricted to the retina (Halestrap and Meridith, 2004). Therefore it will not be further discussed in this work.

In the mouse heart, Dimmer et al. (2000) provided some evidence for MCT4's presence on the RNA level but the only MCT isoform that has been found in the mammalian heart on the protein level is the MCT1 (Bonen, 2001; Evans et al., 2002; Johannsson et al., 2001).

At this point, it should be briefly mentioned that in some studies an electrogenic lactate transporter (SMCT) that does not couple the lactate transport to  $H^+$  but to  $Na^+$  has been reported in the heart (Martin et al., 2006; Paroder et al., 2006). But this finding is controversial. Srinivas et al. (2003) could detect the mRNA of the SMCT with northern blot, whereas Gopal et al. (2004) could not detect the SMCT mRNA in mouse heart samples. Xiao and Allen (2000) performed sodium imaging on rat cardiomyocytes. They induced cytosolic sodium load by lactate application. But when they inhibited the NHE with cariporide, the lactate-induced sodium load was gone, which indicates the absence of a sodium-dependent lactate transporter in rat cardiomyocytes.

However, all evidence points to the MCT1 as major lactate transporter in cardiomyocytes. Therefore,  $H^+$  buffering and muffling may directly contribute to the lactate transport.

## **1.5 Acid/Base regulation and lactate transport**

The lactate transport into cardiomyocytes is coupled via MCT to H<sup>+</sup> transport. Therefore H<sup>+</sup> buffering and muffling potentially interfere with lactate transport. The slow intracellular H<sup>+</sup> diffusion as compared with its diffusion in unbuffered aqueous solution ( $8-12 \times 10^{-7} \text{ cm}^2/\text{s}$  and  $9.3 \times 10^{-5} \text{ cm}^2/\text{s}$ , respectively (Vanysek, 2000; Zamboni et al., 2003)) may cause an accumulation of H<sup>+</sup> where it enters the cell (Vaughan-Jones et al., 2002). According to this slow cytosolic H<sup>+</sup> diffusion, Spitzer et al. (2002) formulated the hypothesis that H<sup>+</sup> micro domains might form. In the case of lactate uptake into cardiomyocytes this would mean that H<sup>+</sup> would accumulate in close proximity to the MCT in the cytosol. Thus, the inward directed H<sup>+</sup> gradient would get reduced and the lactate uptake would slow down. In the presence of CO<sub>2</sub>/HCO<sub>3</sub><sup>-</sup> buffer, the cytosolic H<sup>+</sup> mobility increases by a factor of 2.7 (Zamboni et al., 2003), therefore the formation of H<sup>+</sup> micro domains during lactate uptake might reduce. This increased H<sup>+</sup> mobility in CO<sub>2</sub>/HCO<sub>3</sub><sup>-</sup> buffer depends on the catalytic activity of the CA (Spitzer et al., 2002). In addition, the increased buffer capacity in the presence of CO<sub>2</sub>/HCO<sub>3</sub><sup>-</sup> buffer would reduce the cytosolic acidification that is caused by MCT mediated lactate uptake. Consequently, lactate uptake into cardiomyocytes might be increased in CO<sub>2</sub>/HCO<sub>3</sub><sup>-</sup>-buffered conditions, depending on CA's catalytic activity. Spitzer et al. (2002) refer the observed effect of CA activity on cytosolic H<sup>+</sup> mobility to cytosolic CA. But, as previously mentioned, the cytosolic activity of CA in cardiomyocytes is controversial. In contrast, there is strong evidence for extracellular CA activity on cardiomyocytes. Several authors report a functional interaction of extracellular CA and NBC (Alvarez et al., 2003; Morgan et al., 2007; Loiselle et al., 2004; Orłowski et al., 2012, Stock and Schwab, 2009). Theparambil et al. (2014) could observe a strong impact of the NBC on the buffer capacity in cultured mouse astrocytes. Therefore, the effect of CA on the H<sup>+</sup> mobility in CO<sub>2</sub>/HCO<sub>3</sub><sup>-</sup> buffer, as reported by Spitzer et al. (2002), might also be due to an indirect effect via NBC.

Wetzel et al. (2001) could show that inhibition of extracellular CA inhibits lactate uptake into skeletal muscle. This observation might point to a functional interaction of MCT and extracellular CA. But if it is taken into account that a functional interaction of MCT and NBC has been observed when expressed in *Xenopus laevis* oocytes (Becker et al., 2008), then it might

be that the observed effect of extracellular CA on lactate uptake (Wetzel et al., 2001) is the result of an indirect CA/MCT interaction via NBC ( $CA \rightarrow NBC \rightarrow MCT$ ).

Beside a catalytic effect of CA on the lactate flux, an interaction of MCT and CA, independent of CA's catalytic activity, was found.

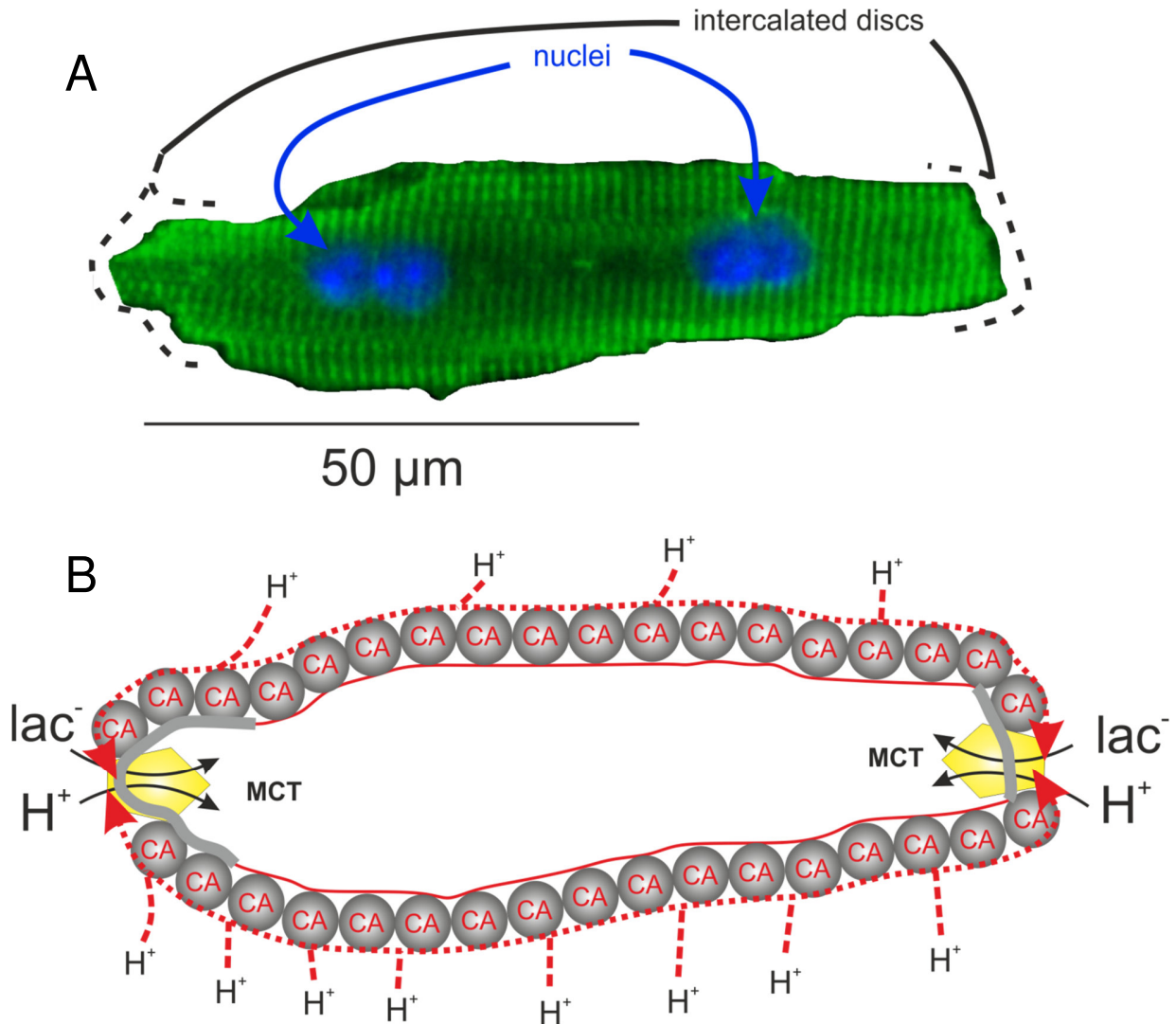


**Figure 1** Scheme of potential non-catalytic interaction of MCT1 and extracellular CAs in mouse

**A** Isolated cardiomyocyte from a p15 mouse. The nuclei are stained with Hoechst and are shown in blue. The green signal results from an unspecific approach in immunocytochemistry for CAII. Nevertheless, it nicely highlights the cell's sarcomeres. **B** Hypothetical model of non-catalytic interaction of MCT and extracellular CA. The MCTs are mainly located in the intercalated discs, which are indicated as grey strings.

In *Xenopus* oocytes, heterologously expressing MCT1 and the intracellular CAII, the lactate uptake was faster than in oocytes expressing MCT1 alone, even when treated with the CA inhibitor 6-Ethoxy-2-benzothiazolesulfonamide (EZA) (Becker et al., 2005).

This interaction was also observed for the extracellular CAs CAIV (Klier et al., 2013) and CAIX (Michael Klier, unpublished data). The observed effect was finally formulated as hypothetical H<sup>+</sup> collecting/scattering antenna, formed by membrane associated CAs (Becker et al., 2011). Basically, CAs are thought to provide conductor quality for H<sup>+</sup> along cell membranes, independent of their catalytic activity. Like this, the low cytosolic H<sup>+</sup> mobility could be compensated. Such “antennae” might also include other proteins than CA’s, especially outside the heterologous expression system, but CA’s are likely to form the essential link between MCT and H<sup>+</sup> conductor.

This “antenna” might enhance lactate uptake into cardiomyocytes. Especially if it is taken into account that MCT1 is reported to be mainly expressed at the rather small area of intercalated discs (Garcia et al., 1994; Johannson et al., 2001). Like this, the whole cell surface would form an H<sup>+</sup>-catchment area of the very locally active MCT (Figure 1).

Another pH regulator that might contribute to the lactate uptake into cardiomyocytes is the Na<sup>+</sup>/H<sup>+</sup> exchanger (NHE). As its name already explains, this membrane transporter provides the exchange of Na<sup>+</sup> and H<sup>+</sup>. Since the gradient for sodium is steeply inward directed, the NHE provides an acid extruding activity. The NHE1 is the only isoform known to be expressed in the heart (Ch’en et al., 2008).

Similar to MCT and NBC, NHE1 may interact with CAs. For NHE1 and CAII, functional and physical interactions were described (Li et al., 2002; Orłowsky and Grinstein, 2004).

The contribution of NHE1 to lactate uptake into the heart is controversial. On the one hand, NHE1 contains an H<sup>+</sup>-sensitive domain that will allow transport activity only beyond a particular threshold of H<sup>+</sup> concentration (Wakabayashi et al., 1997). Leem et al. (1999) reported an increase of NHE-dependent acid extrusion at pH < 6.9 in guinea-pig cardiomyocytes. Thus, the NHE may support the lactate uptake via MCT if the cytosolic pH drops below pH 6.9. According to Kempainen et al. (2002) the human blood lactate level may reach a concentration of 10 mM at strong physical activity. If it is assumed that this would lead to a cytosolic load from 0 to 10 mM lactate and that the buffer capacity is 50 mM (Leem et al. 1999), the cytosolic pH would



drop by  $\Delta\text{pH}$  0.2. Consequently, only in cells with a basal  $\text{pH} \leq 7.1$  the cytosolic raise in lactate concentration from 0 to 10 mM would cause a drop in cytosolic pH that may reach pH 6.9 and therefore potentially activate the NHE. The average basal pH in cardiomyocytes is reported to be pH 7.2 (Vaughan-Jones et al., 2009), so that just individual cardiomyocytes might possess a basal  $\text{pH} \leq 7.1$ . Additionally, the basal cytosolic lactate level might not be zero and the raise in blood lactate level would not occur instantaneously. Thus, the gradient for lactate influx might be lower than assumed and cellular pH regulating mechanisms might be able to maintain the cellular pH meanwhile the cell is loading lactate. Therefore, the involvement of NHE in lactate uptake via MCT appears to be unlikely.

On the other hand, the NHE1 was found to be mainly located in intercalated discs (Garciaarena et al., 2013; Halestrap et al., 1997), which is the same subcellular localization that had been reported to show the highest MCT1 level, as mentioned above. This co-localization indicates the possibility of a functional interaction of MCT1 and NHE1 in cardiomyocytes.

In Figure 2, pH regulating processes potentially involved in lactate transport in cardiomyocytes are summarized. CAs might support the lactate flux in a catalytic-dependent manner by supporting the  $\text{H}^+$  mobility and the buffer capacity via NBC. In addition, CAs might participate in an  $\text{H}^+$  conductor along the intra- and extracellular cell surface that counteracts the low intracellular  $\text{H}^+$  mobility and thereby supports the MCT. If active, the NHE could counteract the cytosolic  $\text{H}^+$  load, caused by lactate uptake via MCT.

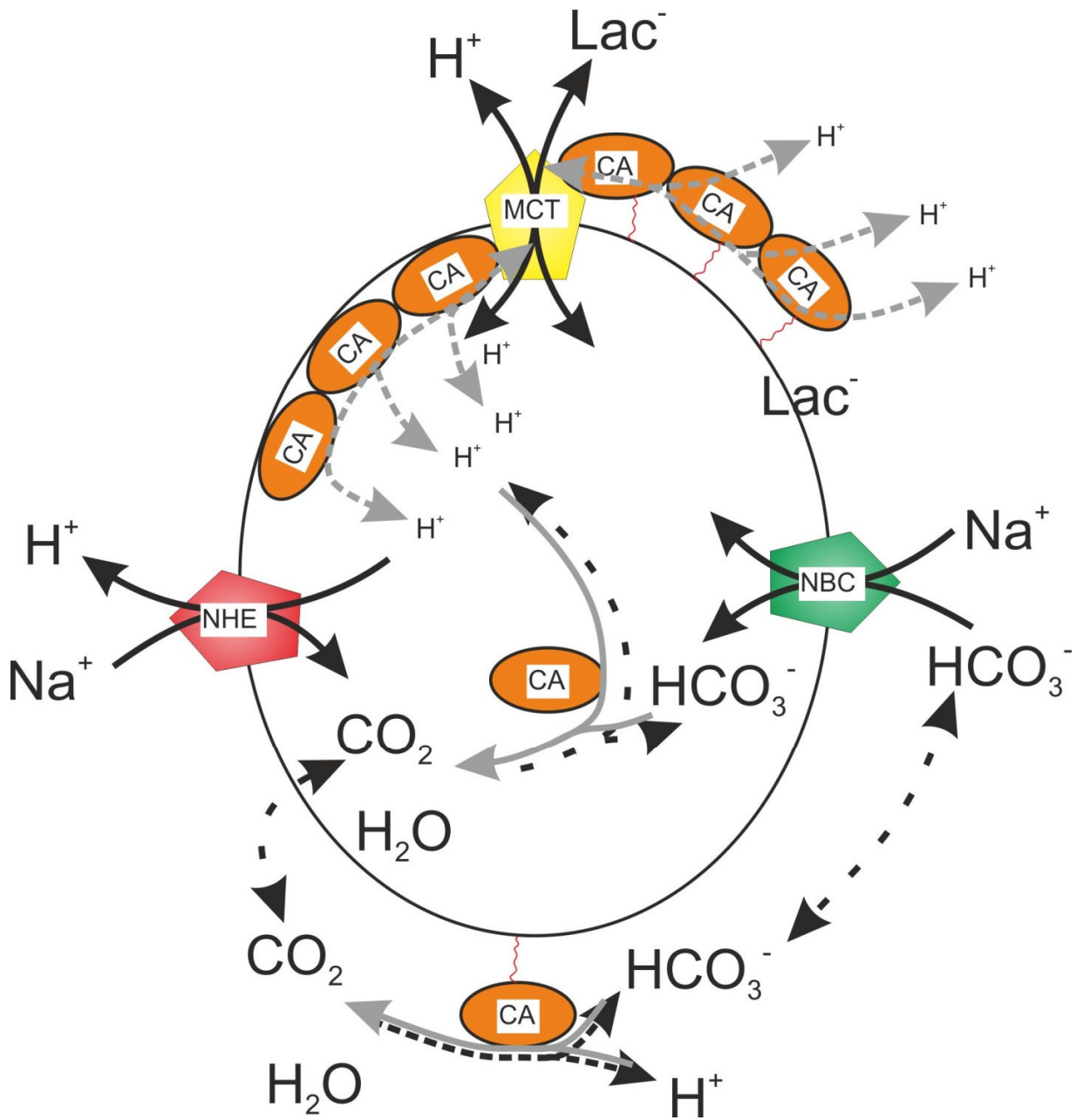


**Figure 2** Acid/base regulation potentially involved in cardiomyocytes' lactate uptake

Extra- and intracellular CAs may support the lactate uptake, depending on CA's catalytic activity and in a non-catalytic manner. The cardiomyocytes' main acid extruders are NHE and NBC. Those are known to provide functional interaction with CAs. MCT: monocarboxylate transporter; NBC: Na<sup>+</sup>/HCO<sub>3</sub><sup>-</sup> co-transporter; NHE: Na<sup>+</sup>/H<sup>+</sup> exchanger; CA: carbonic anhydrase

## **1.6 Motivation**

Cellular pH regulation (Figure 2) and metabolism are complex when considered individually. However, their interplay is obvious as it is widely believed that cellular activity goes along with H<sup>+</sup> release. In muscle, pH regulation defines performance. Messonnier et al. (2007) described a positive correlation of skeletal muscle work rate and the abundance of the proteins MCT1, MCT4, NHE and CAIV. The origin of cytosolic H<sup>+</sup> might be multifaceted and probably includes ATP hydrolysis and CO<sub>2</sub> production. While the protons released at ATP hydrolysis will be trapped inside the cell and might therefore be reused to build up the H<sup>+</sup> gradient between mitochondrial matrix and intermembrane space (Robergs et al., 2004), CO<sub>2</sub> might leave the cell and acidify the extracellular space and neighbouring cells, too. At least in oxidative tissues, such as heart, it is likely that CO<sub>2</sub> production is the main source of H<sup>+</sup> (Gevers et al. 1977). The release of CO<sub>2</sub> depends on the consumption of substrates in the citric acid cycle, which might link it, via CA and NBC activity, to the uptake of lactate.

Therefore, the goal of this work was the investigation of the potential interplay of pH regulation, respiration and lactate uptake into mouse cardiomyocytes.

## 2. MATERIALS & METHODS

---

### 2.1 Cardiomyocyte isolation and cultivation

Cardiomyocytes were isolated from  $p20 \pm 2$  mouse hearts. The isolation method described here was newly developed for this project, based on transcatheter perfusion (Figure 3) and the accumulated experience of several authors (Schlüter and Piper, 2005; Zhou et al., 2000; O'Connell et al., 2003; Louch et al., 2011; Sutherland et al., 2003; Volz et al., 1991). The major difference to the methods published until now is the omission of a Langendorff apparatus from an isolation protocol of adult cardiomyocytes, which provides a cheap and simple alternative. *Additional explanations to the procedure are shown in italics.*

- 1) The animals were sacrificed by cervical dislocation or were decapitated
- 2) The chest was opened with sharp scissors so that the heart got accessible
- 3) The perfusion pump (ISMATEC) was started at a speed of 0.5 ml/min (perfusion with carbogen gassed Yog-Mod (Yogananda-modified, pH 7.2, room temperature; Table 1)).

*If the solution is already pumped out of the cannula when it gets injected, introduction of air bubbles to the vascular system is avoided. The solution was composed according to the recipe of Mr Markandeya (Markandeya et al., 2011) and modified with a low sodium concentration according to the findings by Ver Donk and Borgers (1991), Ruiz-Meana et al. (1999) and Ruiz-Meana and García-Dorado (2009), who described that  $\text{Na}^+$  may pass myocardial gap-junctions and propagate in the syncytium, causing cytosolic  $\text{Ca}^{2+}$  overload.  $\text{Ca}^{2+}$ -free solution was used on the one hand to disrupt connections at intercalated discs, according to the findings of Muir (1967), and on the other hand to avoid hypercontraction due to excessive  $\text{Ca}^{2+}$  influx. A pH between 7.0 and 7.2 was chosen according to the findings by O'Connell et al. (2003) and Kitakaze et al. (1988), who described better cell performance in slightly acidic environment. BDM is a standard drug to inhibit myocardial contraction. Its interaction with the myosin/actin complex is described by Gwathmey et al. (1991). Potential side-effects are mentioned by Borlak and Zwadlo (2004). The benefit of using taurine reaches from preventing apoptosis*

during ischemia (Devi and Anuradha, 2009), which may partially occur during the preparation procedure, to stabilization of the cell membrane (Huxtable and Bressler, 1973).

- 4) The perfusion was connected to the left ventricle via a cannula
- 5) The perfusion speed was increased to 1 ml/min for 2 min
- 6) The right atrium was opened so that fluid could leave the circuit.

*Otherwise the circular system would burst sometime in an uncontrolled manner, which might work too.*

- 7) The perfusion speed was increased to 2 ml/min for 3 min
- 8) The pump was briefly switched off and the perfusion tube was transferred to collagenase containing perfusion solution (collagenase A from Roche; 0.5 mg/ml).

*Even though the solution was calcium free, the collagenase was expected to be active due to calcium released by the cardiomyocytes.*

- 9) After 4 min, 8 ml of 0.5% trypsin solution was added to the collagenase-containing medium (so the volume got filled up to 40 ml and the final trypsin concentration was 0.125 %).

*In previous attempts, treatment with collagenase alone was not sufficient to liberate the cells from the tissue. As consequence, the cells were destroyed in steps 12 and 14. Addition of trypsin, even though rough and unspecific, solved this problem.*

- 10) Perfusion for 15 min.

*It appeared to be helpful to give some heart massage with forceps to support the capillary perfusion at this point.*

- 11) The ventricles were cut below the atria and transferred to a petri dish
- 12) The ventricles were covered with 2 ml enzyme solution (from 9) and plucked to parts with sharp forceps

- 13) The tissue was transferred to a new petri dish (≈ 5 cm) filled with 4 ml of enzyme solution (from step 9) + 200 µl Insulin-Transferrin-Selenium-medium (ITS-medium; see at step 25) and stored in an incubator at 37°C/ 5% CO<sub>2</sub> for 15 min.

*Transferring the tissue parts to a new petri dish was helpful to remove dead, surficial cardiomyocytes, erythrocytes and debris, which may disturb cell attachment in step 22.*

- 14) The plastic tip of a 1000 µl pipette was cut with sterile scissors and then briefly flamed to get a smooth pipette mouth

- 15) Cells were liberated by gentle pipetting

- 16) The fragments that did not dissociate were removed and the cell suspension was transferred to a 15 ml tube containing 4 ml sterile filtered Yog-Mod and 1 ml ITS-medium (the suspension was carefully added to the surface of the solution so that the cells had to sink to the bottom).

*Most authors recommend to reintroduce Ca<sup>2+</sup> in a stepwise manner after the liberation procedure, since immediate application of 2 mM Ca<sup>2+</sup> will cause cytosolic calcium overload, followed by hypercontraction and cell death. Here, calcium was reintroduced in two steps (16 and 19) by mixing the calcium-free Yog-Mod solution and the ITS-Medium, containing 1.8 mM Ca<sup>2+</sup>. Calcium reintroduction at room temperature instead of 37°C was described as beneficial by O'Connell et al. (2003).*

- 17) The cell suspension was stored at room temperature (RT) for 20 min to let the cells settle down, then the cell suspension was centrifuged for 3 min at 300 x g

- 18) The supernatant was discarded except for the lowest ml and the cells were resuspended in the remaining solution.

- 19) The suspension was transferred to a new 15 ml tube with 3 ml sterile filtered Yog-Mod and 2 ml ITS-Medium.

- 20) The cell suspension was stored at RT for 20 min to let the cells settle down, then the tube was centrifuged for 3 min at 300 x g

21) In the meantime, petri dishes were coated with matrigel. A drop of 1.5  $\mu$ l matrigel was placed in the centre of the petri dish and smeared with a sterile cell scraper on a patch of approximately 0.5 cm in diameter. Coated petri dishes were incubated for matrigel polymerization at 37°C for 20-30 min.

*It is important not to apply the gel too thick, otherwise it will swell and detach including the cells on it.*

22) The supernatant was discarded except for the lowest 1000-100  $\mu$ l, in which the cells were resuspended.

23) Finally, a drop of 50  $\mu$ l of suspension was added to a matrigel coated petri dish and settled for 1 h in the incubator at 37°C/ 5% CO<sub>2</sub>.

24) Cellular membrane integrity after the preparation was checked by Hoechst and propidium iodide application (Figure 4).

25) If the cells were intended for cultivation, after 1 h the petri dishes were filled with 2 ml ITS-medium (Table 2).

*The utilization of DMEM D7777 was due to the availability since it's one of the standard media used in this laboratory, but it was favoured over M199 according to Li et al. (2003) who described a reduced presence of coxsackie-adenovirus receptor in M199, which resulted in lower viral transduction yield. The benefits of taurine were mentioned above (step 3). Cultivation of cardiomyocytes for more than 1 day was problematic with media containing BDM. After a very helpful tip by Chad Touchbarry via Researchgate ([www.researchgate.net](http://www.researchgate.net)), blebbistatin was used instead of BDM according to Kabaeva et al. (2008), who could show longer survival of cultured adult mouse cardiomyocytes if blebbistatin was used instead of BDM. In this work, the same beneficial effect of blebbistatin was observed. ITS was used instead of FCS (which was leading to circularization of cardiomyocytes) according to the findings of Sambrano et al. (2002) and Volz et al. (1991). Lactate was added because this work was focusing on lactate transport and the availability of lactate was thought to stimulate lactate transport mechanisms. However, addition of lactate (5 mM) seemed to improve cell viability. Matrigel as coating material was used because of its' laminin content, which was*

reported to provide good attachment of cardiomyocytes (Rogers et al., 2009; Lundgren et al., 1985) and specifically acts on  $\beta_1$ -integrin surface receptors (Terracio et al., 1991), mimicking the interaction with extracellular matrix of the in vivo situation.

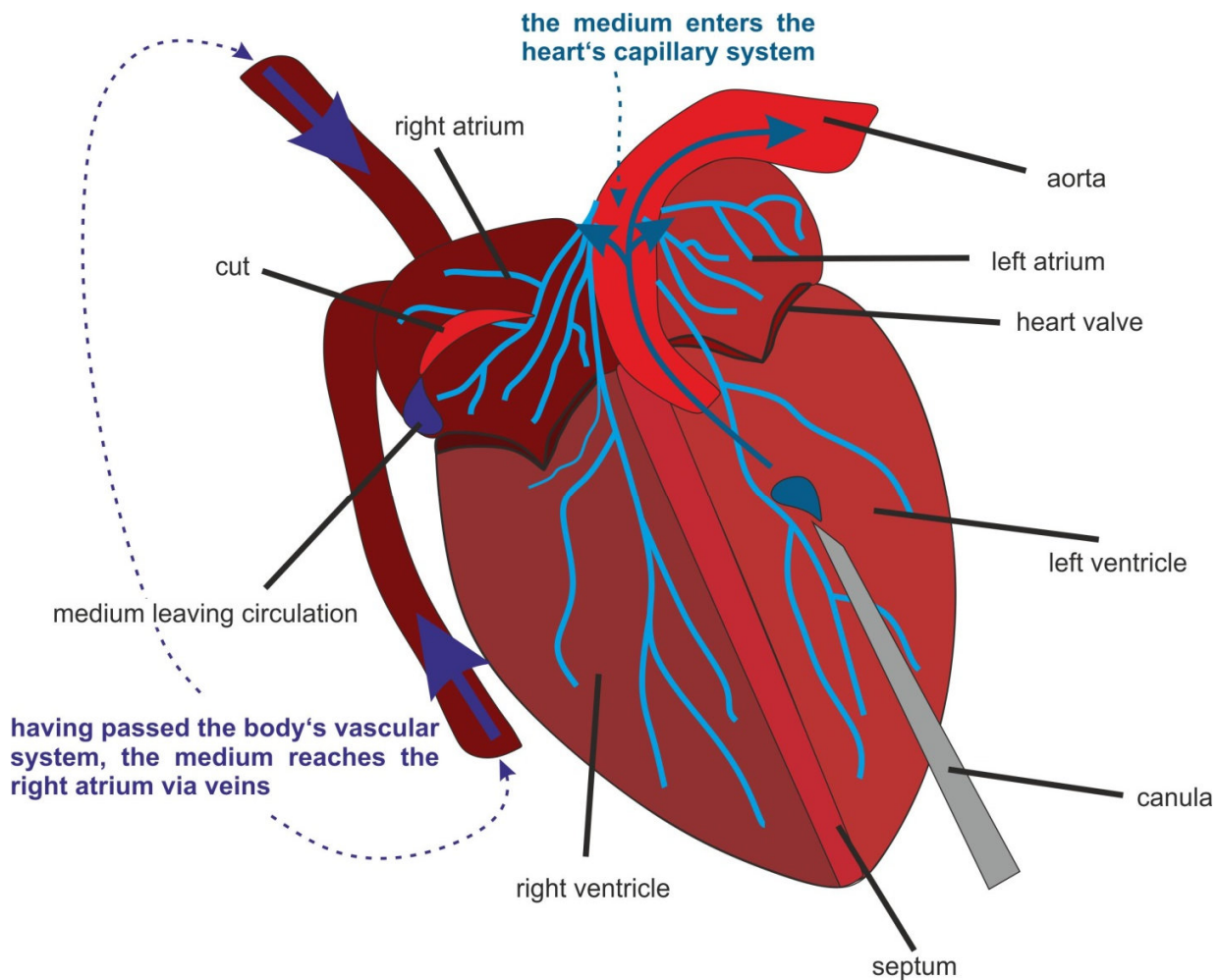


**Figure 3** Scheme of myocardial perfusion

The arrows indicate the direction of perfusion. The medium was pumped into the left ventricle so that it had to leave the heart via the aorta. The heart arteries will branch off the aorta. As the vessel system will produce a resistance, the medium is thought to be forced into the heart's capillary system from where it will finally drain into the right atrium. With a small cut in the right atrium the circuit got opened here so that the heart can be perfused.



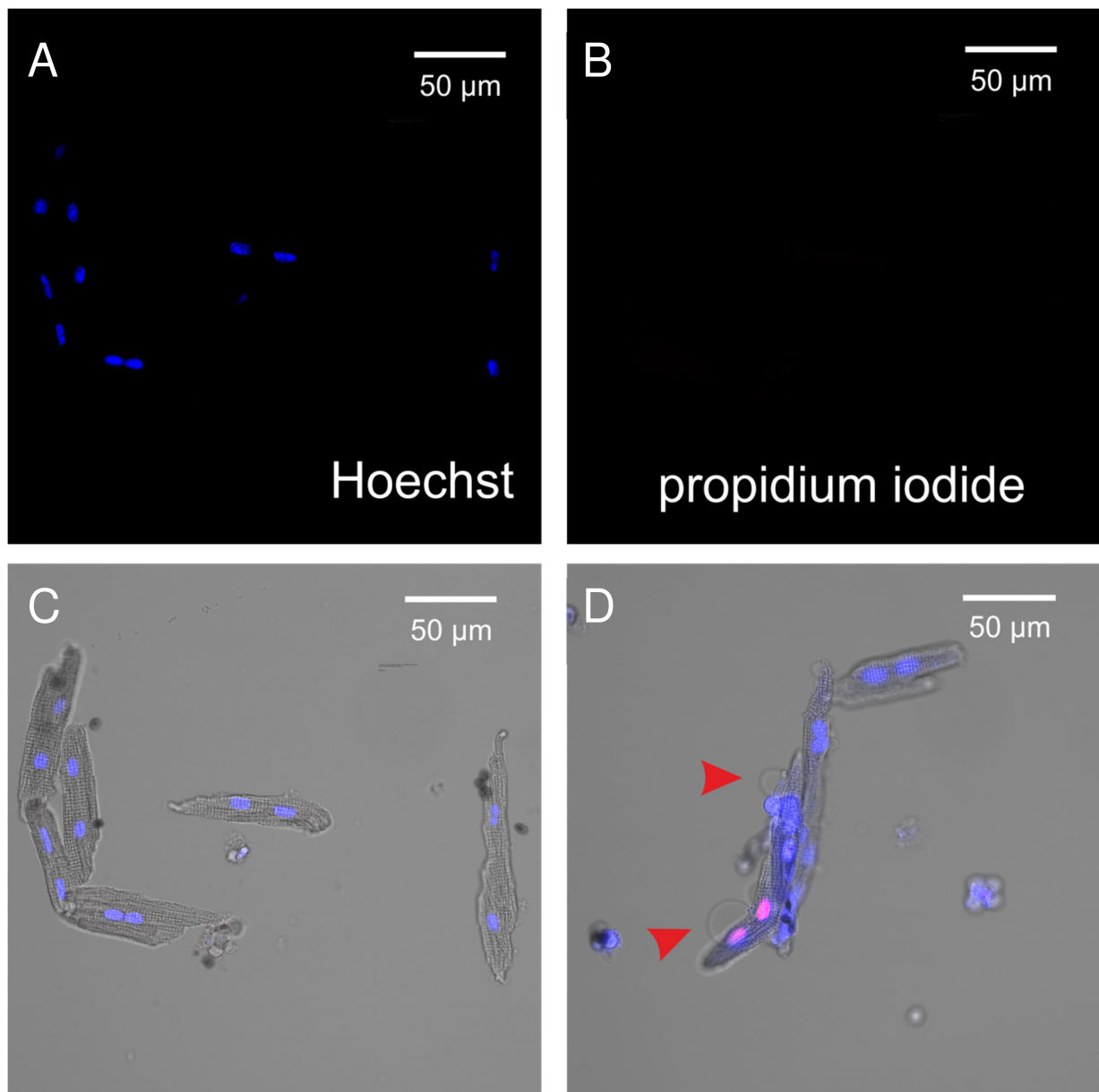


**Figure 4** Test for cell viability after isolation

Cells were treated with Hoechst 33342 (16  $\mu\text{M}$ ; **A**) and propidium iodide (1.5  $\mu\text{M}$ ; **B**). Hoechst is membrane permeable and will therefore label nuclei of all cells. Propidium iodide is membrane impermeable and will only label dead or damaged cells. **C** Overlay of A, B and transmission light. **D** Overlay of Hoechst, propidium iodide (**red**) and transmission light from another frame, showing a propidium iodide-positive cell. The **red arrow heads** indicate apoptotic blastula.

**Table 1** Medium for cardiomyocytes isolation (Yog-Mod)

<b>Chemicals in Yog-Mod</b>	<b>concentration</b>
NaCl (Carl Roth)	56 mM
KCl (Sigma Aldrich)	2.4 mM
KH <sub>2</sub> PO <sub>4</sub> (Riedel de Haën)	0.6 mM
Na <sub>2</sub> HPO <sub>4</sub> (Riedel de Haën)	0.6 mM
MgSO <sub>4</sub> (Sigma Aldrich)	3.2 mM
NaHCO <sub>3</sub> (Merck)	15 mM
Taurine (Sigma Aldrich)	5 mM
HEPES (Carl Roth)	10 mM
Glucose (Sigma Aldrich)	5.5 mM
Saccharose (Carl Roth)	120 mM
2,3-Butanedione monoxime (BDM) (Sigma Aldrich)	10 mM

**Table 2** Medium for cultivation of cardiomyocytes (ITS-Medium)

<b>Chemicals in ITS-Medium</b>	<b>concentration</b>
DMEM D7777 (Sigma Aldrich)	1x
Taurine (Sigma Aldrich)	2 mM
NaHCO <sub>3</sub> (Merck)	8 mM
Creatine (Sigma Aldrich)	1.85 mM
Blebbistatin (Sigma Aldrich)	25 µM
insulin transferrin selenium (ITS) supplement (100x; Gibco)	5x
Na <sup>+</sup> -lactate (Sigma Aldrich)	5 mM
Penicillin-Streptomycin (Sigma-Aldrich)	10 ml/l

**Table 3** Further materials used for cardiomyocytes cultivation

<b>Materials</b>
Lactate sensor <i>Laconic</i> (Vector Biolabs)
Pyruvate sensor (Gift from Felipe Barros)
Petri dish (Falcon 0160)
15 ml Tube (Orange Scientific)
ECM-Gel (Matrigel; Sigma Aldrich)

## 2.2 Imaging

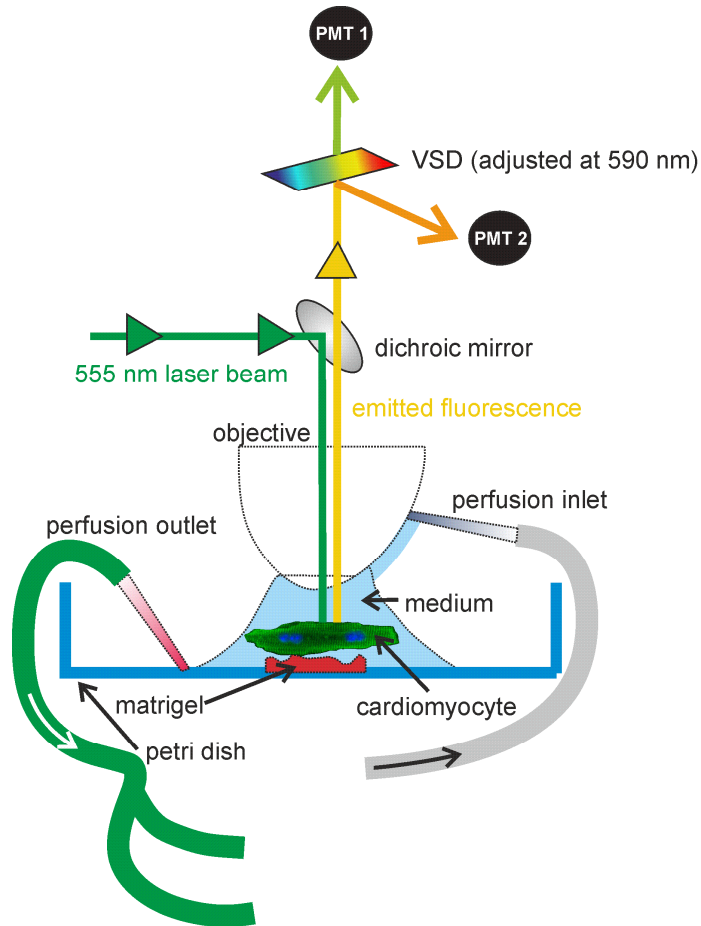


**Figure 5** Scheme of the imaging setup used at the LSM 700

Schematic setting, used for imaging experiments at the Zeiss LSM 700. The isolated cardiomyocytes were fixed to a petri dish with matrigel. The medium was pumped with a peristaltic pump to the objective where it ran to the lens. The medium was pumped out of the petri dish with the same pump, but the outlet was connected to two tubes so that it ran twice as fast as the inlet. SNARF was excited with a 555 nm laser. The emitted light was split into two spectra at 590 nm. The lactate sensor *Laconic* was excited with a 405 nm laser and the resulting emission spectrum was split at 508 nm according to Figure 11. VSD: variable secondary dichroic mirror. PMT: photon multiplier.

All imaging experiments were performed with a Zeiss LSM 700 confocal microscope. The petri dishes of the cell cultures were used as bath chamber. The bath was perfused with a peristaltic pump (Ismatec) at a speed of 2 ml/min. The solution was entering the bath by running down the objective. This was leading to an immediate application in the focus and abolished the

common imaging problem of air bubble trapping. With the same peristaltic pump, the solution was pumped back from the bottom of the petri dish. To keep the volume as small as possible and to avoid spill over, the solution outlet was connected to two tubes, connected to the pump, so that the outlet would be about twice as fast as the inlet (Figure 5). Thus, inlet and outlet speed were coupled to each other and imaging disturbances caused by the perfusion were reduced.

**Table 4** Dyes used for pH imaging

Dye	Solvent	Company	Concentration used
SNARF 5F (cytosolic pH sensor)	DMSO	Invitrogen (S 23923)	100 $\mu$ M
Fluorescein-DHPE (membrane bound pH sensor)	Ethanol or DMF	Invitrogen (F 362)	85 $\mu$ M

**Table 5** Inhibitors used in imaging experiments

Inhibitor	Solvent	Company	Concentration used
EZA (CA inhibitor, membrane permeable)	DMSO	Sigma Aldrich	30 $\mu$ M
AR C155858 (MCT1 inhibitor)	DMSO	AstraZeneca/Tocris	300 nM
S0859 (NBC inhibitor)	DMSO	Sanofi-Aventis	30 $\mu$ M
NaN <sub>3</sub> (respiratory chain complex IV inhibitor)	H <sub>2</sub> O	Fluka	5 mM
Cariporide/ HOE642 (NHE1 inhibitor)	DMSO	Santa Cruz Biotechnology	30 $\mu$ M

**Table 6** Recipe of HEPES-buffered imaging solution.

The pH was adjusted to 7.4 with NaOH. For CO<sub>2</sub>/HCO<sub>3</sub><sup>-</sup>-buffered imaging solution, 26 mM of NaCl were substituted with 26 mM NaHCO<sub>3</sub>. CO<sub>2</sub>/HCO<sub>3</sub><sup>-</sup>-buffered was contentiously gassed with carbogen (95% O<sub>2</sub> / 5% CO<sub>2</sub>).

<b>Chemical</b>	<b>Concentration</b>
NaCl (Carl Roth)	130 mM
KCl (Sigma Aldrich)	1 mM
KH <sub>2</sub> PO <sub>4</sub> (Riedel de Haën)	1.2 mM
MgSO <sub>4</sub> (Sigma Aldrich)	3.2 mM
Taurine (Sigma Aldrich)	5 mM
HEPES (Carl Roth)	5 mM
D-glucose (Sigma Aldrich)	5.5 mM
Saccharose (Carl Roth)	15 mM
BDM (Sigma Aldrich)	5 mM

## 2.2.1 H<sup>+</sup> imaging

### 2.2.1.1 H<sup>+</sup> imaging (SNARF)

SNARF- (SemiNAphthoRhodaFluor) 5F 5-(and -6)-carboxylic acid (Invitrogen) is a pH sensitive fluorescent dye. Its emission spectrum shows an isosbestic point at about 590 nm (Figure 6), which provides the possibility of ratio metric imaging.

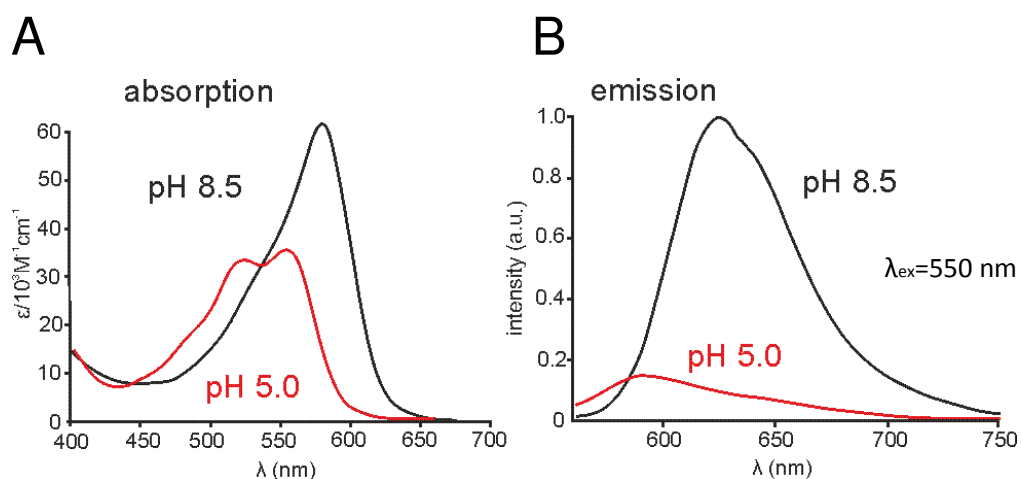
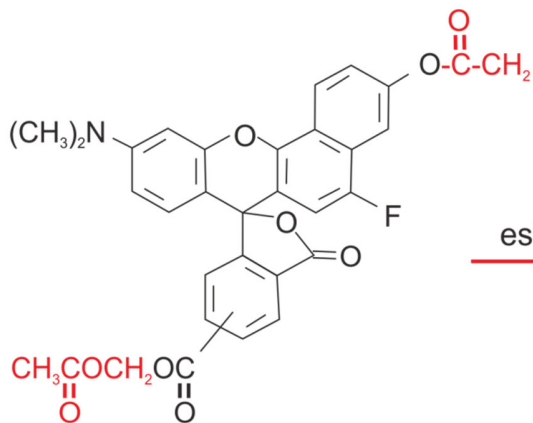


**Figure 6** Fluorescence properties of SNARF-5F

**A** The pH-dependent absorption is shown. **B** The pH-dependent emission when excited at 550 nm is shown. This figure was modified from Hille et al., 2008.

The emission spectrum fraction shorter than 590 nm is gaining intensity, whereas the emission spectrum fraction longer than 590 nm is losing intensity with increasing H<sup>+</sup> concentration. In this work, these two fractions of the emission spectrum were separated with a dichroic mirror (VSD) and recorded separately on two different PMTs (photon multiplier) (Figure 5).

## SNARF ester



## SNARF acid

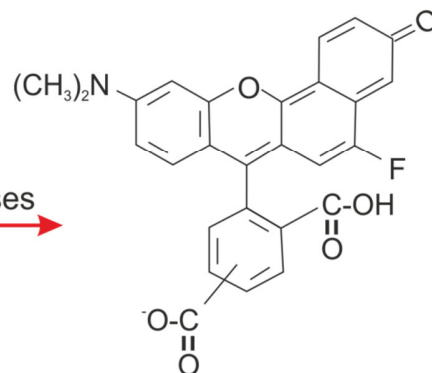


**Figure 7** Chemical structure of SNARF

The chemical structure of the membrane-permeable ester form and the membrane impermeable acid form of SNARF are shown (modified from Invitrogen). Cleaved parts are shown in **red**.

Finally, the signal  $<590$  nm was divided by the signal  $>590$  nm, which resulted in a signal ratio, therefore it is called ratiometric. Ratiometric imaging has the advantage over non-ratiometric imaging, that most artefacts due to multiple disturbances that may occur during a measurement, especially in perfused systems, will have the same impact on both emission fractions. Therefore they will be neutralized in the ratio. Also the incubation time of the dye or the exact concentration loaded do not alter the signal. In Figure 8 the effect of cytosolic  $H^+$  concentration changes in the SNARF emission fractions  $<590$  nm and  $>590$  nm are shown. With the program ImageJ and the plugin "ratioplus", a ratio signal from the  $<590$  nm and the  $>590$  signal was formed. Drifts that are present in the single fractions are almost absent from the ratio signal. To measure the  $H^+$  kinetics, the ratio signal was noise filtered with a low pass filter and a threshold of 0.012 Hz. From this noise filtered signal, the derivative with respect to the time was formed with the program clampfit (Axon Instruments).

The dye was applied as membrane permeable ester (acetoxymethyl ester: AM) to the cells. In the cytosol unspecific esterase did cleave the ester from the fluorescent molecule, leaving a carboxyl group that gave a charge to the dye (Figure 7). As a consequence, SNARF was trapped inside the cell. The cardiomyocytes were stained with imaging solution (Table 6) containing 50-100  $\mu M$  SNARF for 10-15 min at room temperature in the setup. Due to staining in the bath chamber, it was possible to take snapshots from time to time and thereby follow the



staining. For pH measurements, SNARF was excited with the 555 nm laser. The scanning frequency was 0.2 Hz.

For pH imaging experiments, liberated cardiomyocytes were produced as described under cardiomyocytes isolation and cultivation (p.24). Experiments to measure the lactate induced acidification were performed at the day of preparation within 2-3 h after the animal had been sacrificed.

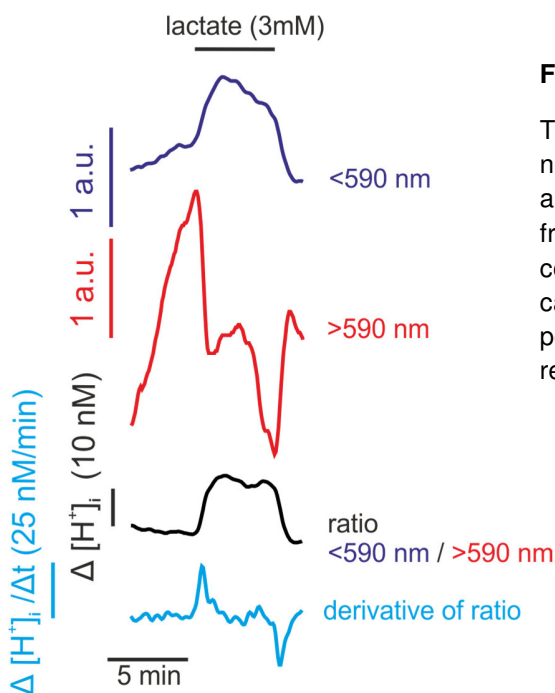


**Figure 8** SNARF recordings

The emission spectrum of SNARF-5F, excited at 555 nm, was split into a fraction shorter than 590 nm (**purple**) and longer than 590 nm (**red**). The signals of both fractions were used to form the ratio (**black**), which was converted to  $H^+$  concentrations according to the calibration (Figure 9). For the analysis of  $[H^+]_i$  changes per time, the derivative of the calibrated ratio signal with respect to the time was used (**blue**).

The solutions used for pH imaging experiments were based on the Yog-Mod solution from the cardiomyocyte isolation procedure since the cells remained viable in that environment. For the composition of HEPES-only-buffered solution see Table 6. For  $CO_2$ -buffered solution, 26 mM of NaCl of HEPES-only-buffered solution were substituted by 26 mM  $NaHCO_3$  and the solution was gassed with carbogen (95%  $O_2$  + 5%  $CO_2$ ). For lactate-,  $NH_4Cl$ - and high  $K^+$ -containing solutions, NaCl was substituted in the adequate amount. For 0  $Na^+$ -solution, NaCl was substituted by NMDG (N-Methyl-D-glucamin) and HCl. The pH of all solutions was, if not mentioned otherwise, adjusted to 7.4.

All **inhibitors** used were dissolved in DMSO (Table 5). All experiments were performed at room temperature.

### **2.2.1.2 Calibration (SNARF)**

To convert the ratiometric imaging data to pH or H<sup>+</sup> concentration values, the system had to be calibrated. This was done with the help of nigericin (Sigma-Aldrich), which is an antibiotic that incorporates into the cell membrane and shows an H<sup>+</sup>/K<sup>+</sup> exchanger property. The cell membrane is anyway permeable for K<sup>+</sup> due to Na<sup>+</sup>/K<sup>+</sup> ATPase and K<sup>+</sup> inward rectifier (Zobel et al., 2003) activity.

Therefore, K<sup>+</sup> entering or leaving the cell via nigericin together with a proton may just be replenished. This means that the intracellular H<sup>+</sup> concentration may adjust to the extracellular levels without any restriction. By measuring the SNARF ratios at defined extracellular pH (6.0, 6.5, 7.0, 7.5, and 8.0), calibration curves for H<sup>+</sup> and pH calibration were produced (see Figure 9).

The equation describing the fit was determined to be:  $Y = 44.851 X^{0.1368}$ . Y stands for the ratio values measured with SNARF, whereas x stands for the H<sup>+</sup> concentration. For the pH imaging experiments, only y is known. To know X, the formula had to be converted:  $X = (Y/44.851)^{(1/0.1368)}$ . Then, all SNARF ratio values were converted according to this equation to H<sup>+</sup> concentration values.

The medium used for the calibration was HEPES-only-buffered solutions as described above, containing 20 mM HEPES instead of 5 mM. NaCl was substituted with KCl (130 mM) to mimic intracellular K<sup>+</sup> levels. The pH was adjusted with NaOH.

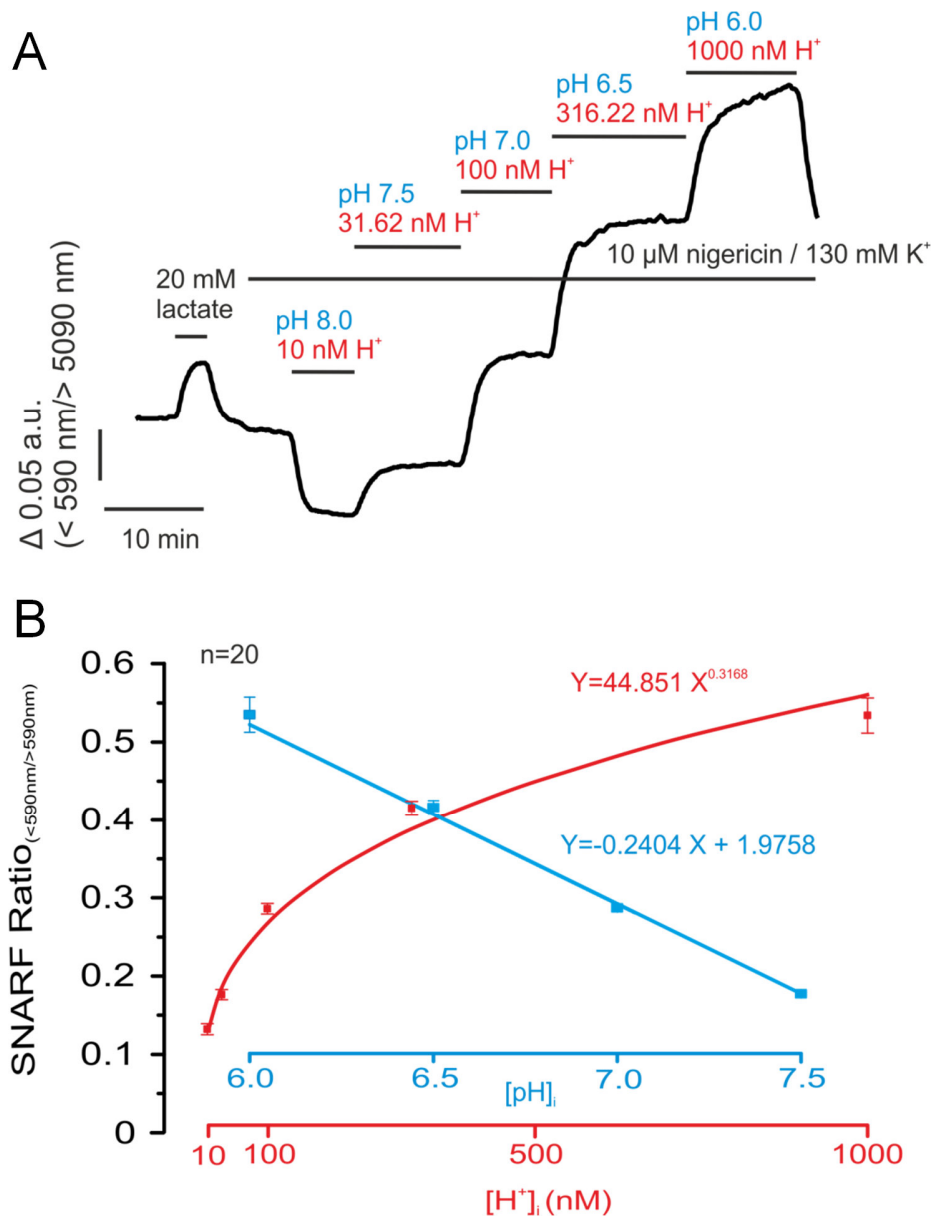


**Figure 9** Calibration of the SNARF-imaging setup

**A** Recording of the calibration procedure. **B** Calibration curves  $H^+$  and pH calibration. The exponential fit for  $H^+$  calibration can be described by the following equation:  $Y = 44.851 X^{0.3168}$ . The linear fit for pH calibration is described by the following equation:  $Y = -0.2404 X + 1.9758$ . Errors are shown as standard error.

### 2.2.1.3 Determination of H<sup>+</sup> buffer capacity and acid/base flux

The cytosolic H<sup>+</sup> buffer capacity was determined by the use of butyric acid. In an aqueous environment, the acid will be in an equilibrium of its acid [HBut] and base equivalent [But<sup>-</sup>]. This equilibrium is described by the Henderson-Hasselbach- Equation:

$$(1) \text{pH} = \text{pK}_s + \log ([\text{But}^-]/ [\text{HBut}])$$

As butyric acid is membrane permeable (Walter and Gutknecht, 1984) it can enter the cell independent of membrane transporters. Because the bath chamber is continuously perfused, its volume can be considered as infinite. Therefore, [HBut]<sub>i</sub> is assumed to be equal to [HBut]<sub>o</sub>. Based on this assumption and the Henderson-Hasselbach-Equation, the cellular H<sup>+</sup> buffering capacity was determined. The pK<sub>s</sub> value for butyric acid is known to be 4.82 (German Wikipedia, 14.10.2013) and the extracellular pH was set to a known value (pH 7.4). As a defined concentration of sodium butyrate [NaBut] was used (1 mM), the concentration of undissociated acid in medium and cytosol, was calculated with the Henderson-Hasselbach-Equation:

$$(2) 7.4 = 4.82 + \log (([\text{NaBut}] - [\text{HBut}])/ [\text{HBut}])$$

$$(3) 7.4 = 4.82 + \log ((1 \text{ mM} - [\text{HBut}])/ [\text{HBut}])$$

$$(4) [\text{HBut}] = 0.00262337 \text{ mM}$$

With H<sup>+</sup> imaging, the minimal cytosolic pH during extracellular application of HBut (0.00262337 mM) was determined. By the use of the Henderson-Hasselbach-Equation [But<sup>-</sup>] was determined for the minimal pH (for example, the minimal pH reaches 7.3):

$$(5) 7.3 = 4.82 + \log ([\text{But}^-]/ 0.00262337 \text{ mM})$$

$$(6) 10^{7.3-4.82} = [\text{But}^-]/ 0.00262337 \text{ mM}$$

$$(7) 0.79 \text{ mM} = [\text{But}^-]$$

This means that the extracellular application of sodium butyrate (1 mM) resulted in a cytosolic But<sup>-</sup> concentration of 0.79 mM at the maximal acidification. In addition, the cytosolic H<sup>+</sup> load or pH change was measured to be 5.82 nM or Δ pH 0.0535 (at a basal [H<sup>+</sup>]<sub>i</sub> of 44.4 nM). Since

each But<sup>-</sup> formation must go along with one H<sup>+</sup> release, the cytosolic H<sup>+</sup> content was increased by 0.79 mM. The ratio of the cytosolic H<sup>+</sup> load (here 0.79 mM) and the change of free cytosolic H<sup>+</sup> (here 5.82 nM) is the so called buffer ratio ( $\rho$ ):

$$(8) \rho = \Delta [\text{But}^-]_i / \Delta [\text{H}^+]_i$$

$$\rho = 135,738.83$$

The ratio of the cytosolic H<sup>+</sup> load and  $\Delta$  pH is the so called buffer capacity ( $\beta$ ):

$$(9) \beta = \Delta [\text{But}^-]_i / \Delta [\text{pH}]_i$$

$$\beta = 14.77 \text{ mM}$$

If the cytosolic ability of H<sup>+</sup> buffering is known, the acid/base flux ( $J_{A/B}$ ) can be calculated. To do this, the measured kinetics of cytosolic H<sup>+</sup> concentration or pH changes were multiplied with  $\rho$  or  $\beta$ , respectively.  $\rho$  was found to depend on  $[\text{H}^+]_i$  in an exponential manner. Therefore, an additional possibility to determine  $J_{A/B}$  is the use of the fit describing the relation of  $\rho$  and  $[\text{H}^+]_i$ . To do so, the SNARF measurement was calibrated in H<sup>+</sup> and noise filtered. Then, its first derivative with respect to the time was formed with clampfit (Figure 8). Next, the H<sup>+</sup> calibrated recording was converted to a buffer ratio recording with the fit describing the relation of  $\rho$  and  $[\text{H}^+]_i$  and was named “adaptive buffer ratio”. Then, the derivative was multiplied with the adaptive buffer ratio. The resulting trace is  $J_{A/B}$  per time. The maximal fluxes per application were analysed.

### **2.2.1.2 H<sup>+</sup> imaging (Fluorescein-DHPE)**

Fluorescein-DHPE (N-(fluorescein-5-thiocarbamoyl)-1,2-dihexadecanoyl-sn-glycero-3-phosphoethanolamine; Invitrogen) is a pH sensitive fluorescent dye that contains a lipophilic part that incorporates into cell membranes (Figure 10).

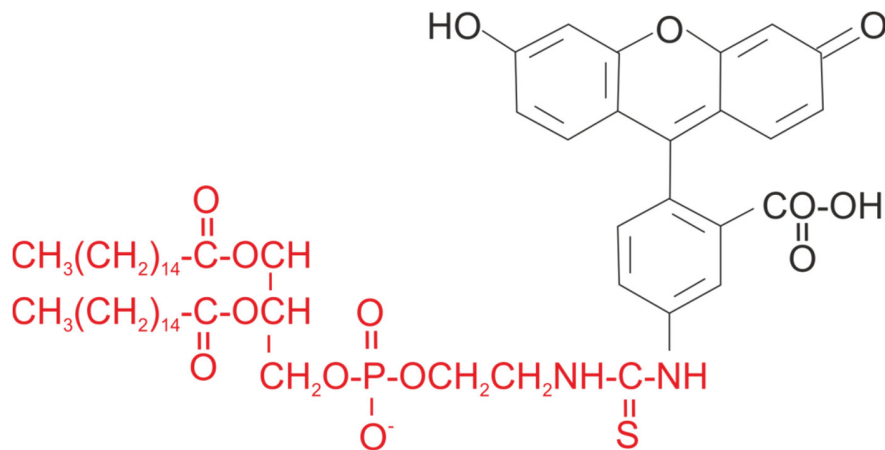


**Figure 10** Chemical structure of Fluorescein DHPE (modified from Invitrogen)

The fluorescein is shown in **black**. The 1,2-dihexadecanoyl-sn-glycero-3-phosphoethanolamine (DHPE) is shown in **red**.

The measurements were performed with the LSM 700. The dye was excited with the 405 nm and the 488 nm laser, which allowed ratiometric imaging or with the 488 nm laser alone. Application of the 405 nm laser was problematic, since the used contraction inhibitor blebbistatin shows fluorescence when it is excited with the 405 nm laser. Since blebbistatin showed a different bleaching behaviour than Fluorescein-DHPE, ratio metric measurements did tend to have a strong drifting. Before cells were loaded with the dye, blebbistatin had to be bleached until no further bleaching was observed. Since bleaching may be phototoxic to the cells, this procedure is far from being ideal. An additional problem in ratio metric imaging with Fluorescein-DHPE was the scanning nature of the microscope. The picture will be generated by scanning the sample line by line. This is time consuming and therefore limited the maximal scanning rate at the used settings to about 1-2 Hz. For ratiometric imaging it is necessary to scan each picture twice; once at 405 nm and once at 488 nm excitation. Due to the time needed for scanning, the second picture will be delayed and therefore it does not fit exactly. As consequence, the noise may become very intense and could even, in extreme cases, completely cover the pH signals.

Even though problematic, the advantages of ratiometric imaging are explained in H<sup>+</sup> imaging - SNARF (p.35). But the experience gained during this work suggest that Fluorescein-DHPE can

be used for ratio metric imaging in the LSM 700, but might perform better in a non-scanning system.

Calibration for Fluorescein-DHPE measurements was performed by application of HEPES-only-buffered solutions (Table 6), containing 50 mM HEPES instead of 5 mM, that had been adjusted to a defined pH. The strong buffering should force the cell surface pH to the defined pH of the applied solution.

## **2.2.2 Lactate imaging**

### **2.2.2.1 Transduction**

For lactate imaging, cardiomyocytes were prepared as described under “cardiomyocyte isolation and cultivation” (p.24) until step 22. Per batch, 6 petri dishes were settled with cardiomyocytes. After cell settlement, the 50 µl drop was removed from the petri dish to avoid a waste of virus on unattached cells. Next, 5 µl of an adenovirus-stock ( $4.8 \times 10^{10}$  PFU; Vector Biolabs), containing the FRET-based lactate sensor *Laconic* (Lactate optical nano indicator from CECs; San Martin et al., 2013), were mixed with 95 µl of ITS-medium. The lactate sensor is based on LldR, a transcription regulating protein from *Escherichia Coli* that performs a conformation change upon lactate binding (Aguilera et al., 2008). San Martin et al. (2013) took advantage from this feature and combined it with the fluorescent proteins mTFP and Venus. Those Fluorescent proteins change their distance when the LldR binds lactate, which results in an altered FRET-signal.

According to Du et al. (2004), murine and human cardiomyocytes transduce best with serotype 1 adenovirus, but the here used serotype 5 did also work. On 4 petri dishes 25 µl of virus-containing ITS-medium were added each. The remaining 2 petri dishes were covered with 25 µl ITS-medium each as control. After 2 h incubation at 37°C/ 5% CO<sub>2</sub>, the petri dishes were filled up with 2 ml ITS-medium each. After 2 days of cultivation, the medium was exchanged with fresh ITS medium, lacking blebbistatin. This was necessary because blebbistatin produced some fluorescence (also described by Lucas-Lopez et al., 2005) when excited with the 405 nm Laser. Interestingly, at this stage of cultivation, the absence of a contraction inhibitor did not seem to affect the cell viability or shape.

### 2.2.2.2 Lactate imaging

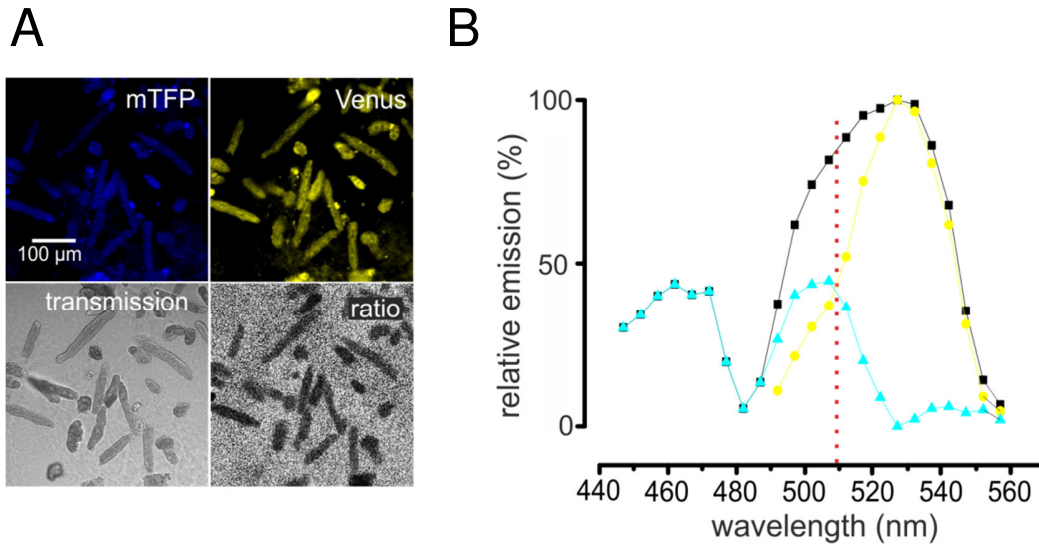


**Figure 11** Expression of *Laconic* in mouse cardiomyocytes

**A** Isolated cardiomyocytes 3 d after transduction. **B** Fluorescence properties of *Laconic*, as determined with the  $\lambda$ -stack function of the LSM 700. The total emission spectrum of *Laconic* when excited with 405 nm is shown in **black**. The emission spectrum of *Laconic* when only the *Venus* is excited with 488 nm is shown in **yellow**. The emission spectrum of mTFP when excited with 405 nm is shown in **cyan**. The dotted line indicates the used splitting point of CFP and YFP signal at 508 nm.

Transduced cardiomyocytes were used 3-4 d after transduction. The imaging experiments were performed with a ZEISS LSM 700 confocal microscope. For setup details see Figure 5. To induce FRET in the lactate sensor *Laconic*, the mTFP (CFP variant; see Ai et al., 2006) was excited with a 405 nm laser. To determine the optimal splitting point of the emission spectrum in mTFP and *Venus* (YFP variant) dominated fractions, the total emission spectrum of *Laconic*, when excited with 405 nm and the *Venus* spectrum alone, when excited with 488 nm were recorded (Figure 11).



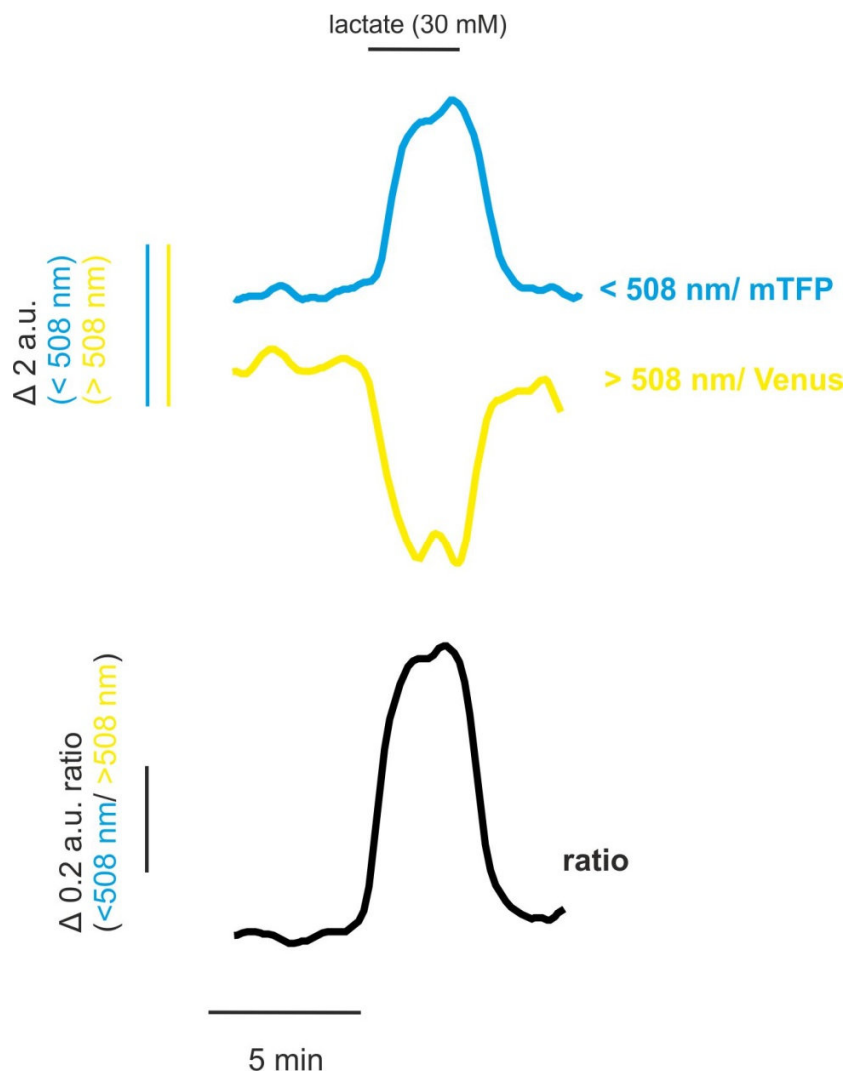


**Figure 12** Example recording of lactate imaging in cardiomyocytes with *Laconic*

The ratio is shown in black whereas the mTFP fraction is shown in cyan and the Venus fraction is shown in yellow.

Accordingly, the *Laconic* emission spectrum was split at 508 nm. The resulting mTFP and Venus signals could be used for ratio metric imaging, due to their contrary behaviour on lactate concentration changes. Since lactate binding will increase the distance of mTFP and Venus, a rise in cytosolic lactate concentration will increase the mTFP signal but decrease the Venus signal (Figure 12).

The same solutions as described for SNARF measurements were used (Table 6).

### 2.2.3 Pyruvate imaging

The cardiomyocytes were isolated and transduced as described for the lactate sensor. The pyruvate sensor is described by San Martin et al. (2014). Similar as for the lactate sensor *Laconic*, a transcription regulating protein was used. PdhR, a pyruvate binding protein, from *Escherichia Coli* was combined with mTFP and Venus and called *Pyronic* (pyruvate optical nano indicator from CECs). The used imaging setup and settings were the same as for lactate imaging.

For pyruvate-containing solutions, NaCl was substituted by NaPyruvate in imaging solution.

### 2.2.4 Statistical analysis

The calibrated SNARF recordings were analysed with the program clampfit (Axon Instruments). Marco Alt found its suitability for analysis of imaging data (Stridh et al., 2012). To determine the H<sup>+</sup> or pH kinetics, derivatives with respect to the time of the calibrated recordings were produced with clampfit. Because the noise was faster than the signals, the noise was reduced with a noise filter at a threshold of 0.012 Hz in clampfit, before the derivatives were calculated. The resulting trace showed  $\Delta[\text{H}^+]/\Delta t$  or  $\Delta[\text{pH}]/\Delta t$ , depending on the calibration. The *Laconic* and *Pyronic* recordings were treated in the same way. The maximal kinetic during an application was measured. Significance was tested with paired or unpaired students't tests ( $P \leq 0.05$  \*,  $P \leq 0.01$  \*\*,  $P \leq 0.001$  \*\*\*).

## 2.3 Western blot

### 1. Lysate preparation

Tissue samples were transferred to 1.5 ml centrifugation tubes and covered with 4% SDS (sodium dodecyl sulfate; MP Biomedicals), containing protease inhibitor (Roche product number 11836170001). Then, lysate was produced by ultrasonic treatment (30s). To remove particles and jellylike remnants, samples were centrifuged at 14,000 x g for 5 min and only the supernatant was kept for experiments. Cell culture samples were collected in 4% SDS containing protease inhibitor and transferred to 1.5 ml to centrifugation tubes. Jellylike remnants were dissolved by scratching the tube several times across the rack for 1.5 ml tubes. For cardiomyocyte samples, liberated

cardiomyocytes were centrifuged for 5 min at 14,000 X g, the supernatant was removed and the pellet was covered with 4% SDS, containing protease inhibitor. Finally the tube was vortex treated to dissolve the pellet. Lysates from MCT1 or MCT2 expressing *Xenopus laevis* oocytes were provided by Michael Klier and Christina Schüler, respectively.

## 2. Determination of protein concentration

The protein concentration of the samples was determined with the bicinchoninic acid (BCA) -test (Pierce® BCA Protein Assay Kit Thermo scientific 23225) and an ELISA reader.

## 3. Gel electrophoresis

For gel electrophoresis, samples were prepared in the following manner: Total volume<sub>(sample electrophoresis)</sub> = volume tissue sample<sub>(20 µg protein; 65% of total volume)</sub> + volume sample buffer (Invitrogen NP0007)<sub>(25% of total volume)</sub> + volume reducing agent (Invitrogen NP0004)<sub>(10% of total volume)</sub>. Accordingly, the total volume<sub>(sample electrophoresis)</sub> was calculated as follows: Volume tissue sample<sub>(20 µg protein; 65% of total volume)</sub> / 0.65. Ready-to-use polyacrylamide gels from Invitrogen or Expedeon were used. As protein size indicator, 10 µl of the Novex® Sharp Protein Standard (Invitrogen LC5800) was added per gel. For the electrophoresis, the device provided by Invitrogen (XCell SureLock™ Mini-Cell EI0001) was used. The outer chamber was filled with 600 ml 1x MOPS buffer (Invitrogen NP0001), whereas the inner chamber was filled with 200 ml 1 x MOPS buffer (Invitrogen NP0001), containing 500 µl NuPage antioxidant (Invitrogen NP0005). The gel was started with 100 V and a security threshold of 60 mA for 10 min and then continued for 50 min with 200 V and a security threshold of 120 mA.

## 4. Western blot

The western blot was performed with the device from Invitrogen (XCell SureLock™ Mini-Cell + XCell II™ Blot Module). As blotting solution, 300 ml NuPAGE® Transfer Buffer (Invitrogen LC2000), containing 30 ml methanol and 300 µl NuPage antioxidant (Invitrogen NP0005), was used. Sponge pads and nitrocellulose membranes (Invitrogen

LC2006) were incubated for approximately 30 min in blotting solution before they were used. When membrane, gel and sponge pads had been transferred to the blotting chamber, the latter one was incorporated into the XCell *SureLock*<sup>TM</sup> Mini-Cell (Invitrogen) and filled with blotting solution. The outer chamber was filled with distilled water for cooling. The blotting was performed at 60 V for 100 min.

#### 5. Protein detection

The protein detection was performed with HRP (horse radish peroxidase)-labelled secondary antibodies and luminol based luminescence. First, the membrane was briefly incubated in Ponceau staining (Sigma Aldrich), which gives a red staining to any kind of protein, to check if the blotting had worked properly. Second, the membrane was incubated for 1 h in blocking solution (Table 8) at room temperature. Then, primary antibody was added to the blocking solution. For antibody details see Table 9. The primary antibody was incubated for 2 h at room temperature. Then, the blocking solution was removed and the membrane was washed for 30 min in distilled water. The secondary, HRP-labelled antibody was applied to the membrane, diluted in blocking solution and incubated for 1 h at room temperature. To finish, the secondary antibody was removed and the membrane was washed for 30 min in distilled water.

#### 6. HRP signal recording

The luminescence was induced by application of 500 µl LumiGlo (Cell Signalling #7003) to the blot. The signal was recorded with a Biorad imager.

**Table 7** Recipe of TBST

The pH was set to 7.5 with NaOH

Chemical	Concentration
Tris-HCl (Carl Roth)	50 mM
NaCl (Carl Roth)	150 mM
Tween20 (Sigma Aldrich)	1%

**Table 8** Recipe of western blot blocking solution

Chemical	Concentration
TBST	1x
BSA (Sigma Aldrich)	1% (w/v)
Casein (Sigma Aldrich)	0.5% (w/v)

**Table 9** Antibodies used for western blot

Primary antibody	Concentration/ dilution used	Secondary antibody	Dilution used
CAII (Millipore AB1828)	50 µg/ml	anti-rabbit (Santa Cruz sc-2004)	1:1000
CAIII (Santa Cruz sc-50715)	4 µg/ml	anti-goat (Santa Cruz sc-2020)	1:1000
CAIV (R&D AF2414)	0.8 µg/ml	anti-goat (Santa Cruz sc-2020)	1:1000
CAXIV (Santa Cruz sc-25602)	50 µg/ml	anti-rabbit (Santa Cruz sc-2004)	1:1000
MCT1 (Millipore AB3538P)	2 µg/ml	anti-chicken (Santa Cruz sc-2428)	1:1000
MCT2 (Millipore AB3542P)	1:500	anti-rabbit (Santa Cruz sc-2004)	1:1000
NBCe1 (Abcam ab78326)	1:500	anti-rabbit (Santa Cruz sc-2004)	1:1000

## 2.4 Immunohistochemistry

Tissue sections (10  $\mu\text{m}$ ) were produced with a cryostat at  $-20^{\circ}\text{C}$ . The sections were mounted on coated glass slides (Superfrost ultra plus; Thermo scientific) and fixed with acetone for 5 min in humid chamber at room temperature. Isolated cardiomyocytes (for procedure see p.24), settled on matrigel coated petri dishes could not be fixed with acetone, since the used petri dishes were made of plastic sensitive towards acetone. Isolated cardiomyocytes were therefore fixed for 5 min at room temperature with the fixing agent *Histofix* (Roth). After fixation, the samples were briefly washed in PBS (phosphate-buffered saline: 130 mM NaCl, 7 mM  $\text{Na}_2\text{HPO}_4$ , 3 mM  $\text{NaH}_2\text{PO}_4$ , pH 7.4) to remove fixing agent remnants. Next, the samples were incubated in blocking solution (Table 10) for 1h at room temperature. After blocking, primary antibody was added to the blocking solution and incubated for 2 h in a humid chamber at room temperature (for detail information see Table 11). Then the antibody solution was removed and the samples were washed for 30 min at room temperature. Secondary antibody, carrying a fluorescent molecule (Alexa Fluor 488 or Alexa Fluor 546) was applied to the samples, diluted 1:1000 in blocking solution, together with the fluorescent DNA staining agent Hoechst 33342 (16  $\mu\text{M}$ ; Life technologies). Finally, the samples were washed for 30 min in PBS. Pictures were taken the same day with the Zeiss LSM 700 confocal microscope.

**Table 10** Recipe of blocking solution for immunohistochemistry.

If a secondary antibody directed against goat was used, goat serum was replaced by donkey serum. The solution was adjusted to pH 7.4

Chemical	Concentration
NaCl (Carl Roth)	130 mM
$\text{Na}_2\text{HPO}_4$ (Riedel de Haën)	7 mM
$\text{NaH}_2\text{PO}_4$ (Riedel de Haën)	3 mM
BSA (Sigma Aldrich)	3% (w/v)
TritonX100	5‰
Goat serum (or donkey serum) (Sigma Aldrich)	1% (v/v)

**Table 11** Antibodies used for immunohistochemistry.

Secondary antibodies were all bought at Invitrogen.

Primary antibody	Concentration used	Secondary antibody	dilution used
CAII (Millipore AB1828)	50 µg/ml	anti-rabbit (A-11008)	1:1000
CAIII (Santa Cruz sc-50715)	4 µg/ml	anti-goat (A-11055)	1:1000
CAIV (R&D AF2414)	0.8 µg/ml	anti-goat (A-11055)	1:1000
CAIX (Novus biologicals NB100-417)	8 µg/ml	anti-rabbit (A-10040 and A-11010)	1:1000
CAXIV (Santa Cruz sc-25602)	50 µg/ml	anti-rabbit (Santa Cruz sc-2004)	1:1000
MCT1 (Millipore AB3538P)	4 µg/ml	anti-chicken (A-11039)	1:1000
MCT4 (Millipore AB3314P)	4 µg/ml	anti-rabbit (A-11008)	1:1000
Slow myosin (Millipore MAB1628)	4 µg/ml	anti-mouse (A-10036)	1:1000

## 2.5 Genotyping of KO animals

### NBC KO

The animals were produced and described by Gawenis et al. (2007). Exon 9 is disrupted.

### CAII KO animals

The CAII KO animals used were produced and described by Lewis et al. (1988). The loss of CAII activity is based on a point mutation in codon 155 if counted from the start codon at position 110 in exon 1 of the gene car2. The codon CAA is changed to TAA, which is a stop codon (Pan et al., 2006).

### CAIV KO

The animals were produced and described by Shah et al. (2005). Exons 1b, 2 and 3 as well as parts of exon 4 were deleted.

## **CAIX KO**

The animals were described by Gut et al. (2002). The enzyme function was disrupted by insertion of a DNA sequence into exon 1.

## **CAXIV KO**

The animals were produced and described by Shah et al. (2005). Exon 4 was deleted.

### **1. DNA-Purification**

A. Tissue sample (ear) got digested in 500 µl Lysisbuffer (Table 13) at 55°C for 3 h

B. Enzymes were heat inactivated (20 min; 95°C)

C. Undissolved parts were removed by centrifugation (15 min 19000 x g)

D. Supernatant was mixed 1:1 with isopropanol and incubated for 20 min at RT

E. Centrifugation for 15 min at 19000 x g

F. supernatant was removed and 500 µl 70% EtOH was added to separate DNA from contaminants (like proteins)

G. Centrifugation (like E)

H. EtOH was removed and the tubes were dried at 78°C (10-20 min)

I. DNA was dissolved in 100 µl TE-buffer (Table 12)

### **2.1 PCR – CAII KO**

A. The protocol is a modified version of that one described by Sjöblom et al (2009).

WT- and KO-PCR master mix were prepared (per reaction: 10 µl Ready-Mix (Sigma); 1 µl 10 µM reverse primer ( CAII r); 1 µl 10 µM forward CAII (WT) respectively forward CAII (KO); 3 µl DNA-free H<sub>2</sub>O). For primer see Table 14 .

B. 5 µl DNA-sample (dissolved in TE-buffer) was added per reaction

C. PCR was performed in a thermo cycler (95°C for 60 s → 53°C for 30s 72°C for 30s; 35 cycles → 72°C for 10 min)



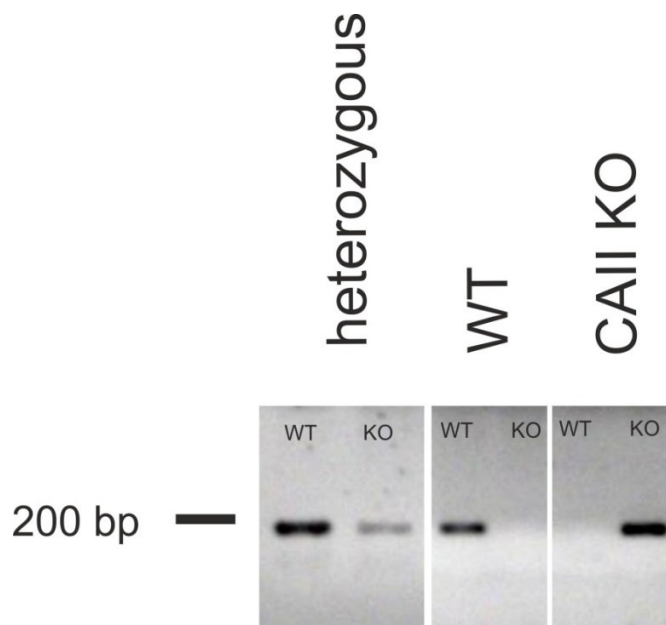


**Figure 13** Genotype determination of CAII <sup>+/-</sup>, CAII <sup>+/+</sup> and CAII <sup>-/-</sup> mice

The wild type (WT) and the knock out (KO) allele were tested in separate PCR reactions, so two PCRs had to be performed per animal.

## 2.2 PCR – CAIV (the genotyping was performed by Ivan Ruminot)

### 2.3 PCR – CAIX KO

- A. WT- and KO-PCR master mix were prepared (per reaction: 10 µl Ready-Mix (Sigma); 1 µl 10 µM reverse primer ( CAIX r); 1 µl 10 µM forward CAIX (WT) respectively forward CAIX (KO); 3 µl DNA-free H<sub>2</sub>O). For primer see Table 14.
- B. 5 µl DNA-sample (dissolved in TE-buffer) was added per reaction
- C. PCR was performed in a thermo cycler (94°C for 90s → 61°C for 60s → 56.5°C for 60s → 72°C for 30s; 35 cycles → 72°C for 10 min)

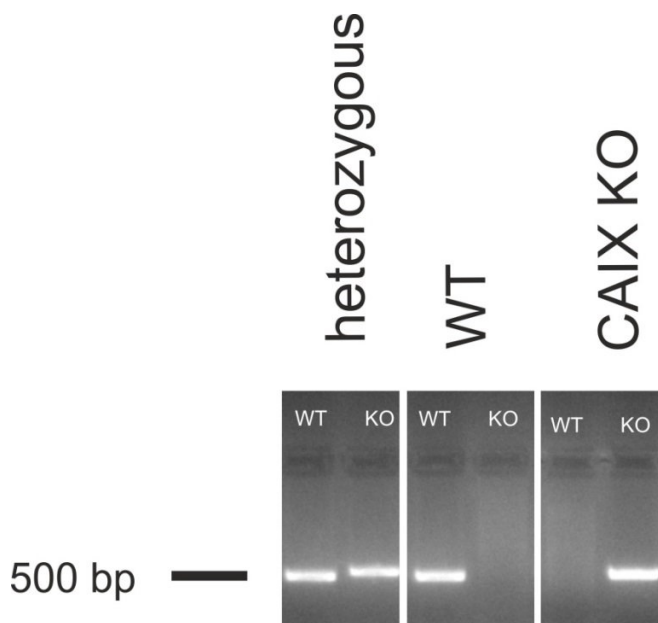


**Figure 14** Genotype determination of CAIX <sup>+/-</sup>, CAIX <sup>+/+</sup> and CAIX <sup>-/-</sup> mice

The wild type (WT) and the knock out (KO) allele were tested in separate PCR reactions, so two PCRs had to be performed per animal. Since the PCR product from the KO allele is bigger than that one from the wild type allele (WT 442 bp and KO 562 bp), the two PCR reactions might possibly be performed in the same tube, but this was not tested during this work.

## 2.4 PCR – CAIXIV

- A. WT- and KO-PCR master mix were prepared (per reaction: 10 µl Ready-Mix (Sigma); 1 µl 10 µM reverse primer; 1 µl 10 µM forward primer; 3 µl DNA-free H<sub>2</sub>O). For primer see Table 14.
- B. 5 µl DNA-sample (dissolved in TE-buffer) was added per reaction
- c. PCR was performed in a thermo cycler (92°C for 45 s → 70°C for 30s; 35 cycles → 72°C for 10 min)

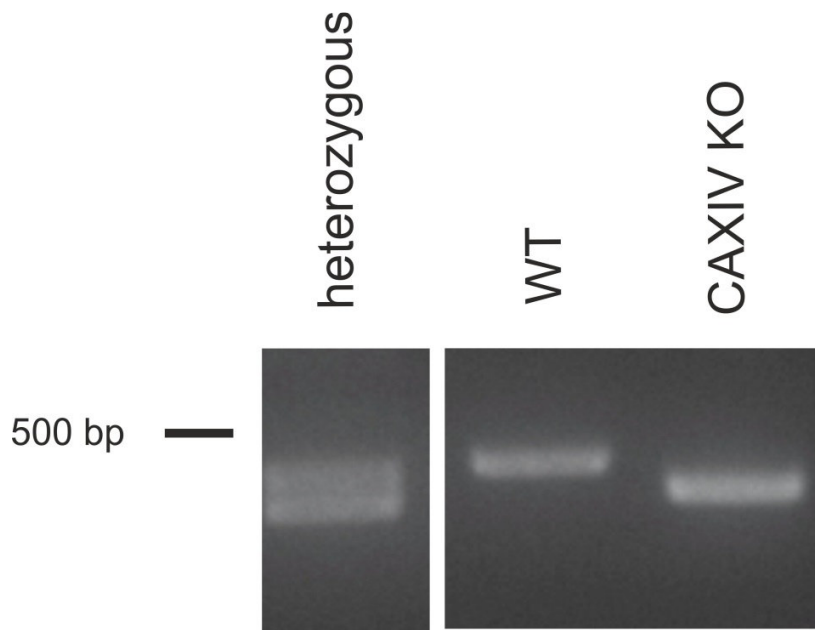


**Figure 15** Genotype determination of CAXIV <sup>+/-</sup>, CAXIV <sup>+/+</sup> and CAXIV <sup>-/-</sup> mice

The PCR products from the wild type (WT) and the knock out (KO) allele were differing in size (WT 420 bp and KO 400 bp) and therefore just one PCR was performed per animal.

## 2.5 PCR – NBC KO (the genotyping was performed by Ivan Ruminot)

### 3 Gel

The samples were loaded on a 2.5 – 3% agarose gel, containing 10µl Roti Safe Staining (Carl Roth) / 100 ml. The electrophoresis was performed at 100 mV for 15 – 20 min.

### 4 Picture

A pictures of the resulting gels were taken with an imager from *INTAS*.

**Table 12** TE-Buffer

The pH was adjusted to 7.5

Chemical	Concentration
Tris-HCl (Carl Roth)	10 mM
EDTA (Sigma Aldrich)	1 mM

**Table 13** Lysis buffer 1x MGB (Modified Gitschier Buffer)

Chemicals	Concentration
Tris (Carl Roth)	67 mM
(NH <sub>4</sub> ) <sub>2</sub> SO <sub>4</sub>	17.7 mM
MgCl <sub>2</sub>	6.5 mM
TritonX-100	5‰
Proteinase K (Carl Roth)	1 µg/µl

**Table 14** Further materials used for genotyping

Material
Isopropanol
70% Ethanol
Roti-Safe GelStain (Carl Roth)
Triton X
<u>Primer- NBC KO</u> Forward Primer 5'TCACAAACCTTTCAGCAAAGAGTGC3' Reverse Primer 5'CAAAGAGCAACAGTCAGACAGC3'
<u>Primer- CAII KO</u> Forward primer f CAII (WT): 5'GATTGGACCTGCCTCAC3' Forward primer f CAII (KO): 5'GATTGGACCTGCCTCAT3' Reverse Primer CAII : 5'TACCTCCGGTAAACTGTTTC3'
<u>Primer- CAIX KO</u> Forward primer (WT): 5'CTCCTATTTCCGATGCACGTACAG3' Forward primer (KO): 5'AGGAGCAAAGCTGCTATTGG3'

<p>Reverse primer: 5'CTTACCTGAGCCTAGATTTGGAAG3'</p>
<p><u>Primer- CAXIV KO</u> Forward primer: 5'AGGCTCCTGCAGCTAAGGTGGGATCAGACG3' Reverse primer: 5'TCCATCCTCTGAGCTCCACTGGACCGAACC3'</p>
<p><u>Primer- CAIV KO</u> <u>CA4K/OE25 5'</u> 5'CACCCTTCATCCTCGTCGGCTATGACCAAAG C3' <u>CA4/OIntron1A 5'</u> 5'TGAGGTCAATTCCCAGCTCCCACATTGTTGC3' <u>CA4K/OExon6 3'</u> 5'TGTGGATCTTGATGGGTTGTTTGTACACAGTCC3'</p>

# 3. RESULTS

## 3.1 Buffer capacity and buffer ratio in ventricular mouse cardiomyocytes

The buffer capacity ( $\beta$ ) and buffer ratio ( $\rho$ ) were determined by SNARF imaging (Figure 16). In HEPES-only,  $\text{CO}_2/\text{HCO}_3^-$  and  $\text{CO}_2/\text{HCO}_3^-$ -buffered solution plus EZA (30  $\mu\text{M}$ ). NaButyrate was applied to the cells at a concentration of 1 mM. The pH of the solutions was set to pH 7.4 and the concentration of butyric acid was calculated, as explained in the Materials & Methods part. The intracellular concentration of butyric acid was assumed be the same as outside. According to the Henderson-Hasselbach equation, the intracellular butyrate concentration at  $[\text{H}^+]_{i,\text{max}}$  was calculated.

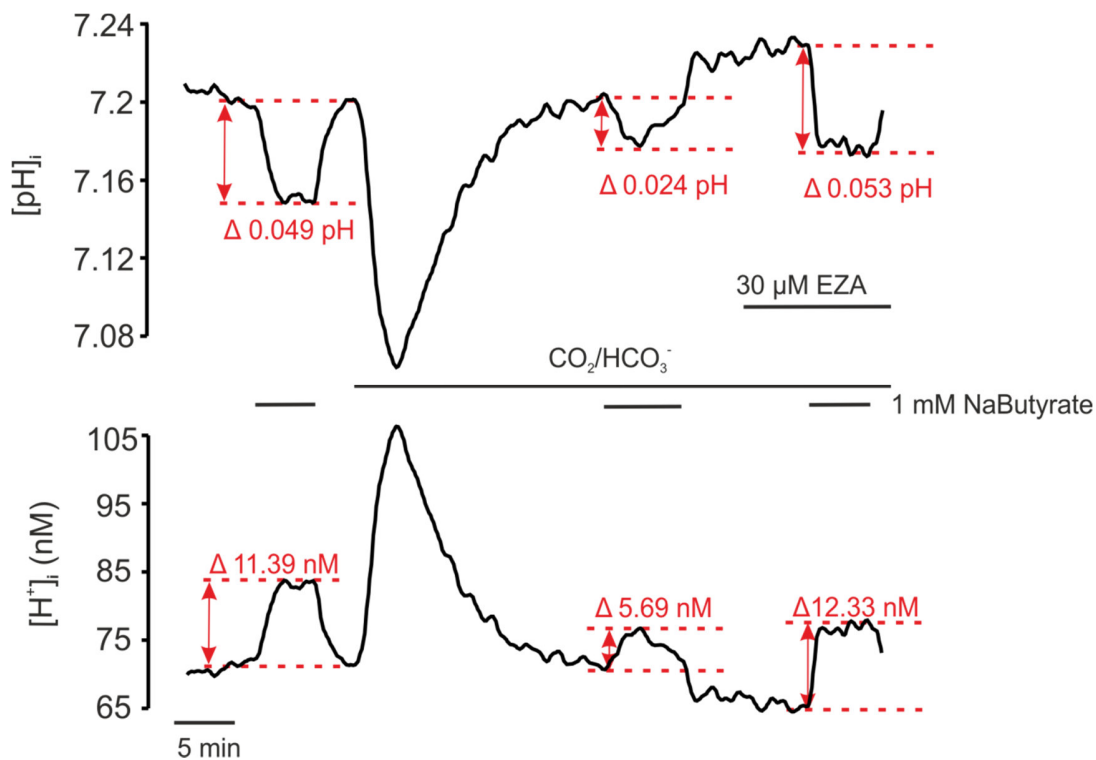


**Figure 16** Determination of  $\beta$  and  $\rho$  in mouse cardiomyocytes

The ability of mouse cardiomyocytes to buffer  $\text{H}^+$  was determined by pH imaging with SNARF. NaButyrate was applied to the cells at a concentration of 1 mM in HEPES-only,  $\text{CO}_2/\text{HCO}_3^-$  and  $\text{CO}_2/\text{HCO}_3^-$ -buffered solution plus 30  $\mu\text{M}$  EZA. The hereby caused intracellular changes in  $\text{H}^+$  concentration are shown in red. One particular example trace is shown.

The averaged values for  $\rho$  are named fixed buffer ratio ( $\rho_{\text{fixed}}$ ) to distinguish it from the adaptive buffer ratio ( $\rho_{\text{adap.}}$ ).  $\beta$  and  $\rho$  are shown in Figure 17 and Table 15.

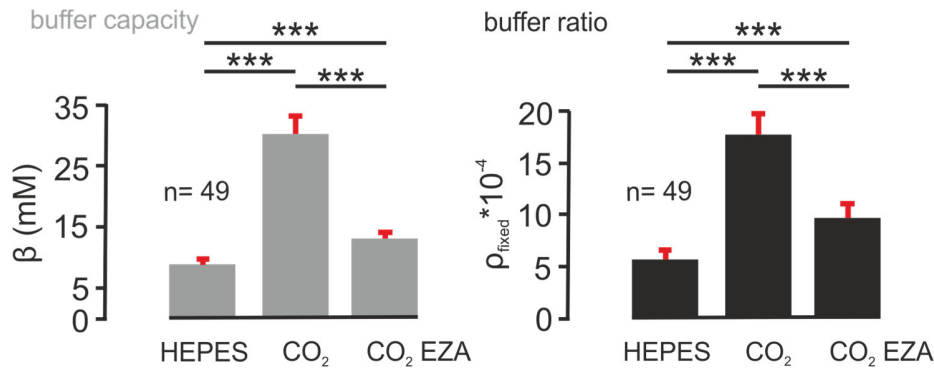


**Figure 17** Buffer capacity ( $\beta$ ) and fixed buffer ratio ( $\rho_{\text{fixed}}$ ) in mouse cardiomyocytes

The buffer capacity and fixed buffer ratios were determined for the HEPES-only-, CO<sub>2</sub>/HCO<sub>3</sub><sup>-</sup>- and CO<sub>2</sub>/HCO<sub>3</sub><sup>-</sup>-buffered + EZA (30  $\mu$ M) conditions. For the values see Table 15.

**Table 15** Buffer capacity ( $\beta$ ) and fixed buffer ratio ( $\rho_{\text{fixed}}$ ) in mouse cardiomyocytes

Buffering conditions	$\beta$ (mM)	$\rho_{\text{fixed}} \cdot 10^{-4}$
HEPES-only	8.8 $\pm$ 0.75	5.6 $\pm$ 0.89
CO <sub>2</sub> /HCO <sub>3</sub> <sup>-</sup>	30.2 $\pm$ 2.9	17.67 $\pm$ 1.98
CO <sub>2</sub> /HCO <sub>3</sub> <sup>-</sup> + EZA (30 $\mu$ M)	13.1 $\pm$ 0.88	9.6 $\pm$ 1.4

The individual buffer ratios and buffer capacities were plotted against the individual basal [H<sup>+</sup>]<sub>i</sub> and pH<sub>i</sub>, respectively (Figure 18). The dependence of the buffer ratio on [H<sup>+</sup>]<sub>i</sub> is described by an exponential fit, that increases when [H<sup>+</sup>]<sub>i</sub> drops. The correlation between pH<sub>i</sub> and buffer capacity is not obvious. Linear fits revealed a slight tendency for the buffer capacity to increase with the pH<sub>i</sub>. The equations of the fits, describing the correlation of [H<sup>+</sup>]<sub>i</sub> and  $\rho$  are  $\rho_{\text{adap. HEPES}} = [\text{H}^+]_i^{-1.5572} \cdot 4.43774 \cdot 10^7$ ,  $\rho_{\text{adap. CO}_2/\text{HCO}_3^-} = [\text{H}^+]_i^{-1.16741} \cdot 2.45908 \cdot 10^7$  and  $\rho_{\text{adap. CO}_2/\text{HCO}_3^- + \text{EZA}} = [\text{H}^+]_i^{-2.13811} \cdot 5.34228 \cdot 10^8$ .

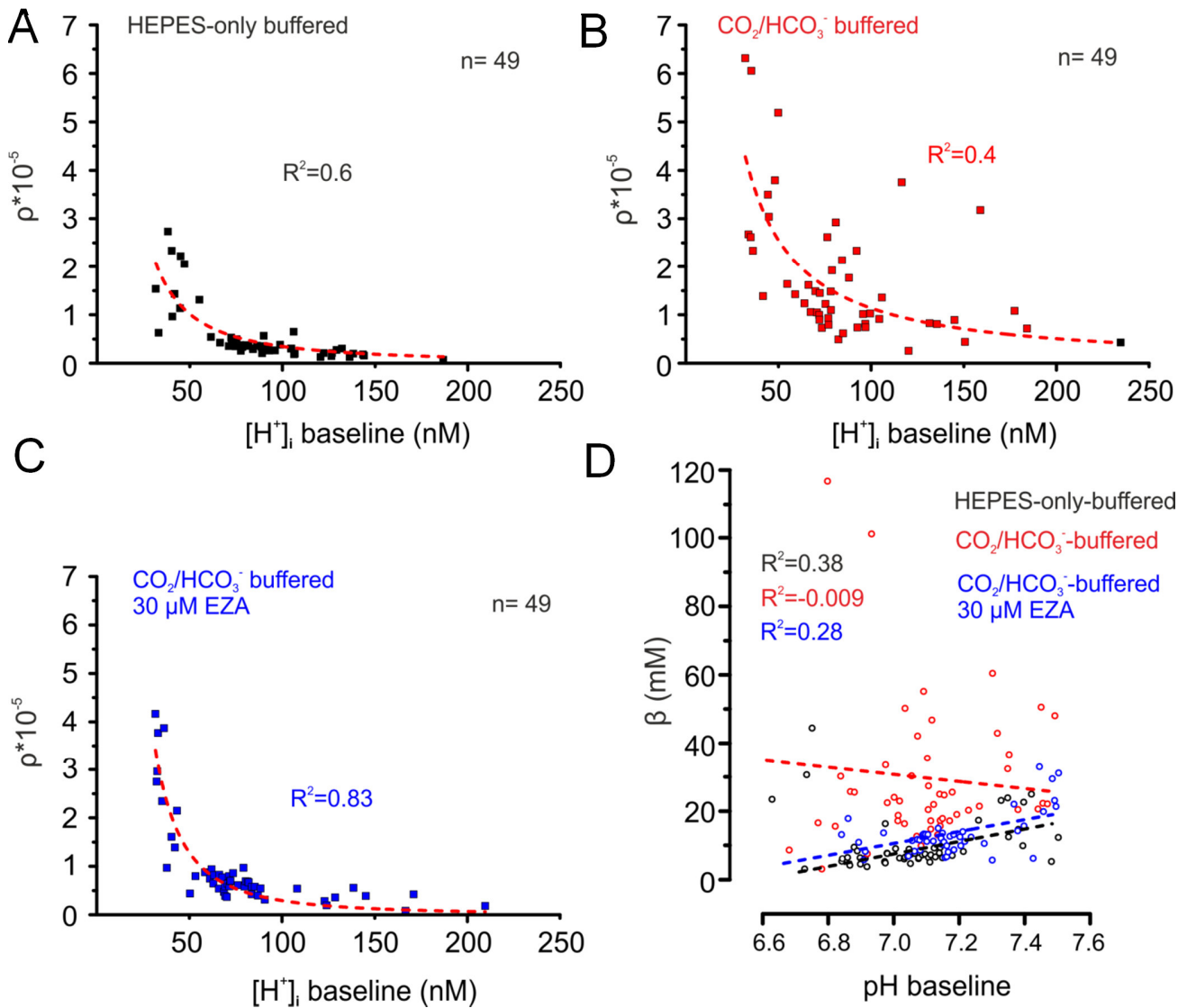


**Figure 18** Impact of basal pH on buffer ratio and buffer capacity

**A** Relation of basal cytosolic H<sup>+</sup> concentration and the buffer ratio in HEPES-only-buffered solution (fit: buffer ratio =  $[H^+]_i^{-1.5572} \cdot 4.43774 \cdot 10^7$ ). **B** Relation of basal cytosolic H<sup>+</sup> concentration and the buffer ratio in CO<sub>2</sub>/HCO<sub>3</sub><sup>-</sup>-buffered solution (fit: buffer ratio =  $[H^+]_i^{-1.16741} \cdot 2.45908 \cdot 10^7$ ). **C** Relation of basal cytosolic H<sup>+</sup> concentration and the buffer ratio in CO<sub>2</sub>/HCO<sub>3</sub><sup>-</sup>-buffered solution in the presence of the CA inhibitor EZA (fit: buffer ratio =  $[H^+]_i^{-2.13811} \cdot 5.34228 \cdot 10^8$ ). **D** relation of basal cytosolic pH and the buffer capacity in **HEPES-only-buffered**, **CO<sub>2</sub>/HCO<sub>3</sub><sup>-</sup>-buffered** and **CO<sub>2</sub>/HCO<sub>3</sub><sup>-</sup>-buffered in the presence of EZA (30 μM)**. The values in A-C were fitted with an exponential, asymptotic fit in origin.



## 3.2 pH regulating proteins and lactate transporter present in mouse cardiomyocytes

### 3.2.1 Carbonic anhydrase in ventricular mouse cardiomyocytes

The enzymatic activity of cytosolic carbonic anhydrase (CA) was tested by application of CO<sub>2</sub>/HCO<sub>3</sub><sup>-</sup>-buffered solution in absence and presence of the CA inhibitor EZA. The scheme of CO<sub>2</sub>-dependent pH changes is shown in Figure 19 A including the potential role of cytosolic carbonic anhydrase. Although the conversion of H<sub>2</sub>O + CO<sub>2</sub> to H<sup>+</sup> + HCO<sub>3</sub><sup>-</sup> takes place spontaneously, cytosolic CA may speed up this process (Stridh et al. 2013). In ventricular mouse cardiomyocytes from WT animals, application of the CO<sub>2</sub>/HCO<sub>3</sub><sup>-</sup> caused a  $\Delta[H^+]_i/\Delta t$  of  $24.5 \pm 2.5$  nM/min in the absence and  $24.7 \pm 2.8$  nM/min in the presence of EZA (30  $\mu$ M) (Figure 19). The  $\Delta[H^+]_i/\Delta t$  during removal of extracellular CO<sub>2</sub>/HCO<sub>3</sub><sup>-</sup> was determined to be  $-24.9 \pm 2.8$  nM/min in WT and  $-38.7 \pm 6.7$  nM/min in CAII<sup>-/-</sup> animals. The unpaired student's *t*test revealed a *P* of 0.087, thus the difference was not significant. The  $\Delta[H^+]_i/\Delta t$  during reintroduction of extracellular CO<sub>2</sub>/HCO<sub>3</sub><sup>-</sup> was determined to be  $28.1 \pm 3.5$  nM/min in WT and  $44.5 \pm 3.8$  nM/min in CAII<sup>-/-</sup> animals (Figure 20). The unpaired student's *t*test revealed a *P* of 0.19, thus the difference was not significant.

Immunohistochemical approaches to determine CAII's presence in mouse cardiomyocytes resulted in clear and defined fluorescence signals but the same kind of signals were observed in CAII knockout animals (Figure 21).

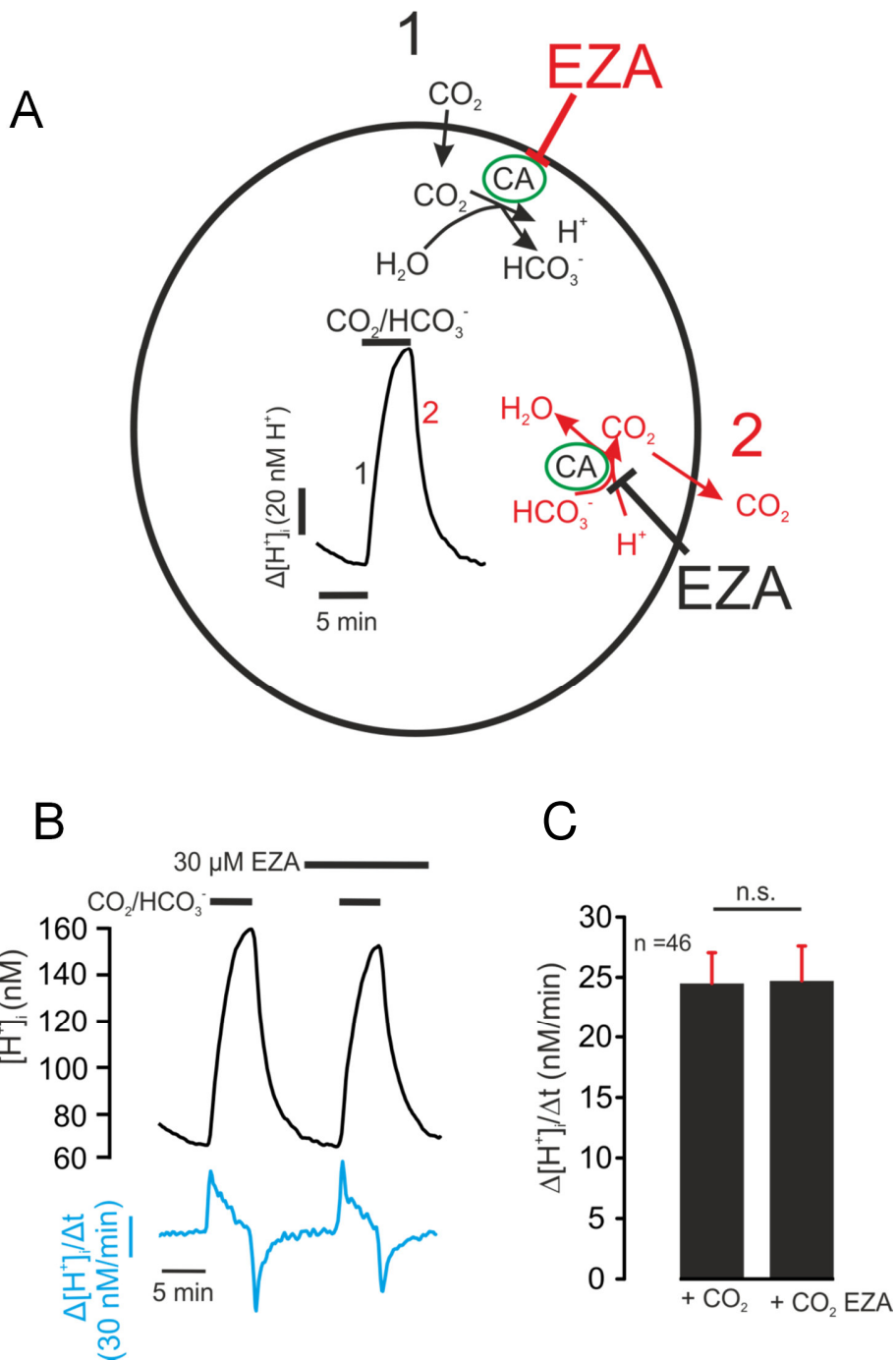


**Figure 19** Test for cytosolic CA activity

**A** Scheme of  $\text{CO}_2/\text{HCO}_3^-$ -induced changes of cytosolic pH. **B** Recordings of cytosolic  $\text{H}^+$ -imaging are shown in **black**. The kinetic of  $\text{H}^+$  concentration changes is shown in **blue**. **C** Statistics of effect by EZA on cytosolic  $\text{CO}_2$  induced acidification.

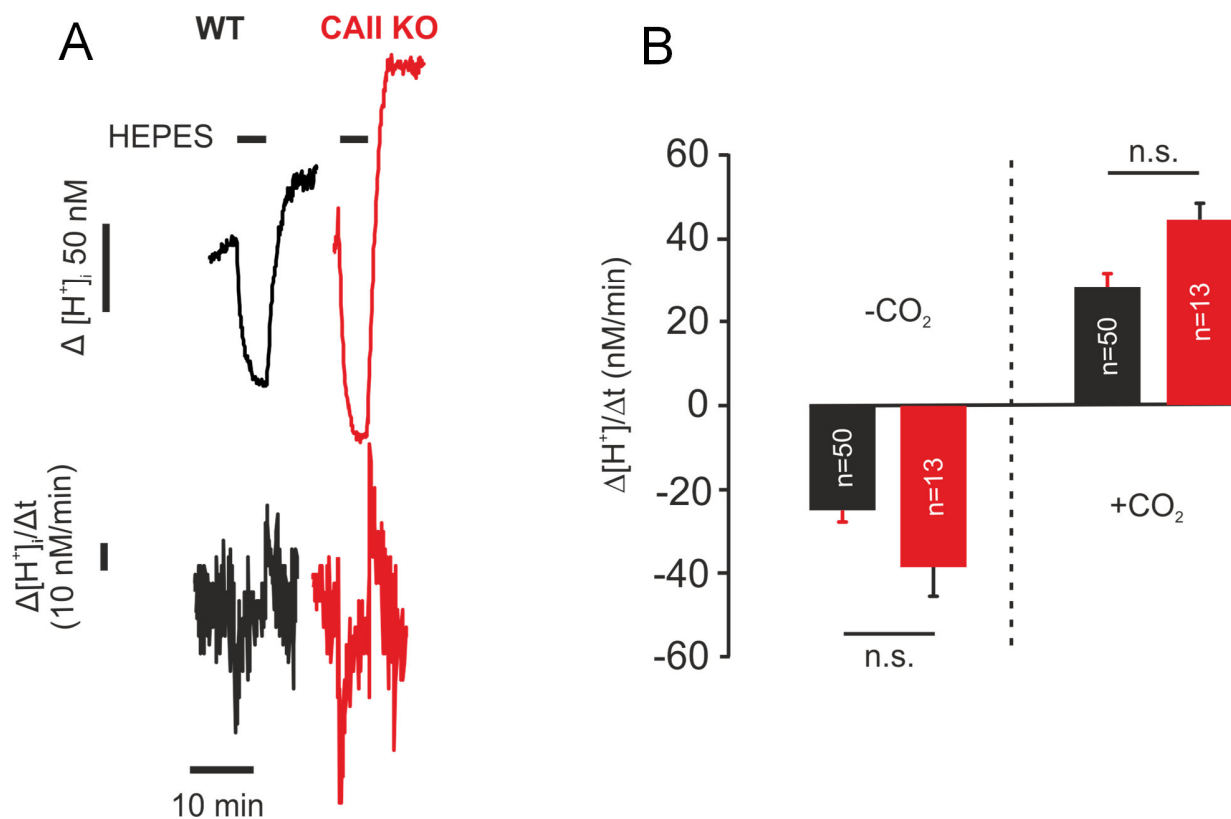


**Figure 20** Cytosolic CA activity in WT and CAII<sup>-/-</sup> cardiomyocytes

The cytosolic H<sup>+</sup> concentration was measured with SNARF in a calibrated system. The cells were alternatively perfused with CO<sub>2</sub>/HCO<sub>3</sub><sup>-</sup> and HEPES-buffered medium (pH 7.4) to measure the CO<sub>2</sub> induced cytosolic pH change in wild type and CAII KO animals. **A** Recordings of CO<sub>2</sub>/HCO<sub>3</sub><sup>-</sup> induced cytosolic H<sup>+</sup> concentration changes in wild type and CAII KO cardiomyocytes. The kinetic of cytosolic H<sup>+</sup> concentration changes is shown below the H<sup>+</sup> recordings. **B** Statistics of effect by EZA on cytosolic CO<sub>2</sub> conversion.

The loss of CAII activity is based on a point mutation in codon 155 (if counted from the start codon at position 110 in exon 1 of the gene *car2*). The codon CAA is changed to TAA, which is a stop codon (Pan et al., 2006). This leads to the possibility that CAII fragments, consisting of the enzymes forepart, were present in the cells and detected by the polyclonal antibodies (Figure 21). Therefore, western blots were performed to detect CAII in wild type and CAII knockout heart samples (Figure 22). In the western blot, no protein was detected by the anti-CAII antibody in CAII<sup>-/-</sup> samples. In the sample from the WT heart, CAII was clearly detected. This is most likely caused by the high erythrocyte content in the heart samples which, contain CAII (Geers et al., 1992; Poole and Halestrap, 1994).

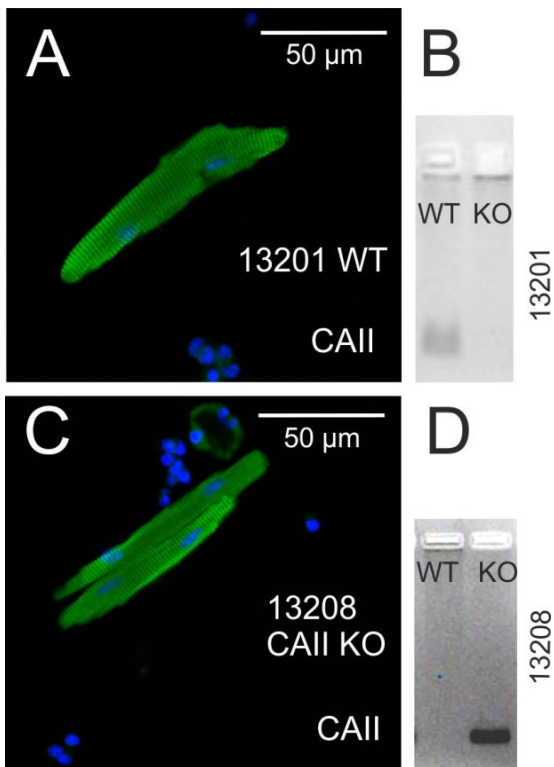


**Figure 21** Detection of CAII in WT and CAII<sup>-/-</sup> cardiomyocytes

**A** Isolated cardiomyocyte from wild type animal (p20, black 6) with identification number 13201. CAII was detected with an anti-CAII antibody and is shown in **green**, nuclei were stained with Hoechst (**blue**).

**B** PCR product from genotype confirmation of animal 13201. Only the wild type allele was detected (WT).

**C** Isolated cardiomyocyte from CAII<sup>-/-</sup> animal (p20, black 6) with identification number 13208. CAII was detected with an anti-CAII antibody and is shown in **green**, nuclei were stained with Hoechst (**blue**).

**D** PCR product from genotype confirmation of animal 13208. Only the KO allele was detected (KO).

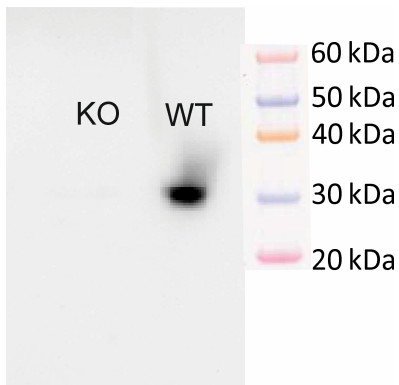


**Figure 22** CAII detection in mouse heart with western blot

20 µg of the lysate from WT and CAII<sup>-/-</sup> (KO) heart were loaded on each lane. In the knockout sample no signal was observed.

It was found that the antibody used for CAII detection could also detect the CAIII (Figure 23), providing the possibility that the signal observed in Figure 21 results from unspecific binding to CAIII.

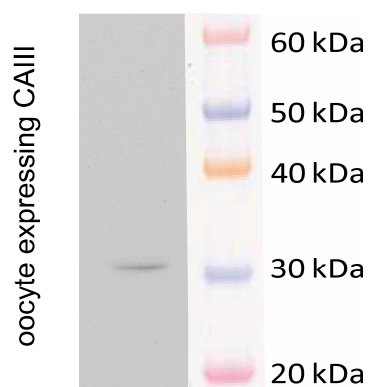


**Figure 23** CAII antibody detects CAIII

20  $\mu\text{g}$  of the lysate of *Xenopus* oocytes heterologously expressing CAIII were loaded on the gel. The western blot was used for CAII detection. The positive signal in oocytes expressing CAIII confirmed the unspecific binding of the CAII antibody to CAIII.

The CAIII had been reported to be rather insensitive to inhibition with EZA and its  $K_i$  was determined to be as high as 60  $\mu\text{M}$  (Geers et al., 1992;  $K_i$  value for CAI: 25 nM,  $K_i$  value for CAII: 8 nM, Brzozowski et al., 2010). Therefore, the absence of an effect by EZA on the  $\text{CO}_2/\text{HCO}_3^-$  induced  $\Delta[\text{H}^+]/\Delta t$  does not exclude the presence of CAIII from the cytosol.

CAIII's presence in ventricular mouse cardiomyocytes was tested with an immunohistochemical approach in heart tissue (Figure 24).

As positive control, a cryostat section of the soleus muscle was used for CAIII detection as the soleus muscle is known to provide a strong CAIII presence (Shiels et al., 1982). The oxidative nature of the shown muscle was confirmed by immunocytochemistry, detecting slow myosin, present in oxidative muscle fibres (Figure 24 B). In the mouse heart the CAIII was not detected (Figure 24 C).

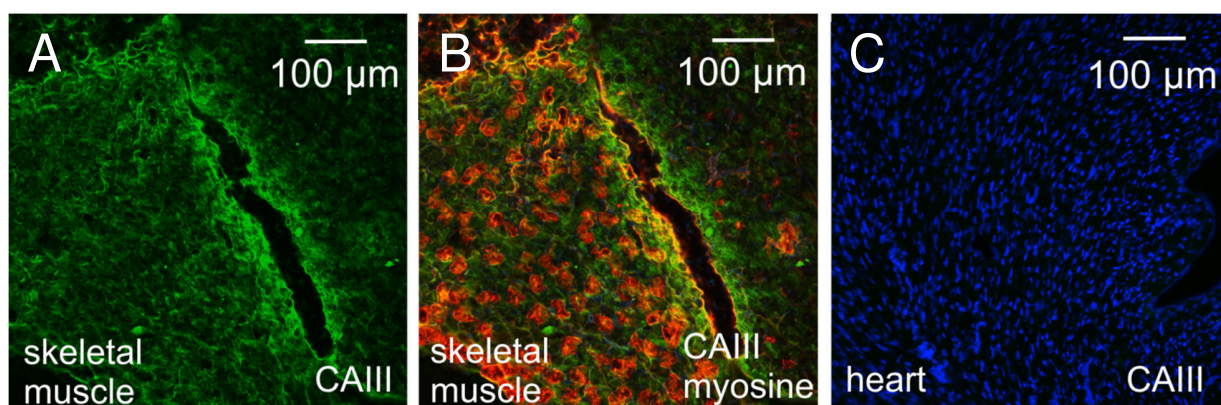


**Figure 24** CAIII in skeletal and heart muscle.

**A** Cryostat section of lower hind limb (p20, black 6 mouse) with CAIII stained **green**. **B** CAIII staining (A) stacked with slow myosin staining (**red**; indicates oxidative myocytes). **C** Cryostat section of mouse heart (p 19, black 6) with CAIII stained **green** (absent) and nuclei were stained with Hoechst (**blue**).

Extracellular CA activity was measured by alternating application of HEPES-only and CO<sub>2</sub>/HCO<sub>3</sub><sup>-</sup>-buffered solution in absence and presence of the CA inhibitor EZA. Figure 25 A, the scheme of this experiment is shown. The circle is meant to mimic a cell. Above this cell, an example trace of an H<sup>+</sup> imaging experiment from the cell surface is shown. During this recording, CO<sub>2</sub>/HCO<sub>3</sub><sup>-</sup> were applied and removed again. When HCO<sub>3</sub><sup>-</sup> reaches the cell surface, it will be partially converted to CO<sub>2</sub> and water. Hereby it will bind protons, so that the H<sup>+</sup> concentration at the cell surface drops. The speed of this pH change is dependent of pH regulatory mechanism, like carbonic anhydrase (CA).

This is the same protocol as used for the cytoplasmic CA activity. To measure the cell surface pH, the pH sensitive fluorescent dye Fluorescein-DHPE was used. In contrast to the experiments performed with the cytosolic pH sensor SNARF, in measurements of the pH on the cell surface with DHPE fluorescein, the application of the CA inhibitor EZA reduced the  $\Delta[H^+]_o/\Delta t$  during CO<sub>2</sub>/HCO<sub>3</sub><sup>-</sup> application by 53.2% and the  $\Delta[H^+]_o/\Delta t$  during CO<sub>2</sub>/HCO<sub>3</sub><sup>-</sup> removal was reduced by 48% (Figure 25).

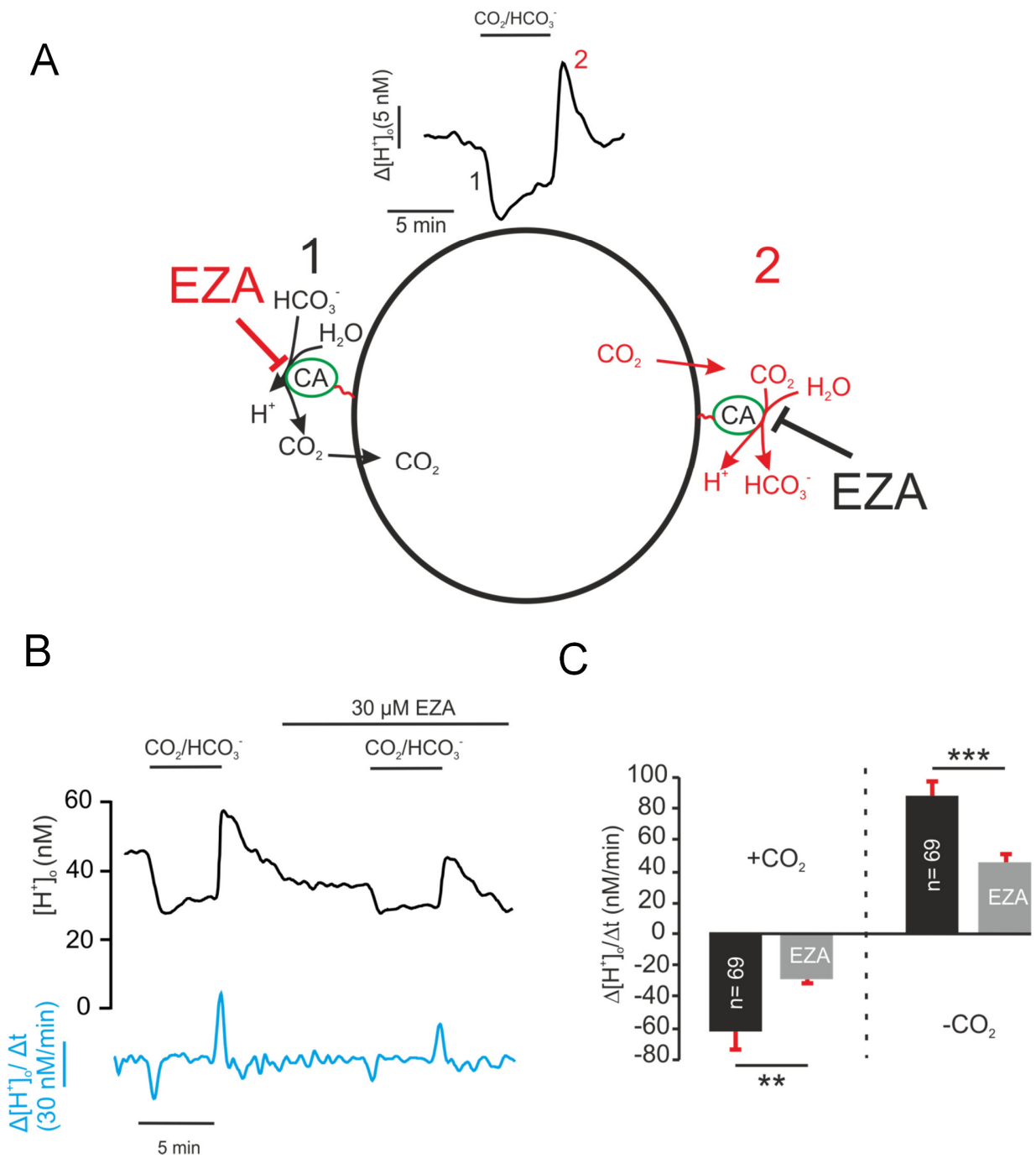


**Figure 25** Activity of extracellular CA on mouse cardiomyocytes

**A** Scheme of  $\text{CO}_2/\text{HCO}_3^-$  induced changes of surface pH **B** Recordings of  $\text{H}^+$ -imaging that were noise filtered Hz (black). The kinetics of surface  $\text{H}^+$  concentration are shown in blue. **C** Statistics of the EZA effect on  $\Delta[\text{H}^+]_o/\Delta t$ .



The origin of this extracellular CA activity was further investigated by protein detection techniques. Candidates for extracellular CAs were CAIV, CAIX and CAXIV as they were found to be present in mouse cardiomyocytes by Scheibe et al. (2006).

Immunohistochemical approaches revealed CAIV signals in the ventricle of the mouse heart in acetone fixed cryostat sections, that were absent from CAIV KO animals (Figure 26). Western blots for CAIV detection in heart samples confirmed CAIV's presence in the mouse heart (Figure 26 B). But immunocytochemistry for CAIV detection in dissociated myocardial tissue suggests the origin of those signals in other cell types than cardiomyocytes (Figure 26 A).

In this work it was not achieved to characterize those CAIV positive cells. Since the murine heart is reported to consist of about 30% fibroblasts (Banerjee et al., 2007), those might be likely candidates. Sender et al. (1998) did report CAIV signals in endothelial cells and cardiomyocytes.

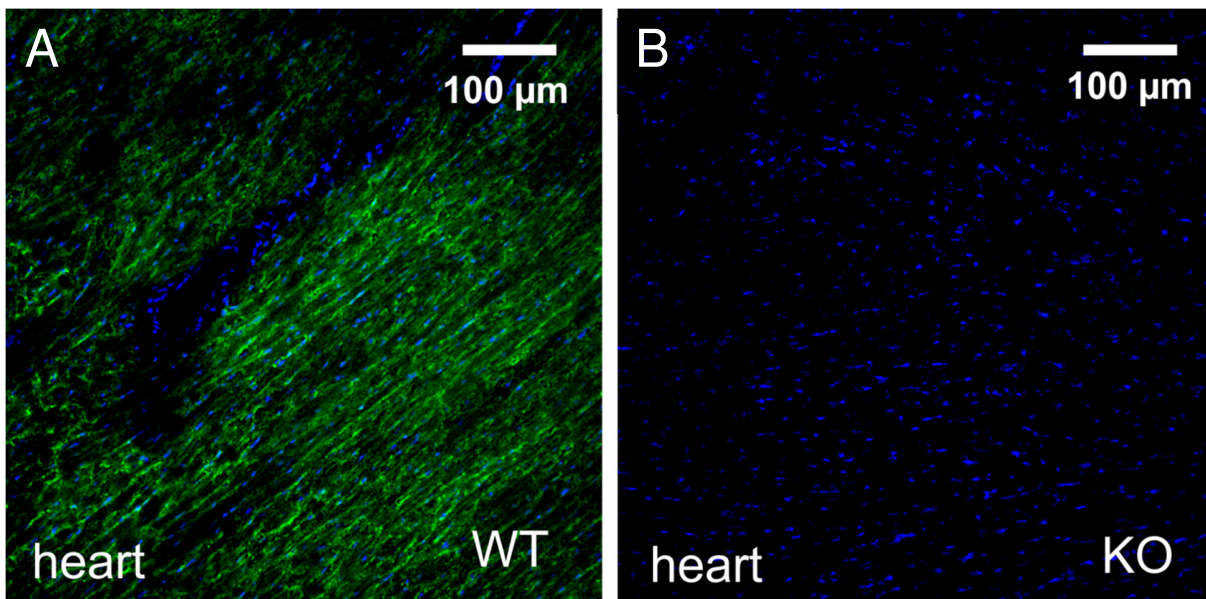


**Figure 26** CAIV in mouse heart

15 µM cryostat sections of wild type (A) and CAIV KO (B) mice from the same litter (p20) were used for CAIV detection. **A** Ventricular cryostat section of a p20 WT mouse. **B** Ventricular cryostat section of a p20 CAIV<sup>-/-</sup> mouse. The CAIV is labelled **green**. The nuclei were labelled with Hoechst and are shown in **blue**.



The CAIX was also detected in the mouse heart and stomach with immunohistochemistry, but the same positive signals were observed in CAIX KO animals (Figure 28). So the used immunohistochemical approach for CAIX detection in mouse heart was not reliable.

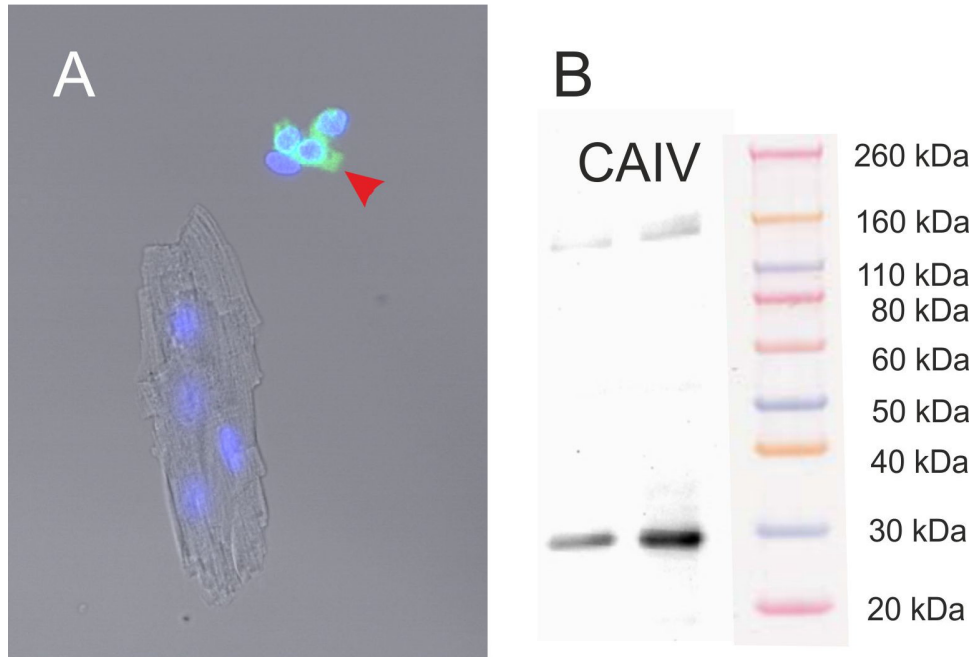


**Figure 27** CAIV detection in dissociated heart sample

**A** Dissociated cardiomyocytes and unidentified CAIV positive cells (arrow head). CAIV is shown in **green**, nuclei were stained with Hoechst and are shown in **blue**. **B** Western blot against CAIV on myocardial tissue lysates. 20  $\mu$ g protein were loaded per lane. Two lanes were loaded with the same sample. P20 wild type black-6 mice were used for this experiment

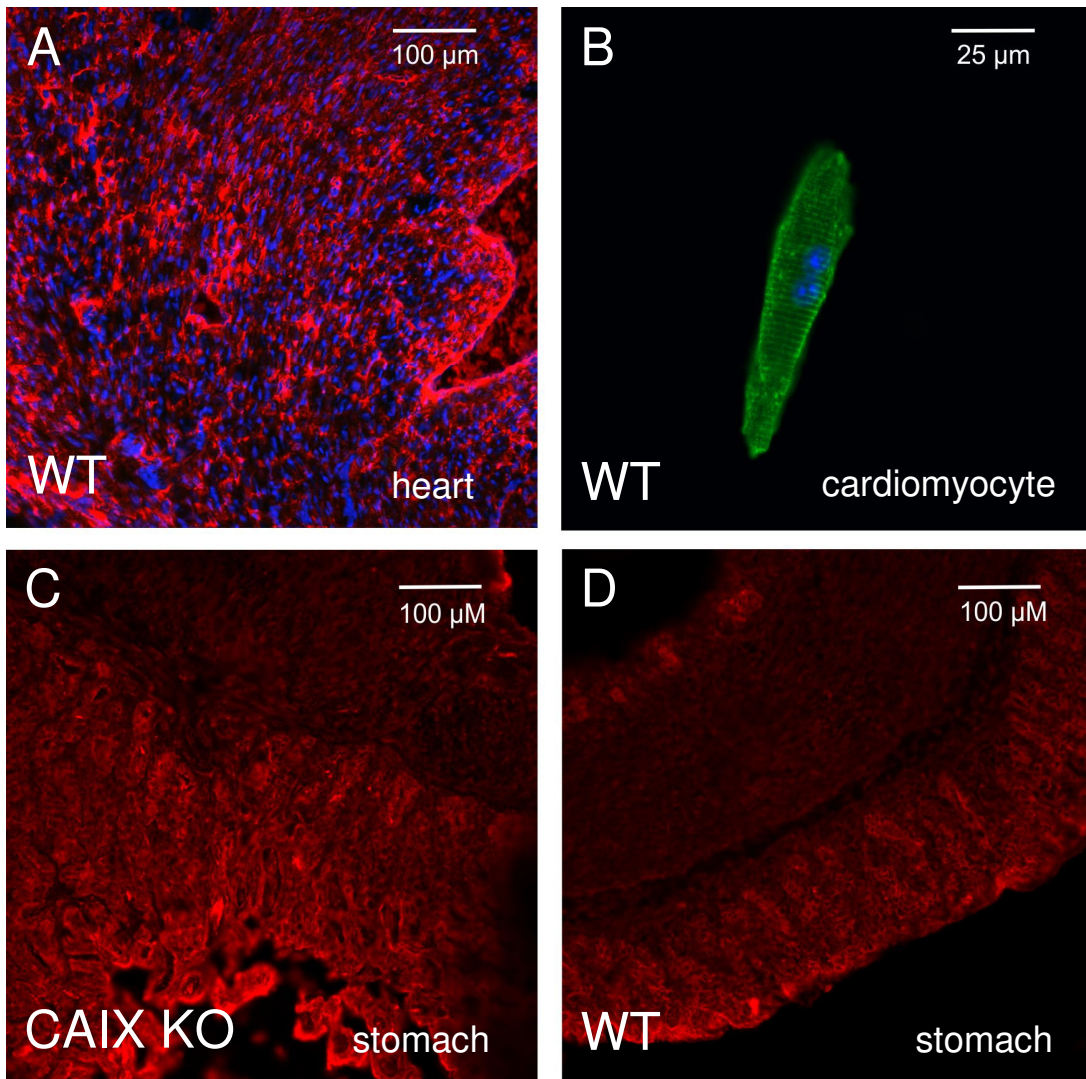


**Figure 28** CAIX in mouse heart and stomach

**A** Cryostat section from wild type (WT) heart (p20, black 6). CAIX is shown in **red** and nuclei are shown in **blue**. **B** Isolated cardiomyocytes from the ventricle (p20, black 6). CAIX detection is indicated in **green**, nuclei were stained with Hoechst (**blue**). **C** Cryostat section from CAIX KO stomach (p34, CAIX<sup>-/-</sup>). CAIX is shown in **red**. **D** Cryostat section from wild type (WT) stomach (p21, black 6). CAIX is shown in **red**.

### 3.2.2 Lactate transporter in mouse cardiomyocytes

The lactate transport into cardiomyocytes is reported to be mediated by MCTs (monocarboxylate transporters) (Halestrap and Meredith, 2004; Koehler-Stec et al., 1998; Vinnakota et al., 2011). Those will transport lactate along with one H<sup>+</sup>. The mainly described MCT in the heart is the MCT1 (Bonen et al., 2001; Garcia et al., 1995; Halestrap et al., 1997; Jackson et al., 1997).

The presence of the MCT1 in mouse cardiomyocytes was first tested by protein detection (western blot and immunohisto- and immunocytochemistry; Figure 29). The protein was detected in western blot of heart samples in four biological replicates (just one is shown; Figure 29 D). Since erythrocytes could not completely be removed from the sample immunocytochemistry detection in dissociated cardiomyocytes (Figure 29 C) was performed and confirmed the presence of MCT 1 in ventricular mouse cardiomyocytes.

To test for a potential involvement of MCT2 in lactate uptake by ventricular mouse cardiomyocytes, the myocardial presence of the transporter was tested with western blot (Figure 29 E). As control, samples of *Xenopus* oocytes, heterologously expressing MCT2, were added to the blot. In three biological replicates (just one is shown) no positive signal for MCT2 was found in mouse heart samples, suggesting its absence from cardiomyocytes.

The presence of the MCT4 in the mouse heart was tested by immunohistochemistry Figure 29 A). As control, cryostat sections of the lower hind limb of the mouse, containing the oxidative soleus muscle and the glycolytic gastrocnemius, were used (Figure 29 B). Since white, glycolytic muscle fibres are reported to show a high MCT4 content whereas red, oxidative muscle fibres are reported to rather contain MCT1 (Fishbein et al., 2002; Pilegaard et al., 1999; Wilson et al., 1998), tissue sections, containing both fibre types were chosen as control for MCT4 detection. The soleus muscle was identified according to its high content of oxidative muscle fibres (Figure 29 B). The staining in Figure 29 clearly shows that MCT4 is present in glycolytic and absent from oxidative muscle.

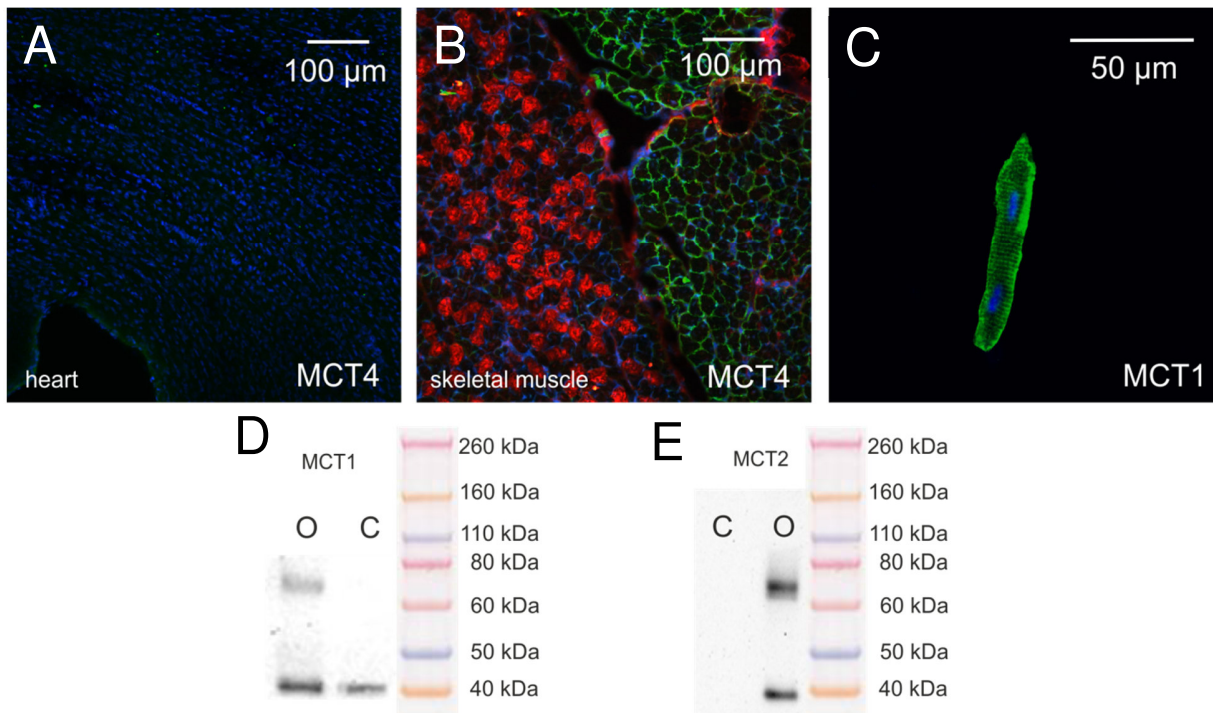


**Figure 29** The presence of MCT1, MCT2 and MCT 4 in mouse cardiomyocytes

**A** Cryostat section of the left ventricle of the mouse heart (p20, black 6 mouse). MCT4 signal is shown in **green** (absent); nuclei are shown in **blue**. **B** Positive control: in a cryostat section of the lower hind limb (p20, black 6 mouse) MCT4 (green) and slow myosin (**red**; indicates oxidative myocytes) were detected; nuclei are shown in **blue**. **C** Isolated cardiomyocyte (p21, black 6), that had been cultured for 24 h prior to MCT1 detection (green); nuclei are shown in **blue**. **D** Western blot with MCT1 detection. 20  $\mu\text{g}$  of cardiomyocyte lysates from 3 different animals (p20 $\pm$  2, Black-6) (C) or 20  $\mu\text{g}$  of lysed *Xenopus* oocytes (O), heterologously expressing MCT1, were loaded per lane, respectively. **E** Western blot with MCT2 detection. 20  $\mu\text{g}$  of cardiomyocyte lysates from 2 different animals (p20 $\pm$  2, Black-6) (C) or 20  $\mu\text{g}$  of lysed *Xenopus* oocytes (O), heterologously expressing MCT2, were loaded per lane, respectively.

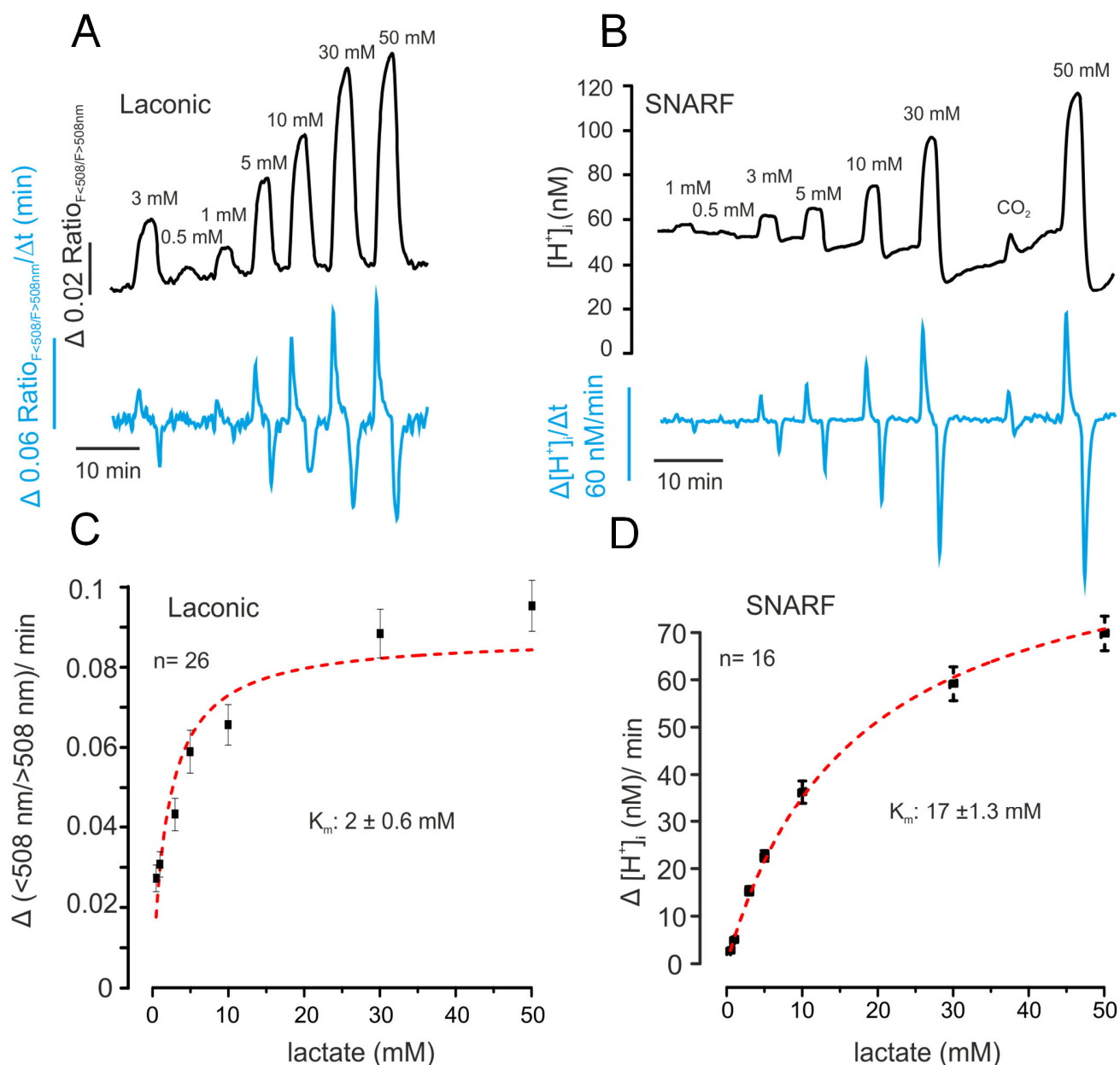


**Figure 30** The  $K_m$  for lactate influx into cardiomyocytes

The  $K_m$  was determined in HEPES-buffered solution (pH 7.4)

**A** Recordings of cells expressing *Laconic* during bath application of different lactate concentrations (black). The kinetics of lactate are shown in blue. **B** Recordings of  $\text{H}^+$ -imaging (SNARF black). The kinetics of  $\text{H}^+$  are shown in blue. **C** Dose-response-curve of lactate influx. The determined  $K_m$  is  $2 \pm 0.6$  mM. **D** Dose-response-curve of lactate induced acidification. The determined  $K_m$  is  $17 \pm 1.3$  mM.

Next  $K_m$  for the lactate influx and the lactate induced  $\Delta[H^+]_i/\Delta t$  into cardiomyocytes was determined.

Since the  $K_m$  of the rat MCT1 for lactate had been determined to be 3.5 mM (Bröer et al., 1998), the  $K_m$  in mouse cardiomyocytes was expected to be similar, if the MCT1 was the dominating lactate transporter. In Figure 30 C and D the  $K_m$  was determined by imaging the kinetic of the lactate influx and the lactate induced acidification during extracellular application of different lactate concentrations (0.5, 1, 3, 5, 10, 30, 50 mM). The Michaelis-Menten fit revealed a  $K_m$  of  $17 \pm 1.3$  mM.

When the  $K_m$  for lactate influx into mouse cardiomyocytes was determined with lactate imaging on cells that artificially expressed the FRET based lactate sensor *Laconic*, a value of  $2 \pm 0.6$  mM was found (Figure 30).

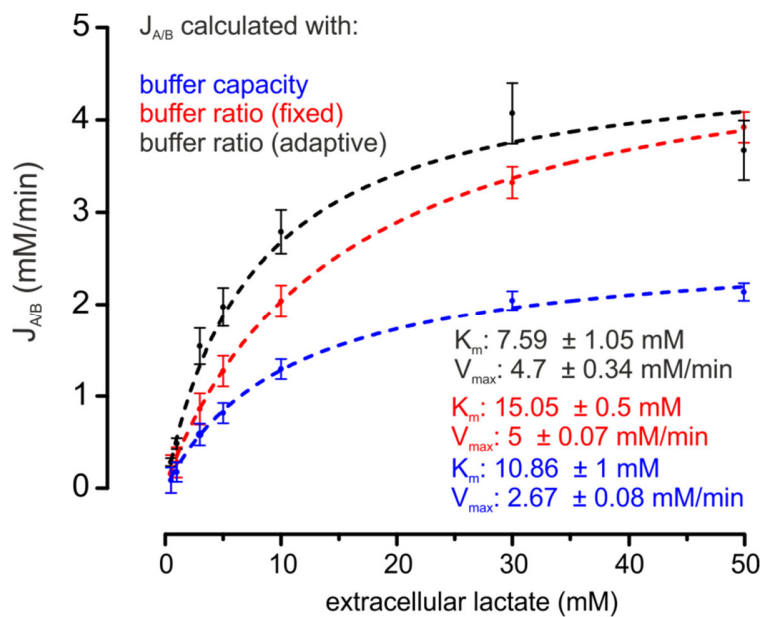


**Figure 31**  $K_m$  of lactate induced  $J_{A/B}$

The lactate-induced acid/base flux ( $J_{A/B}$ ) was calculated from the measured pH kinetics or  $H^+$  kinetics, based on the buffer capacity (blue, 8.8 mM), on the fixed buffer ratio (red, 56089.34) and on the adaptive buffer capacity (black, buffer ratio =  $[H^+]_i^{-1.5572} \cdot 4.43774 \cdot 10^7$ ).

When the  $K_m$  was determined with the  $J_{A/B}$  values, calculated from  $\beta$ ,  $\rho_{\text{fixed}}$  and  $\rho_{\text{adap.}}$ , a strong dependence of the method was observed (Figure 31). The use of  $\beta$ ,  $\rho_{\text{fixed}}$  and  $\rho_{\text{adap.}}$  led to  $K_m$  values of 10.86 mM, 15.05 mM and 7.59 mM, respectively.

### **3.2.3 Sodium bicarbonate co-transporter (NBC) and sodium-proton exchanger (NHE) activity in mouse cardiomyocytes**

A standard method to investigate acid extruding mechanism in cardiomyocytes is the so called  $\text{NH}_4\text{Cl}$  pre-pulse. In Figure 32 A the scheme of  $\text{NH}_4\text{Cl}$  pre-pulse induced  $\Delta[\text{H}^+]_i$  is shown. During  $\text{NH}_4\text{Cl}$  application,  $\text{NH}_4\text{Cl}$  equilibrates with  $\text{NH}_3$  in the extracellular space. The  $\text{NH}_3$  will enter to the cell by diffusion, causing an increase of the intracellular pH by  $\text{NH}_4^+$  formation.  $\text{NH}_4^+$  will enter the cell more slowly than  $\text{NH}_3$  and counteract the rise of pH. It is not perfectly clear how  $\text{NH}_4^+$  enters the cell, but Dart and Vaughan-Jones (1991) could show that the recovery from the rise of cytosolic pH in the sheep heart is independent of  $\text{Na}^+$  and  $\text{Cl}^-$ , which excludes the involvement of the known acid/base transporters (NBC, AE (Anion Exchanger)). They did speculate that this might be caused by unspecific  $\text{NH}_4^+$  influx via  $\text{Na}^+/\text{K}^+$  ATPase or  $\text{K}^+$  channels. When the  $\text{NH}_4\text{Cl}/\text{NH}_3$  is removed from the extracellular environment, cytosolic  $\text{NH}_4^+$  will convert to  $\text{NH}_3 + \text{H}^+$ . The  $\text{NH}_3$  leaves the cell whereas the  $\text{H}^+$  is trapped inside, causing a huge cytosolic acidification. This activates acid extruding mechanisms, so NHE and NBC. With inhibitors or restriction of substrates ( $\text{Na}^+$ ,  $\text{HCO}_3^-$ ), the different acid extruders can be inhibited to dissect the composition of overlapping mechanisms.

The presence of  $\text{HCO}_3^-$ -independent, cariporide-sensitive acid extrusion in mouse cardiomyocytes was tested with the  $\text{NH}_4\text{Cl}$  pre-pulse method. The experiment was performed in the nominal absence of  $\text{CO}_2/\text{HCO}_3^-$  (HEPES-only-buffered solution). In Figure 32, the  $\text{NH}_4\text{Cl}$  pre-pulse was performed once as control, showing all  $\text{CO}_2/\text{HCO}_3^-$ -independent acid extrusion and once in the presence of the NHE1 inhibitor cariporide (Ch'en et al., 2008; Orłowski and Grinstein, 2003). 30  $\mu\text{M}$  cariporide inhibited acid extrusion ( $\Delta[\text{H}^+]_i/\Delta t$ ) by 86% (Figure 33).



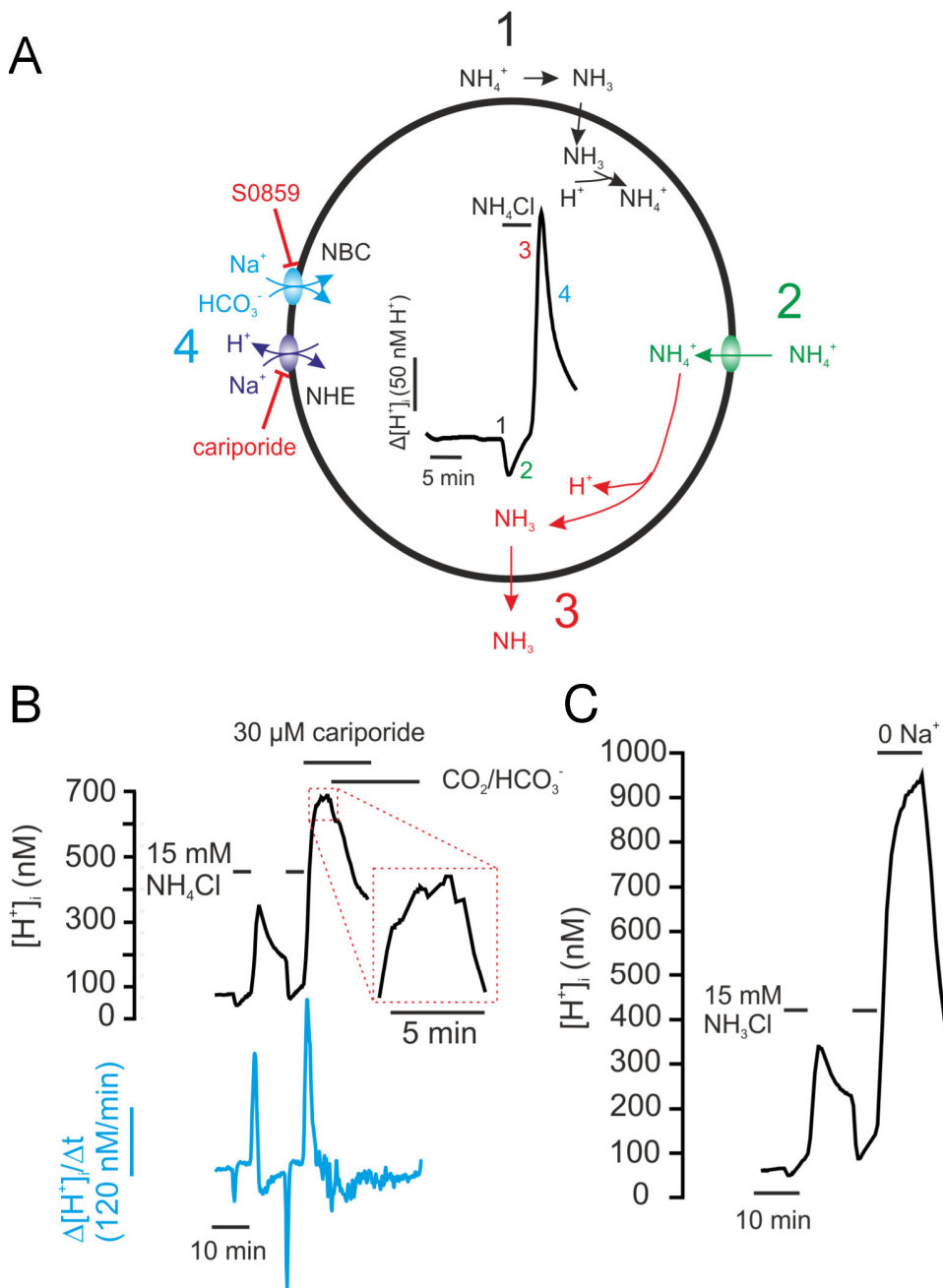


**Figure 32** Acid extruding mechanisms in mouse cardiomyocytes

**A** Scheme of  $\text{NH}_4\text{Cl}$  pre-pulse induced cytosolic  $\text{H}^+$  load. **B** 30  $\mu\text{M}$  of the NHE inhibitor cariporide completely inhibited the acid extrusion in nominal absence of  $\text{CO}_2/\text{HCO}_3^-$ . Introduction of  $\text{CO}_2/\text{HCO}_3^-$  in the presence of cariporide resulted in an increase of cellular pH. The kinetics of  $\text{H}^+$  are shown in blue. **C** In absence of extracellular  $\text{Na}^+$ ,  $\text{CO}_2/\text{HCO}_3^-$ -independent acid extrusion is inhibited. For statistics see Figure 33 and Table 16.



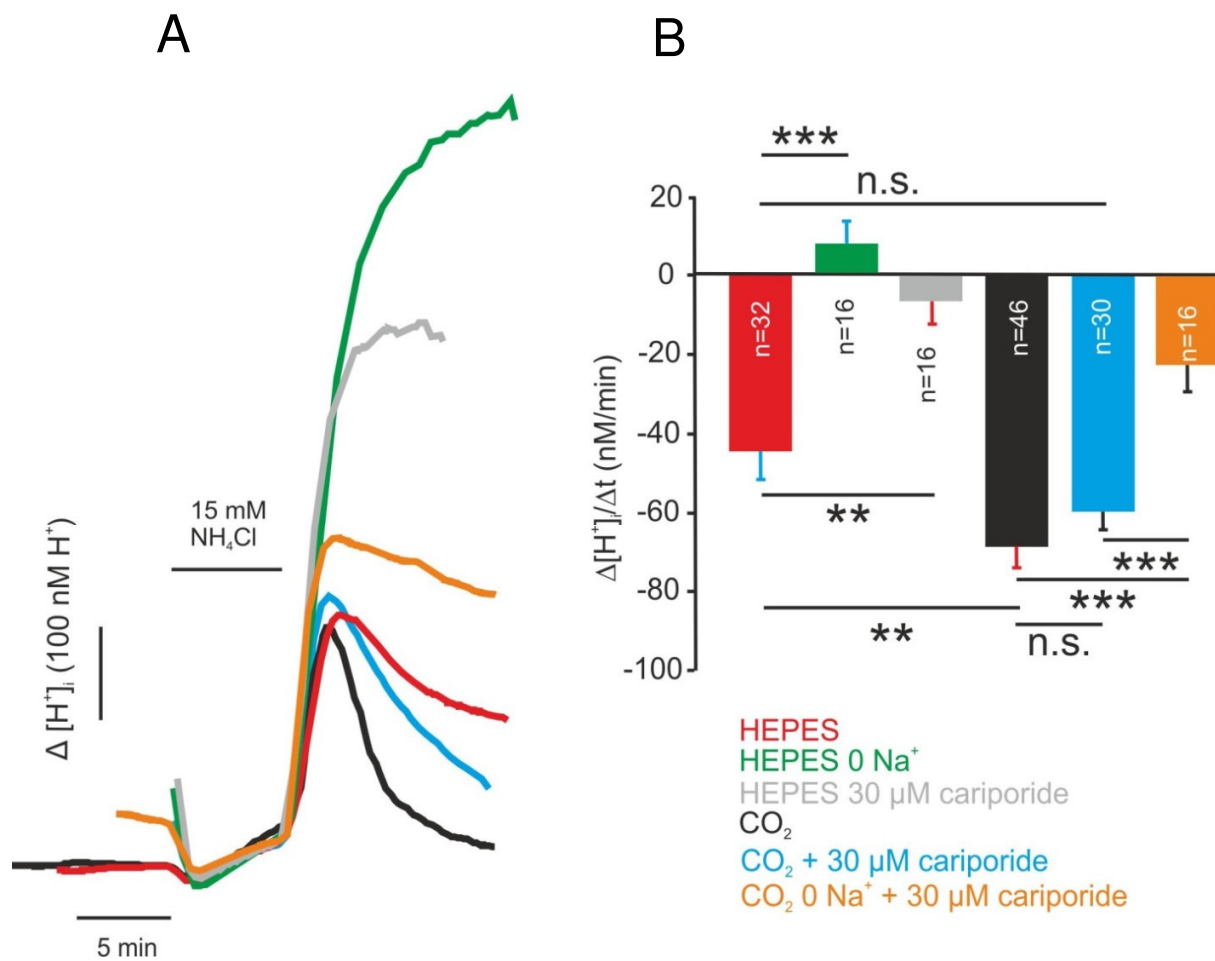


**Figure 33** Dissection of  $\Delta [H^+]_i / \Delta t$  mediating mechanisms after acid load

**A** H<sup>+</sup> recordings from ammonium pre-pulse induced cytosolic acidification in HEPES-buffered solution (red), HEPES-buffered solution without Na<sup>+</sup> (green), HEPES-buffered solution with 30 μM cariporide (grey), CO<sub>2</sub>/HCO<sub>3</sub><sup>-</sup>-buffered solution (black), CO<sub>2</sub>/HCO<sub>3</sub><sup>-</sup>-buffered solution containing cariporide at a concentration of 30 μM (blue) and CO<sub>2</sub>/HCO<sub>3</sub><sup>-</sup>-buffered solution without Na<sup>+</sup> (orange). Sodium dependence of H<sup>+</sup> extrusion was tested with sodium free solutions. **B** Statistics of the acid extrusion shown in A. The maximal  $\Delta [H^+]_i / \Delta t$  of H<sup>+</sup> extrusion after NH<sub>4</sub>Cl removal was analysed.

To test for Na<sup>+</sup> dependence of the cariporide sensitive acid extruder, the NH<sub>4</sub>Cl pre-pulse experiment was performed in the absence of extracellular Na<sup>+</sup> as well. In absence of extracellular Na<sup>+</sup>,  $\Delta [H^+]_i$  became even bigger than in the presence of cariporide and  $\Delta [H^+]_i / \Delta t$  was reduced by 119%.

To test for CO<sub>2</sub>/HCO<sub>3</sub><sup>-</sup>-dependent acid extrusion, in the condition of cariporide inhibited acid extrusion, CO<sub>2</sub>/HCO<sub>3</sub><sup>-</sup> was applied (Figure 32). The cells showed an immediate increase of cytosolic pH.

The acid extruding mechanisms are dissected and compared in Figure 33. The measured  $\Delta[H^+]_i/\Delta t$  is shown in Table 16. The different effects of substrate omission and of inhibitors are shown in Table 17.

**Table 16**  $\Delta[H^+]_i / \Delta t$  after  $NH_4Cl$  pre-pulse

Medium	nM/min	Standard error
HEPES-only	-44.19	7.03
HEPES-only (0 $Na^+$ )	8.54	5.61
HEPES-only (30 $\mu M$ cariporide)	-6.14	5.79
$CO_2/HCO_3^-$	-68.65	5.27
$CO_2/HCO_3^-$ (30 $\mu M$ cariporide)	-59.52	4.65
$CO_2/HCO_3^-$ (cariporide +0 $Na^+$ )	-22.32	5.79

**Table 17** Dissection of  $\Delta[H^+]_i / \Delta t$  contributors after acid load

in HEPES-only	Reduction (%)
cariporide (30 $\mu M$ ) vs. HEPES-only	86.11
0 $Na^+$ in HEPES-only vs. HEPES-only	119.33
in $CO_2/HCO_3^-$ buffer	
cariporide (30 $\mu M$ ) vs. $CO_2/HCO_3^-$	13.3
cariporide (30 $\mu M$ ) and 0 $Na^+$ vs. $CO_2/HCO_3^-$	67.49
cariporide (30 $\mu M$ ) and 0 $Na^+$ vs. cariporide	62.5
<b>Reduction in HEPES-only buffer vs. <math>CO_2/HCO_3^-</math> buffer</b>	<b>35.64</b>

The acid extrusion was also analysed as  $J_{A/B}$  because the exponential behaviour of  $p$  (Figure 18) indicates a strong impact of  $[H^+]_i$  on  $\Delta[H^+]_i/\Delta t$ . This was compensated by the use of  $\rho_{adap}$ . (Figure 34). The determined values for  $J_{A/B}$  are shown in Table 18. The different effects of substrate omission and of inhibitors are shown in Table 19.

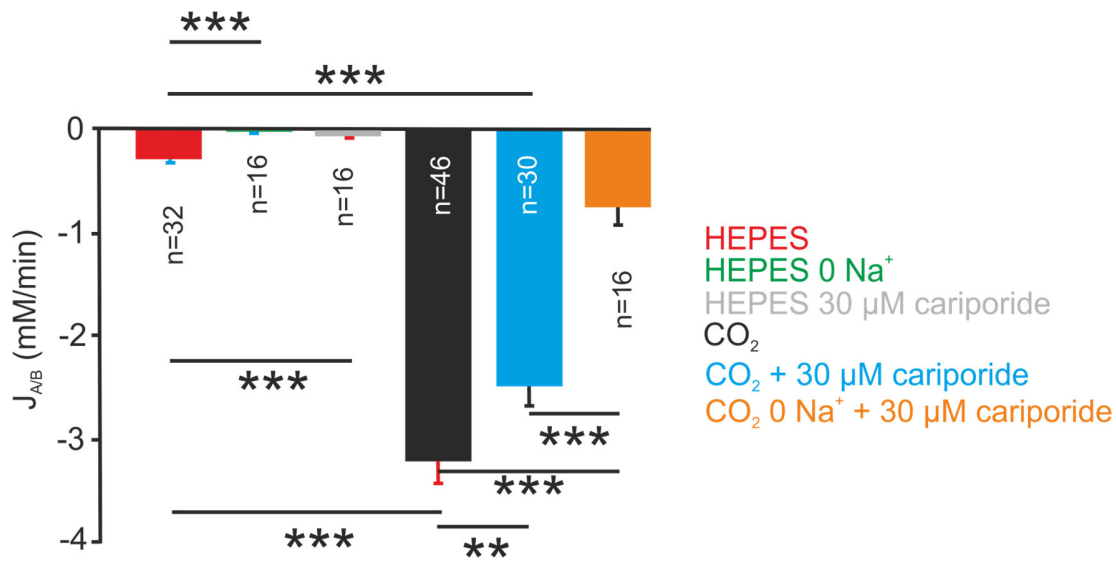


**Figure 34** Dissection of  $J_{A/B}$  mediating mechanisms after acid load

$J_{A/B}$  was calculated according  $p_{\text{adap}}$ , for HEPES-only and  $\text{CO}_2/\text{HCO}_3^-$ -buffered conditions (Figure 18). The values for  $J_{A/B}$  are shown in Table 18.

**Table 18**  $J_{A/B}$  after  $\text{NH}_4\text{Cl}$  pre-pulse

Medium	$J_{A/B}$ (mM/min)	Standard error
HEPES-only	-0.287	0.0267
HEPES-only (0 $\text{Na}^+$ )	-0.017	0.009
HEPES-only (30 $\mu\text{M}$ cariporide)	-0.0637	0.018
$\text{CO}_2/\text{HCO}_3^-$	-3.2237	0.15
$\text{CO}_2/\text{HCO}_3^-$ (30 $\mu\text{M}$ cariporide)	-2.4857	0.195
$\text{CO}_2/\text{HCO}_3^-$ (cariporide +0 $\text{Na}^+$ )	-0.75	0.164

**Table 19** Dissection of  $J_{A/B}$  contributors after acid load

in HEPES-only	Reduction (%)
cariporide (30 $\mu\text{M}$ ) vs. HEPES-only	78.01
0 $\text{Na}^+$ in HEPES-only vs. HEPES-only	94.17
in $\text{CO}_2/\text{HCO}_3^-$ buffer	
cariporide (30 $\mu\text{M}$ ) vs. $\text{CO}_2/\text{HCO}_3^-$	22.9
cariporide (30 $\mu\text{M}$ ) and 0 $\text{Na}^+$ vs. $\text{CO}_2/\text{HCO}_3^-$	76.7
cariporide (30 $\mu\text{M}$ ) and 0 $\text{Na}^+$ vs. cariporide	69.8
Reduction in HEPES-only buffer vs. $\text{CO}_2/\text{HCO}_3^-$ buffer	91.1

### 3.2.3.2 S0859-sensitive and insensitive Na<sup>+</sup>- and HCO<sub>3</sub><sup>-</sup>-dependent H<sup>+</sup> extrusion

To clearly dissect the NBC activity from all other mechanism, the NBC inhibitor S0859 was used.

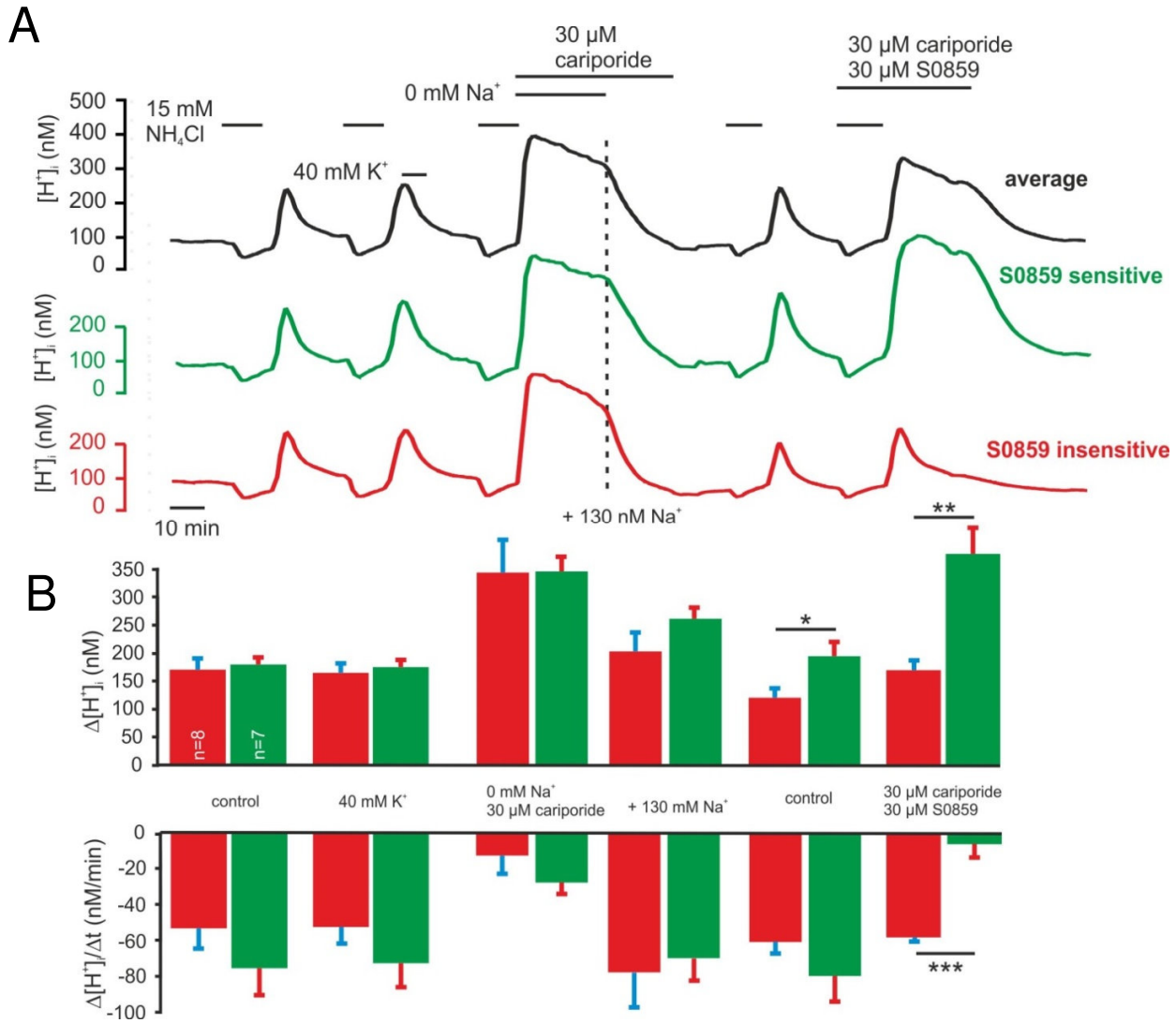


**Figure 35** Mouse cardiomyocytes contain a S0859 sensitive and an insensitive NBC isoform

**A** Recordings from 15 cells were averaged for the average trace (black). High extracellular K<sup>+</sup> (40 mM) did not alter cytosolic pH or H<sup>+</sup> extrusion. In sodium free solution, the H<sup>+</sup> extrusion was significantly reduced, even though not completely abolished. The S0859 showed an inhibiting effect (S0859 sensitive; green) on H<sup>+</sup> extrusion in 7 out of 15 cells, whereas 8 out of 15 cells were S0859 insensitive (red). **B** Statistics of the experiment shown in A. The maximal acidification and the maximal speed of H<sup>+</sup> extrusion after NH<sub>4</sub>Cl removal were analysed. If significance is not indicated, there was no significant difference observed between sensitive and insensitive cell types.

This inhibitor was described by Ch'en et al. (2008) to completely block the NBC activity at a concentration of 30  $\mu\text{M}$  in rat, rabbit and guinea pig cardiomyocytes. In this work the acid extrusion ( $\Delta[\text{H}^+]_i/\Delta t$ ) showed an average reduction of 53% when S0859 (30  $\mu\text{M}$ ) was applied. But the cells did respond in an individual degree to the inhibitor. 62 cells were analysed. In 24%, S0859 reduced acid extrusion ( $\Delta[\text{H}^+]_i/\Delta t$ ) by 90% or more and in 33.9% of the cells acid extrusion was reduced by less than 10%. In Figure 35, a S0859 sensitive and an insensitive fraction are compared.

Depolarization of cardiomyocytes with high extracellular  $\text{K}^+$  (40 mM) did not speed up the acid extrusion from mouse cardiomyocytes (Figure 35) as described by Yamamoto et al. (2005) for guinea pig, rat and rabbit cardiomyocytes. Yamamoto et al. (2005) referred this electrogenic acid extrusion to the NBCe1. The presence of this membrane transporter in mouse cardiomyocytes was tested with western blot. The NBCe1 was detected in WT mouse brain samples but not in WT heart or NBCe1 knock out samples (Figure 36).

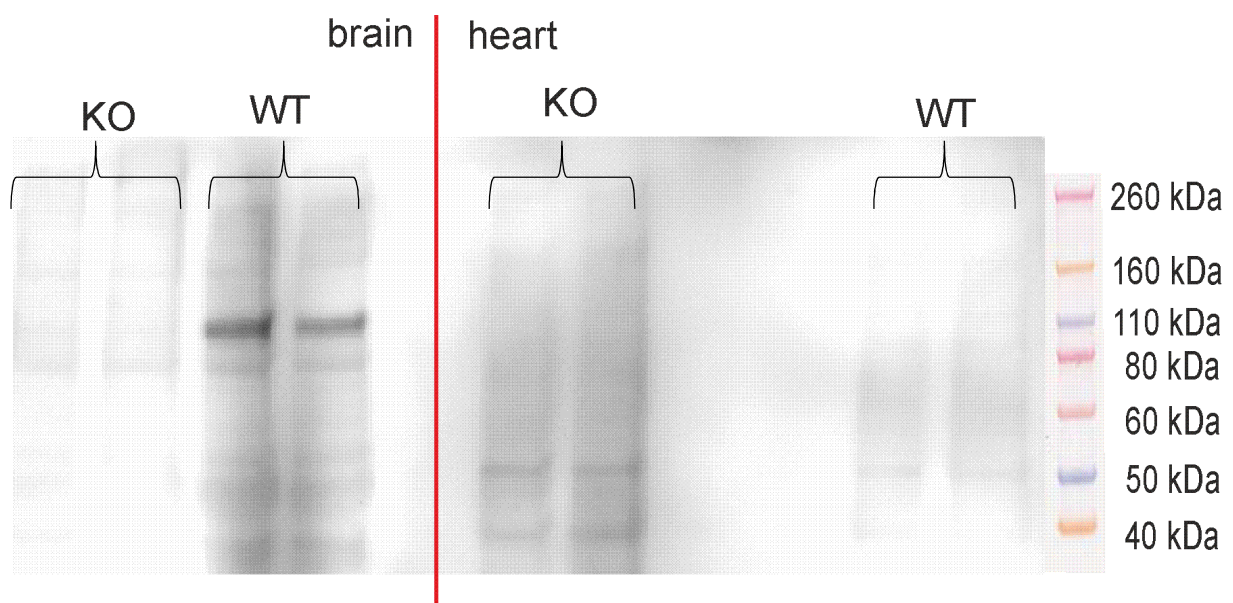


**Figure 36** Western blot with NBCe1 detection

Western blot for NBCe1 detection with brain and heart tissue samples from WT and NBCe1-KO animals. The expected size of NBCe1 is 120 kDa (Garciaarena et al., 2013). Each sample was loaded as pair.

### 3.2.3.3 Na<sup>+</sup>-independent, HCO<sub>3</sub><sup>-</sup>-dependent acid extrusion

In the presence of CO<sub>2</sub>/HCO<sub>3</sub><sup>-</sup>, acid extrusion persisted in Na<sup>+</sup> free solution (as shown in the red and green trace in Figure 35 and Figure 37) but not in its nominal absence (HEPES-only-buffered solution).

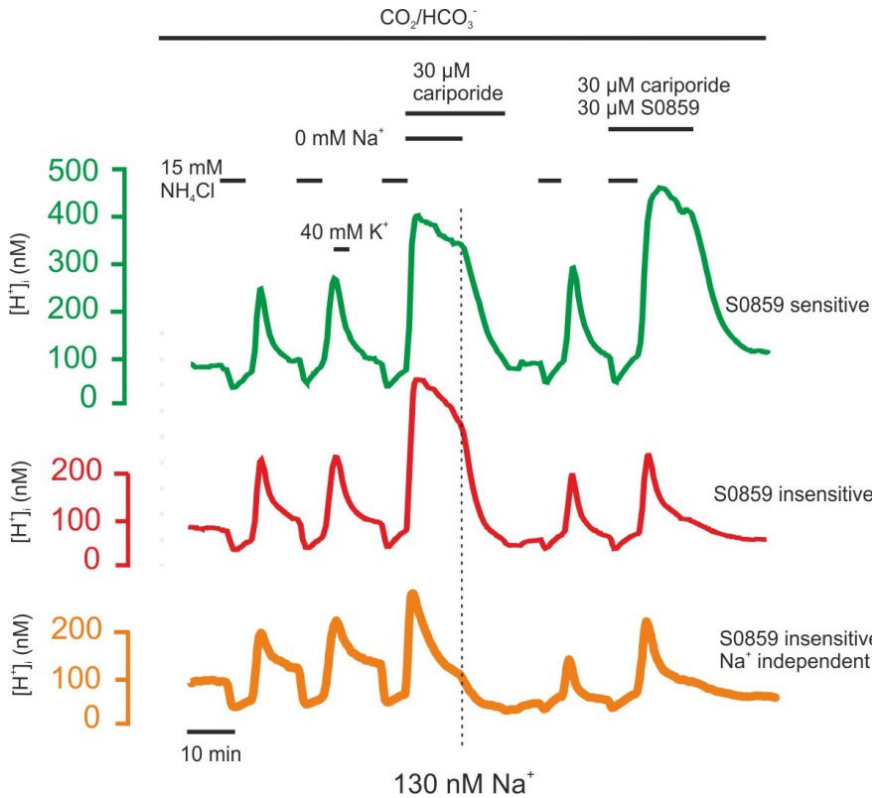


**Figure 37** Na<sup>+</sup>-independent, HCO<sub>3</sub><sup>-</sup>-dependent acid extrusion

The green and red traces are the same as shown in Figure 35. The orange trace was recorded in the same experiment and shows a third type of cardiomyocytes, which extrude H<sup>+</sup>-independent from extracellular sodium.

The pH recordings were noise filtered with the program clampfit at a threshold of 0.012 Hz. For this experiment, a black 6 mouse was used at an age of p19.

In a group of cardiomyocytes (6 out of 30, 20%), the acid extrusion was reduced by less than 10% in the absence of extracellular Na<sup>+</sup> (Figure 37 orange trace).

### 3.2.3.4 Threshold of CO<sub>2</sub>/HCO<sub>3</sub><sup>-</sup>-independent acid extrusion

In HEPES-only-buffered solution, the acid extrusion after NH<sub>4</sub>Cl induced acidification did not reach back the baseline pH but was calculated with an exponential fit to stop at pH 6.82 (Figure 38). In contrast, acid extrusion in CO<sub>2</sub>/HCO<sub>3</sub><sup>-</sup>-buffered solution was calculated to persist until pH 7 was reached.

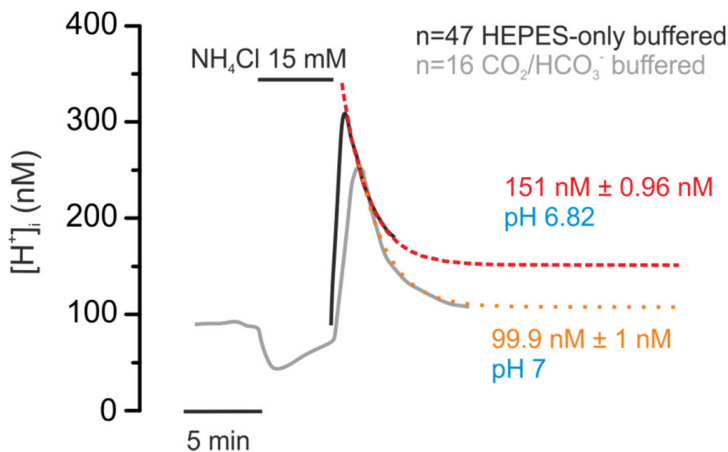


**Figure 38** Threshold of CO<sub>2</sub>/HCO<sub>3</sub><sup>-</sup>-independent acid extrusion

In HEPES buffered solution, the acid extrusion after NH<sub>4</sub>Cl induced acidification stopped before the cytosolic pH reached the baseline. The new baseline after acid extrusion in HEPES-only-buffered solution (**black**) was calculated with the exponential fit:  $Y = 309.98 \cdot \exp(-X/45.62) + 150.86$ . The new baseline after acid extrusion in CO<sub>2</sub>/HCO<sub>3</sub><sup>-</sup>-buffered solution (**grey**) was calculated with the exponential fit:  $Y = 3.56614 \cdot 10^6 \cdot \exp(-X/24.31) + 99.9$ .

The new baselines in HEPES-only and CO<sub>2</sub>/HCO<sub>3</sub><sup>-</sup>-buffered solution were determined at 151 nM H<sup>+</sup> or pH 6.82 and 99.9 nM H<sup>+</sup> or pH 7, respectively.

### 3.2.3.5 Functional interaction of NBC and CA

The cariporide-insensitive, CO<sub>2</sub>/HCO<sub>3</sub><sup>-</sup>-dependent acid extrusion (after NH<sub>4</sub>Cl pre-pulse induced cytosolic H<sup>+</sup> load) was measured in the presence and absence of EZA (30 μM). J<sub>A/B</sub> was calculated with  $\rho_{\text{adap}}$ . (Figure 39). The cariporide insensitive, CO<sub>2</sub>/HCO<sub>3</sub><sup>-</sup>-dependent J<sub>A/B</sub> was determined to be 2.59 ± 0.27 mM/min. In the presence of EZA (30 μM), J<sub>A/B</sub> reduced by 78.4% to 0.56 ± 0.16 mM/min. In Table 20 the J<sub>A/B</sub> as calculated according to  $\rho_{\text{adap}}$  and  $\beta$  are compared.

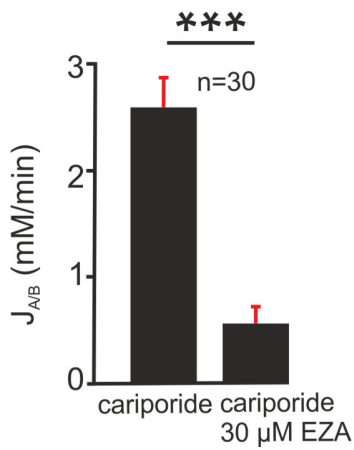


**Figure 39** Effect of EZA on  $\text{HCO}_3^-$ -dependent acid extrusion

The acid extrusion after  $\text{NH}_4\text{Cl}$  induced  $\text{H}^+$  load in absence and presence of EZA (30  $\mu\text{M}$ ). The NHE was inhibited with cariporide (30  $\mu\text{M}$ ). The measured  $\Delta[\text{H}^+]/\Delta t$  was converted to  $J_{A/B}$  with  $\rho_{\text{adap.}}$ .

**Table 20** Effect of EZA on  $\text{HCO}_3^-$ -dependent acid extrusion

Calculation of $J_{A/B}$	$J_{A/B}$ (mM/min) cariporide insensitive	$J_{A/B}$ (mM/min) cariporide insensitive, EZA sensitive	Reduction of $J_{A/B}$ by EZA (30 $\mu\text{M}$ , %)
with $\rho_{\text{adap.}}$	2.59 ± 0.27	0.56 ± 0.16	-78.4
with $\beta$	3.4 ± 0.25	1.6 ± 0.11	-53.3



### 3.3 Lactate flux and physiological implementation

#### 3.3.1 Lactate uptake

The lactate-induced acidification was measured by pH imaging with the cytosolic pH sensor SNARF. Lactate transport was investigated with a lactate concentration of 3 mM because this was the approximate  $K_m$  of myocardial lactate uptake and within the expected range of physiological blood lactate levels (0.64 mM at rest and 1.4 mM after 5 min physical activity; Gertz et al., 1988; up to 10 mM according to Scheuermann et al., 2000).  $H^+$  or pH imaging can be used to determine the lactate flux. This is possible since lactate is transported via MCTs along with  $H^+$ .

Extracellular application of lactate (3 mM) caused  $\Delta[H^+]_i/\Delta t$  of  $20.77 \pm 1.3$  nM/min,  $16.86 \pm 1.2$  nM/min and  $25 \pm 2.5$  nM/min in HEPES-only-,  $CO_2/HCO_3^-$ - and  $CO_2/HCO_3^-$ -buffered conditions in the presence of EZA (30  $\mu M$ ), respectively (Figure 40). Thus,  $\Delta[H^+]_i/\Delta t$  was reduced in  $CO_2/HCO_3^-$ -buffered conditions by 18.8%. Inhibition of CA with EZA (30  $\mu M$ ) increased  $\Delta[H^+]_i/\Delta t$  by 48.7%. The maximal  $\Delta[H^+]_i$  was  $17.4 \pm 1.3$  nM,  $14.3 \pm 1.8$  nM and  $22 \pm 2.9$  nM in HEPES-only,  $CO_2/HCO_3^-$  and  $CO_2/HCO_3^-$ -buffered conditions in the presence of EZA (30  $\mu M$ ), respectively. The basal  $[H^+]_i$  was determined to be  $70.2 \pm 2.6$  nM,  $72.5 \pm 6$  nM and  $66.4 \pm 6.4$  nM in HEPES-only,  $CO_2/HCO_3^-$  and  $CO_2/HCO_3^-$ -buffered conditions in the presence of EZA (30  $\mu M$ ), respectively.

The lactate (3 mM) induced  $J_{A/B}$  was determined according to  $\beta$ ,  $p_{fixed}$  and  $p_{adapt}$ . The  $J_{A/B}$  values are shown in Figure 41 and Table 21. The effects of the buffering conditions on  $J_{A/B}$  are shown in Table 22.

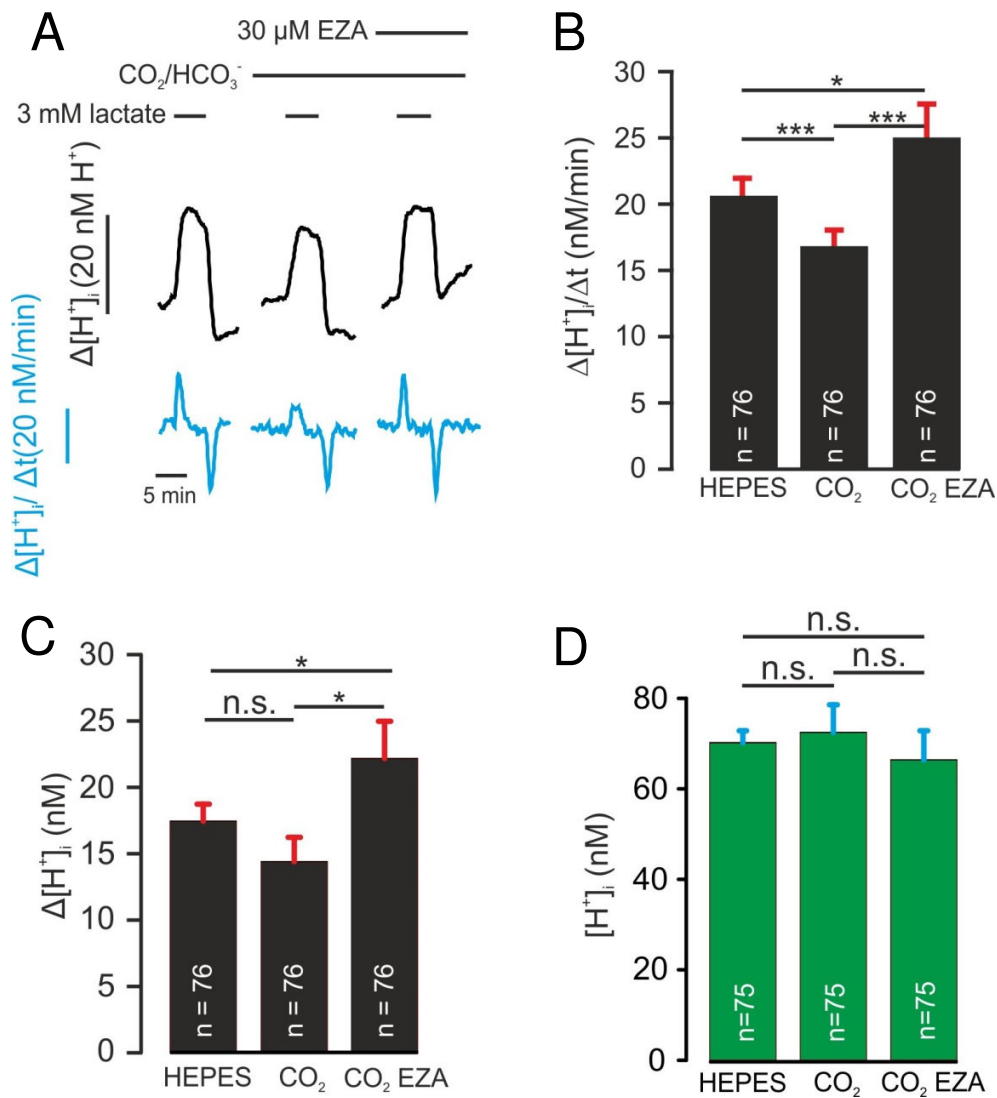


**Figure 40** Measurement of lactate-induced acidification in different buffers

Experiments were performed in mouse cardiomyocytes, loaded with the  $\text{H}^+$ -sensitive dye SNARF-5F in a calibrated system. **A** Recordings of  $\text{H}^+$ -imaging. The lactate induced changes in cytosolic  $\text{H}^+$  concentration are shown in the upper part as **black** traces. In the lower part, the kinetics of  $[\text{H}^+]_i$  are shown in **blue**. **B** Statistics of the lactate induced, cytosolic  $\Delta[\text{H}^+]_i / \Delta t$ . **C** Amplitude of lactate induced acidification with 3 mM lactate **D** Basal cytosolic  $\text{H}^+$  concentration in different buffers.

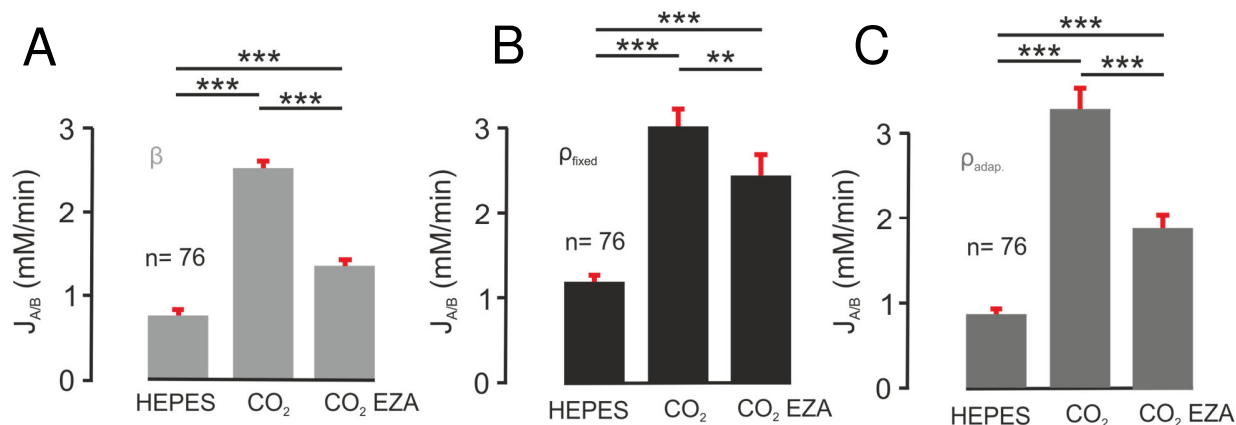


**Figure 41** Lactate (3 mM) induced  $J_{A/B}$  according to  $\beta$ ,  $\rho_{\text{fixed}}$  and  $\rho_{\text{adap}}$ .

**A** Calculated values for lactate influx according to the buffer capacity **B** Calculated values for the acid influx according to  $\rho_{\text{fixed}}$  **C** Calculated values for the acid influx according to  $\rho_{\text{adap}}$ . The values are shown in Table 21.

**Table 21** Lactate (3 mM) induced  $J_{A/B}$  according to  $\beta$ ,  $\rho_{\text{fixed}}$  and  $\rho_{\text{adap}}$

Buffering conditions	$\Delta\text{pH}/\Delta\text{t} \cdot \beta$ (mM/min)	$\Delta[\text{H}^+]_i/\Delta\text{t} \cdot \rho_{\text{fixed}} \cdot 10^{-6}$ (mM/min)	$\Delta[\text{H}^+]_i/\Delta\text{t} \cdot \rho_{\text{adap}} \cdot 10^{-6}$ (mM/min)
HEPES-only	$0.77 \pm 0.057$	$1.17 \pm 0.07$	$0.87 \pm 0.05$
$\text{CO}_2/\text{HCO}_3^-$	$2.52 \pm 0.062$	$2.98 \pm 0.2$	$3.29 \pm 0.25$
$\text{CO}_2/\text{HCO}_3^- + \text{EZA}$ (30 $\mu\text{M}$ )	$1.36 \pm 0.046$	$2.41 \pm 0.24$	$1.88 \pm 0.16$

**Table 22** Effect of buffering condition on  $J_{A/B}$  according to  $\beta$ ,  $\rho_{\text{fixed}}$  and  $\rho_{\text{adap}}$

Buffering conditions	$\beta \Delta J_{A/B}$ (%)	$\rho_{\text{fixed}} \Delta J_{A/B}$ (%)	$\rho_{\text{adap}} \Delta J_{A/B}$ (%)
HEPES-only vs. $\text{CO}_2/\text{HCO}_3^-$	+228.4	+155.7	+276.9
$\text{CO}_2/\text{HCO}_3^-$ vs. $\text{CO}_2/\text{HCO}_3^- + \text{EZA}$ (30 $\mu\text{M}$ )	-46.2	-19.2	-42.8
HEPES-only vs. $\text{CO}_2/\text{HCO}_3^- + \text{EZA}$ (30 $\mu\text{M}$ )	+76.7	+106.6	+115.7

The real lactate flux was determined by lactate imaging with the FRET-sensor *Laconic*. During this work, it was not possible to calibrate the system for lactate imaging, thus the measured  $\Delta[\text{lac}]_i/\Delta t$  is shown in arbitrary units. The measured values are shown in Figure 42 and Table 23. The effect of the buffering system on the lactate flux is shown in Table 24.

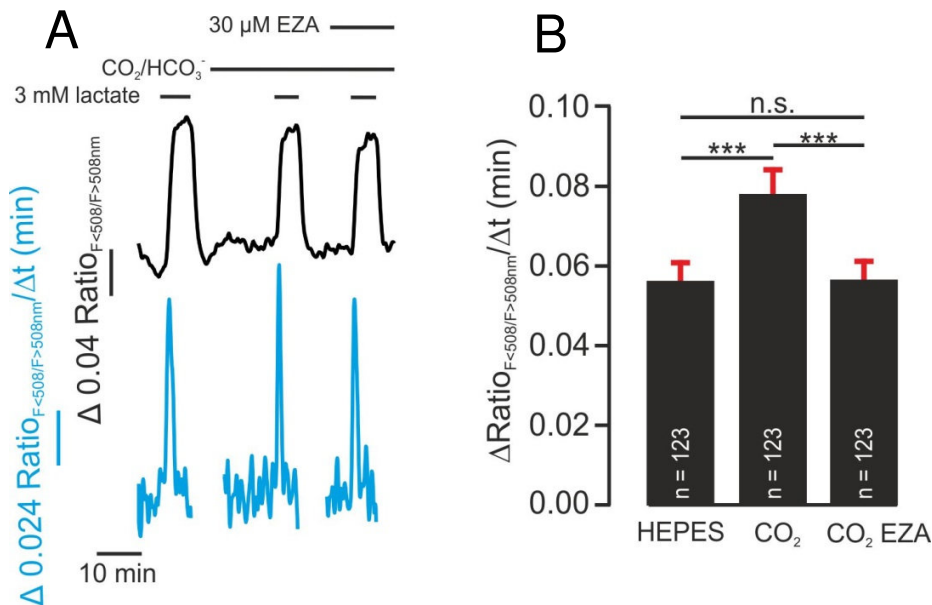


**Figure 42** Lactate uptake measured with *Laconic*

**A** Lactate was applied at a concentration of 3 mM in HEPES-only,  $\text{CO}_2$ -buffered and  $\text{CO}_2$ -buffered solution containing 30  $\mu\text{M}$  of the CA inhibitor EZA. Experiments were performed with cardiomyocytes containing the lactate sensor *Laconic*. Changes in lactate concentration are shown in black, whereas  $\Delta[\text{lac}]_i/\Delta t$  is shown in blue. **B** Statistics of the lactate influx. Significance was tested with a paired student's t test.

**Table 23** Lactate influx during extracellular application (3 mM)

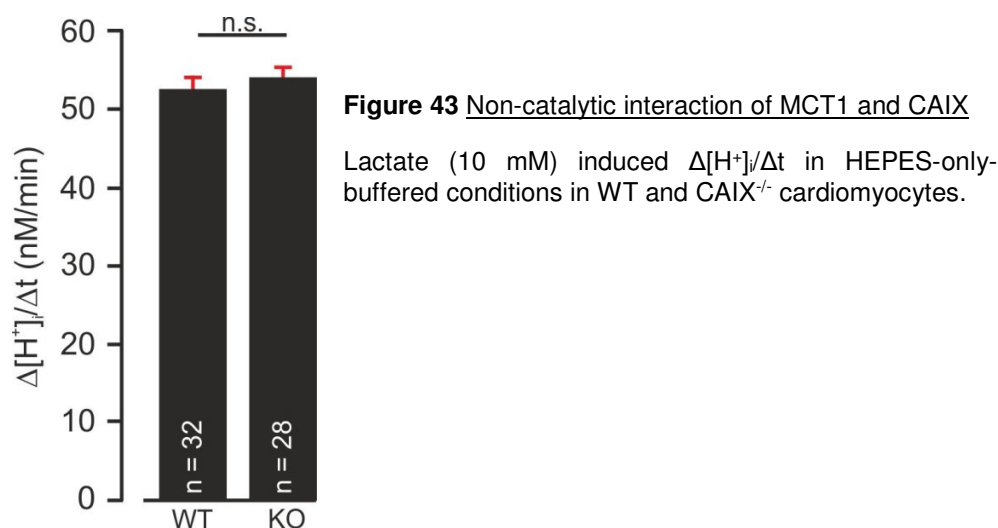
Buffering conditions	$\Delta[\text{lac}]_i/\Delta t$ (a.u./min)
HEPES-only	$0.0566 \pm 0.0047$
$\text{CO}_2/\text{HCO}_3^-$	$0.0782 \pm 0.0065$
$\text{CO}_2/\text{HCO}_3^- + \text{EZA}$ (30 $\mu\text{M}$ )	$0.057 \pm 0.0046$

**Table 24** Effect of buffering system on lactate influx during extracellular application (3 mM)

Buffering conditions	$\Delta[\text{lac}^-]_i/\Delta t$ (a.u./min) (%)
HEPES-only vs. $\text{CO}_2/\text{HCO}_3^-$	+38
$\text{CO}_2/\text{HCO}_3^-$ vs. $\text{CO}_2/\text{HCO}_3^-$ + EZA (30 $\mu\text{M}$ )	-27
HEPES-only vs. $\text{CO}_2/\text{HCO}_3^-$ + EZA (30 $\mu\text{M}$ )	+0.68

### 3.3.2 Non-catalytic interaction of MCT and extracellular CA

For the extracellular CAs CAIV and CAIX a non-catalytic interaction with the MCT1 was observed (Klier et al., 2013 and Michael Klier, unpublished data). CAIV, CAIX and CAXIV were reported in mouse cardiomyocytes by Scheibe et al. (2006). Since the CAIV was found to be absent from mouse cardiomyocytes in this work, a potential non-catalytic interaction of CAIV and MCT was not further investigated. The potential non-catalytic interaction of MCT1 and CAIX was investigated by pH imaging with SNARF in HEPES-only-buffered solution.



Lactate induced  $\Delta[\text{H}^+]_i/\Delta t$  in HEPES-only-buffered conditions was not differing between WT and CAIX<sup>-/-</sup> cardiomyocytes (Figure 43).

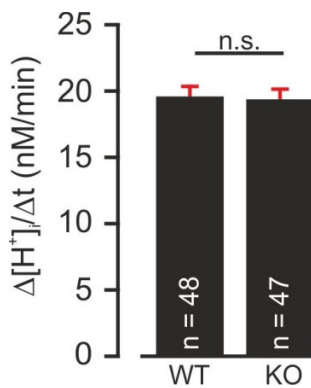


**Figure 44** Non-catalytic interaction of MCT1 and CAXIV

Lactate (3 mM) induced  $\Delta[H^+]_i/\Delta t$  in HEPES-only-buffered conditions in WT and CAXIV<sup>-/-</sup> cardiomyocytes.

The potential non-catalytic interaction of MCT1 and CAXIV was investigated by H<sup>+</sup> imaging with SNARF in HEPES-only-buffered solution. Lactate induced  $\Delta[H^+]_i/\Delta t$  in HEPES-only-buffered conditions was not differing between WT and CAXIV<sup>-/-</sup> cardiomyocytes (Figure 44).

### 3.3.3 Effect of cellular respiration on lactate influx

If lactate is consumed for ATP generation, this must be linked to CO<sub>2</sub> formation. In this work, extracellular CA activity (Figure 25) and its impact on NBC activity are shown (Figure 39). Thus, it was tested if omission of O<sub>2</sub> has an effect on  $\Delta[H^+]_i/\Delta t$  (Figure 45). If extracellular lactate (3 mM) was applied in HEPES-only-buffered solution, gassed with 100% O<sub>2</sub>, the measured  $\Delta[H^+]_i/\Delta t$  was  $11.06 \pm 0.36$  nM/min. In 100% N<sub>2</sub> gassed solution  $\Delta[H^+]_i/\Delta t$  increased by 12.6% to  $12.46 \pm 0.34$  nM/min. When EZA (30  $\mu$ M) was applied in 100% O<sub>2</sub> gassed solution,  $\Delta[H^+]_i/\Delta t$  increased by 8% from  $11.9 \pm 0.3$  nM/min to  $12.9 \pm 0.35$  nM/min.

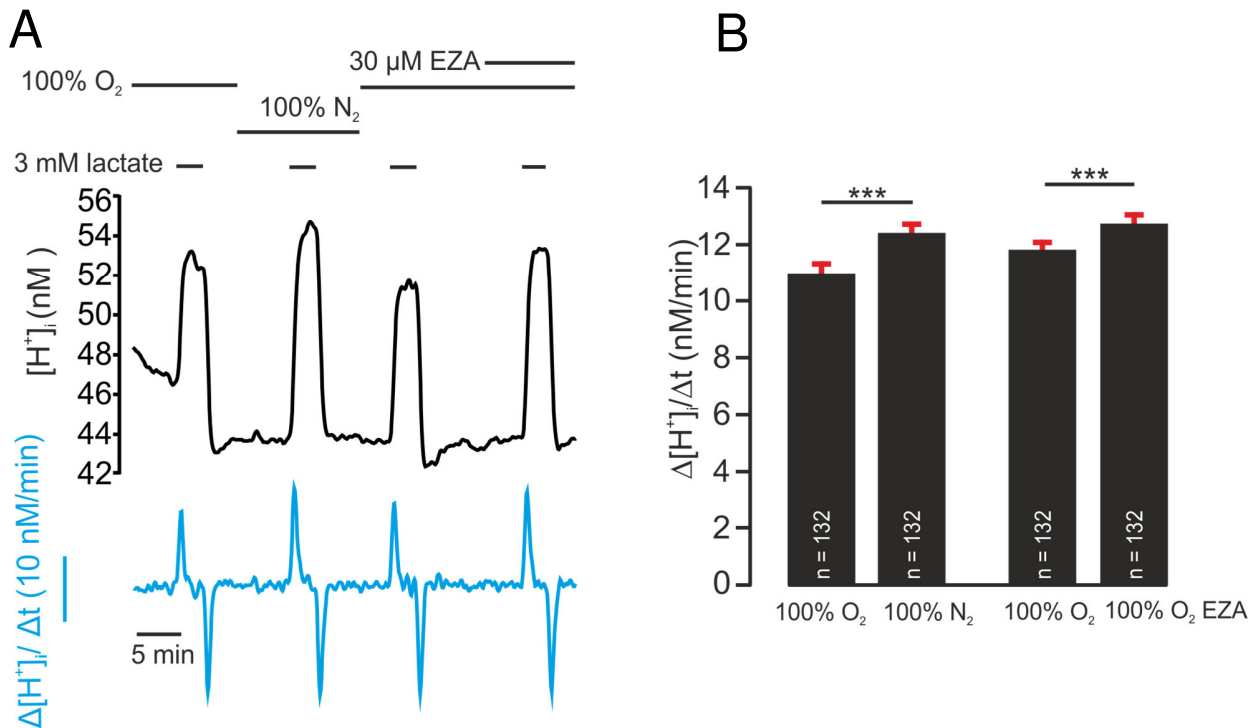


**Figure 45** Effect of cellular respiration on lactate uptake

In HEPES-only-buffered solution, either gassed with 100% O<sub>2</sub> or 100% N<sub>2</sub>, lactate induced H<sup>+</sup> concentration changes were measured. **A** Recordings of H<sup>+</sup>-imaging. The lactate induced changes in cytosolic H<sup>+</sup>-concentration are shown in the upper part as **black** traces. In the lower part, Δ[H<sup>+</sup>]<sub>i</sub>/Δt is shown in **blue**. **B** Statistics of the lactate induced Δ[H<sup>+</sup>]<sub>i</sub>/Δt.

### 3.3.4 Functional interaction of MCT with NHE and/or NBC

#### 3.3.4.1 Impact of NHE on lactate uptake

The effect of NHE on the lactate flux was tested with lactate imaging by the use of the NHE inhibitor cariporide (Figure 46). When lactate (3 mM) was applied in the presence of the NHE inhibitor cariporide (30 μM), Δ[lac<sup>-</sup>]<sub>i</sub>/Δt (0.0183 ± 0.0017 Δa.u./min) was not differing from Δ[lac<sup>-</sup>]<sub>i</sub>/Δt (0.0186 ± 0.0016 Δa.u./min) measured in the absence of cariporide.

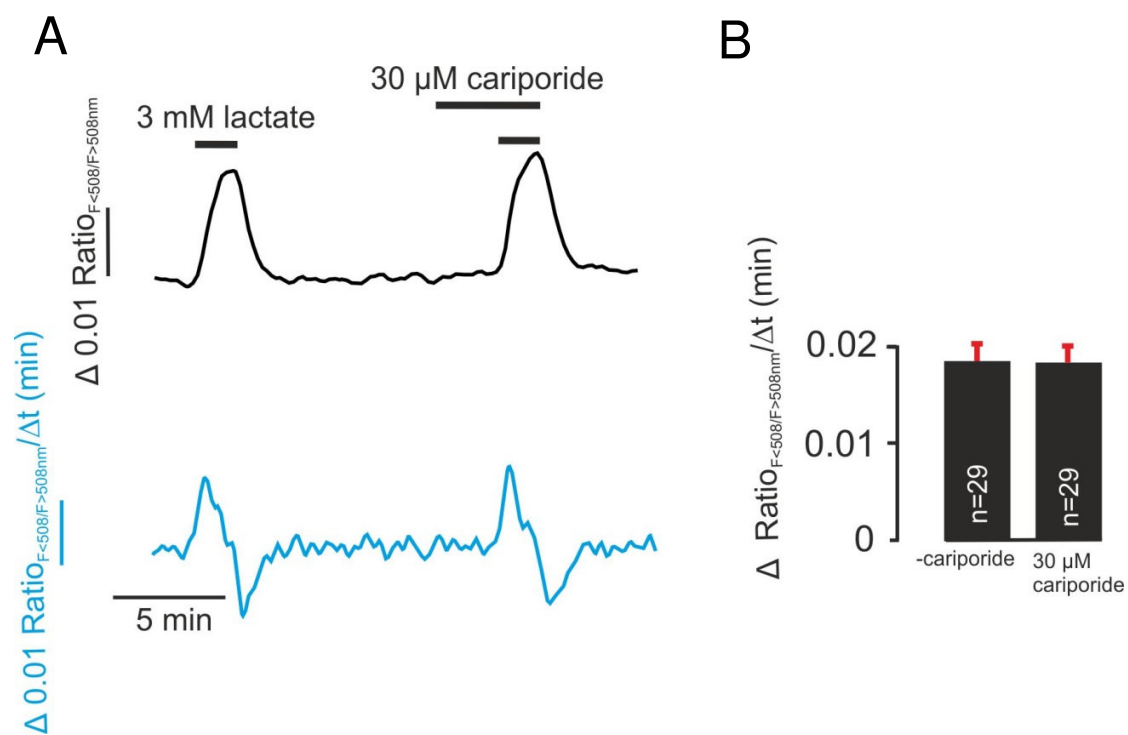


**Figure 46** Effect of NHE on lactate influx

**A** Lactate imaging of cardiomyocytes expressing the lactate sensor *Laconic*. 3 mM lactate were applied in absence and presence of 30  $\mu$ M cariporide.  $\Delta[\text{lac}]_i/\Delta t$  is shown in blue. **B** Statistics. For this experiment, 1 black-6 mouse was used at an age of p20. The measurements were performed at day 4 *in vitro*.



### 3.3.4.2 S0859 inhibits lactate-induced acidification

The impact of the NBC in the lactate transport was tested by utilization of the NBC inhibitor S0859.

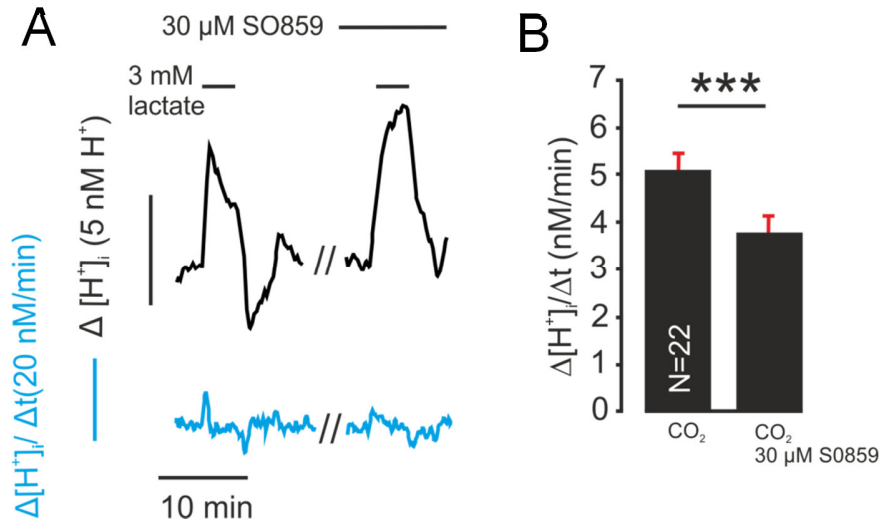


**Figure 47** S0859 inhibits lactate induced  $\Delta [H^+]_i / \Delta t$

**A** 3 mM lactate were bath applied in the absence and presence of the NBC inhibitor S0859. Recordings of  $H^+$ -imaging (**black**).  $\Delta [H^+]_i / \Delta t$  is shown in **blue**. **B** Statistics of  $\Delta [H^+]_i / \Delta t$ .

When lactate (3 mM) was applied to cardiomyocytes in the presence of S0859 (30  $\mu$ M), the lactate induced  $\Delta [H^+]_i / \Delta t$  decreased by 26% from  $5.1 \pm 0.35$  nM/min to  $3.8 \pm 0.25$  nM/min (Figure 47).

### 3.3.5 Lactate metabolism

Experiments to test cardiomyocytes' lactate metabolism were performed with cells artificially expressing the lactate sensor *Laconic*. Lactate was applied at a concentration of 3 mM in the presence of glucose (1 mM). When the lactate signal had been in a plateau for 10 min, the MCT inhibitor ARC155858 was added at a concentration of 300 nM (Figure 48). The intracellular lactate concentration dropped with a  $\Delta [lac^-]_i / \Delta t$  of  $0.0027 \pm 0.00036$   $\Delta a.u. / \text{min}$ .

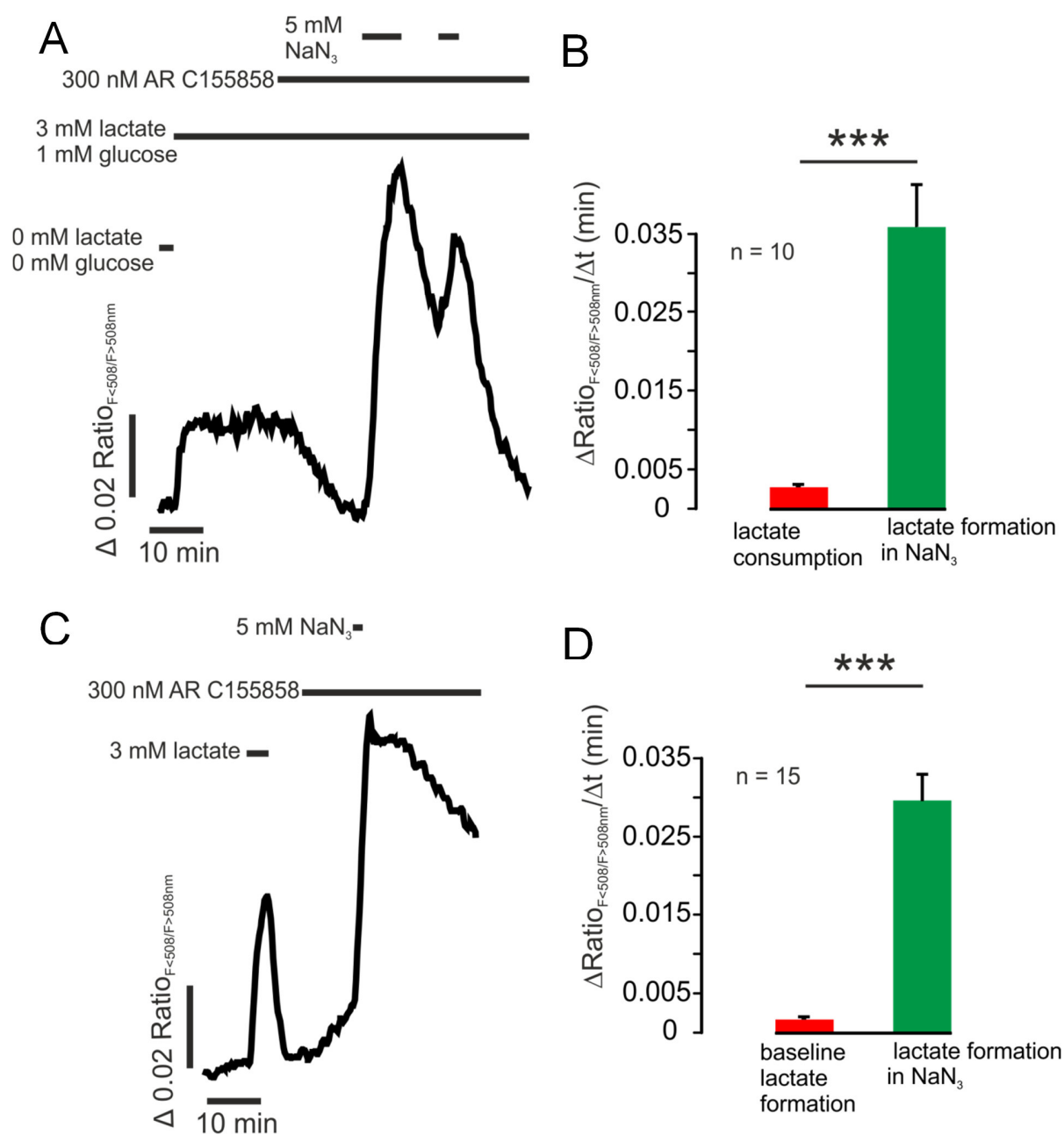


**Figure 48** Lactate metabolism in mouse cardiomyocytes

**A** Averaged recording of 5 *Laconic* (lactate sensor) expressing cardiomyocytes. In presence of lactate (3 mM), the MCT1/MCT2 inhibitor AR C155858 was bath applied to prohibit lactate exchange. **B** Statistics of drop and rise of  $[\text{lac}]_i$  in presence of AR C155858 after cellular lactate load and inhibition of the respiratory chain with  $\text{NaN}_3$ , respectively. **C** Averaged recording of 13 cardiomyocytes expressing the lactate sensor *Laconic*. **D** Statistics of the rise of  $[\text{lac}]_i$  after application of AR C155858 and after inhibition of the respiratory chain with  $\text{NaN}_3$ , respectively.

When the respiratory chain was inhibited with  $\text{NaN}_3$  (5 mM) in the presence of ARC155858 (300 nM), the intracellular lactate concentration rose with a  $\Delta[\text{lac}]_i/\Delta t$  of  $0.035 \pm 0.0054$

$\Delta$ a.u./min. When ARC155858 was applied in the absence of extracellular lactate, the intracellular lactate concentration rose with a  $\Delta[\text{lac}^-]_i/\Delta t$  of  $0.002 \pm 0.00036 \Delta$ a.u./min.

The inhibition of MCT with ARC155858 after cellular lactate load caused a decrease of intracellular lactate concentration. If this was due to lactate consumption, cellular uptake of lactate must have been converted to pyruvate. This was tested with pyruvate imaging (Figure 49). When lactate was applied to cardiomyocytes expressing the pyruvate sensor *Pyronic*, an increase in  $[\text{lac}^-]_i$  was observed.

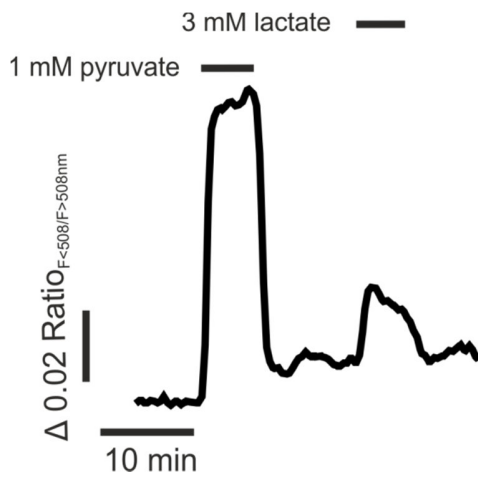


**Figure 49** Cytosolic conversion of lactate to pyruvate

Recording of a cardiomyocyte, expressing the pyruvate sensor. 1 mM pyruvate and 3 mM lactate were bath applied. N=10

# 4. DISCUSSION

---

## 4.1 Discussion - Proteins (CAs, MCTs, NBC and NHE in mouse cardiomyocytes)

### 4.1.1 Discussion - Proteins - Carbonic anhydrases in mouse cardiomyocytes

#### 4.1.1.1 Intracellular carbonic anhydrase

Intracellular CA activity in ventricular rat cardiomyocytes was reported by Schroeder et al. (2013) and Villafuerte et al. (2014). In western blot experiments, Alvarez et al. (2013 and 2007) detected the cytosolic CAII in human, rat and mouse heart, Schroeder et al. (2013) detected the CAII in the rat heart, too. In contrast, Geers et al. (1992), Vuillemin and Pexieder (1997) and Vandenberg et al. (1996) report evidence for the absence of CAII from rabbit, post natal mouse and ferret cardiomyocytes, respectively. Roughton (1935) reports the complete absence of CA activity from the heart, but does not specify which species had been investigated.

Attempts to detect the CAII in mouse cardiomyocytes with immunohistochemistry resulted in signals in WT and CAII<sup>-/-</sup> animals. There was a minimal chance that the signal in the CAII<sup>-/-</sup> animals might have been caused by CAII fragments. But this can be excluded because CAII signals were absent from CAII<sup>-/-</sup> samples in Western blot experiments. If CAII fragments would have caused the signals in CAII<sup>-/-</sup> cardiomyocytes, a protein, smaller than CAII should have been detected in the Western blot. Thus, it must be concluded that CAII detection with immunohistochemistry failed due to unspecific antibody binding. In western blot experiments, the CAII was detected in the WT heart but this is most likely due to erythrocytes that could not be completely removed from the sample (Geers et al., 1992) and which contain CAII (Sly and Hu, 1995). Intracellular CA activity was not observed in mouse cardiomyocytes in this work. This conclusion is based on the finding that the CA inhibitor EZA (30  $\mu$ M) did not have a significant effect on the intracellular CO<sub>2</sub>-induced acidification. When the same experiment was performed with MCF-7 cells (Somayeh Jamali, personal communication) or with 10  $\mu$ M EZA in astrocytes from brain slices (Stridh et al., 2012), CA inhibition resulted in a significant reduction in the speed of CO<sub>2</sub>-induced acidification. Astrocytes and MCF-7 cells are reported to contain CAII (Stridh et al., 2012 and Somayeh Jamali, personal communication, respectively). Therefore, in cardiomyocytes a similar effect should have been observed if cytosolic, EZA

sensitive CA would have been present. This led to the last option for intracellular CA activity in mouse cardiomyocytes: the CAIII. This isoform has been reported to have a comparatively high  $K_i$  for EZA (60  $\mu\text{M}$ ; Geers et al., 1992) and therefore might not have been inhibited at a concentration of 30  $\mu\text{M}$ . In addition, western blot experiments revealed that the used antibody for CAII detection also detects CAIII. But in immunohistochemistry experiments, no signals for CAIII were observed in mouse heart sections. Signals for CAIII in the soleus muscle, as reported for the rat soleus muscle (Shiels et al. 1982), confirmed that antibody and staining procedure worked, so that it can be concluded that CAIII is absent from the mouse heart, as previously reported by Tweedie and Edwards (1989).

However, the live cell imaging experiments by Schroeder et al. (2013) and Villafuerte et al. (2014) provide strong evidence for cytosolic CA activity in rat cardiomyocytes. The discrepancy between this work and the reports by Schroeder et al. (2013) and Villafuerte et al. (2014) about intracellular CA activity might be due to the fact that they have been working on rat, whereas experiments in this work have been performed with mouse cardiomyocytes.

#### 4.1.1.2 Extracellular carbonic anhydrase

Different membrane bound, extracellular CAs have been reported in mouse cardiomyocytes. Scheibe et al. (2006) reported the isoforms CAIV, CAIX and CAXIV on the protein level in mouse cardiomyocytes. Alvarez et al. (2013) detected the CAIV and CAXIV in the human and mouse heart. Sender et al. (1998) reported the CAIV in the human and rat heart. Furthermore, Geers et al. (1992) could detect CA activity in the membrane fraction of lysed rabbit hearts and Vandenberg et al. (1996) could observe CA activity at the sarcolemma of cardiomyocytes from the ferret heart. In this work, the presence of extracellular, EZA-sensitive CA activity on mouse cardiomyocytes was confirmed by  $\text{H}^+$  imaging. But it was not clarified which isoform is responsible for the observed activity.

Scheibe et al. (2006) compared wild type and CAIV-KO animals in western blot and immunocytochemistry experiments. In their study they detect the CAIV in heart samples of wild type animals but not in CAIV-KO animals, indicating that the antibody used is specific. In immunocytochemistry experiments they found a CAIV signal in mouse cardiomyocytes that was abolished by antibody pre-absorption and absent from CAIV-KO animals. Their approach includes all possible controls and therefore it must be considered valid. In contrast, in this work

the CAIV was detected in the mouse heart with western blot at the correct size of approximately 30 kDa (Klier et al. 2013). With immunohistochemistry experiments on sections of the WT and in CAIV KO mouse heart, the CAIV was detected in the WT samples but was absent from the CAIV KO. This indicates that antibody and staining procedure lead to specific signals. However, immunocytochemistry on dissociated heart samples revealed that the CAIV signals are not derived from cardiomyocytes, but from round cells that were not further identified during this work. Since the murine heart is reported to consist of about 30% fibroblasts (Banerjee et al., 2007), those might be likely candidates.

The CAIX was found to be hypoxia and cancer associated and provides therefore hope as new target for cancer therapies (Ivanov et al., 1998; Pastorekova et al., 2004; Potter and Harris, 2008; Robertson et al., 2004). As the CAIX grows more and more interesting as potential cancer target, more and more research is focusing on this isoform. Recent research questions an exclusive relation to cancer. Orlowski et al. (2012) reports the CAIX in rat cardiomyocytes, whereas Scheibe et al. (2006) found the CAIX in mouse cardiomyocytes. Hilvo et al. (2004) could not find CAIX mRNA in the mouse heart, but in several other tissues, including lungs, kidney, liver, stomach and intestine (see also: Gut et al., 2002 and Pan et al., 2012). If CAIX's presence in the human heart would be confirmed, its use as cancer therapy target might be questioned. Anyway, CAIX's presence in the heart would be surprising because the CAIX is reported to be linked to hypoxia (Wykoff et al., 2000), which is not expected to occur in healthy myocardial tissue. Therefore, CAIX's presence in the mouse heart would need to be hypoxia-independent and mediated by some other pathways than via hypoxia-inducible factor 1 (HIF-1). However, CAIX's presence in mouse cardiomyocytes was neither confirmed nor excluded in this work. With immunohistochemistry, CAIX signals were detected in heart sections as well as in stomach sections. In CAIX<sup>-/-</sup> animals, CAIX signals were present in stomach sections, too. This can be either explained by unspecific antibody binding or by CAIX fragments in the KO animal. In the CAIX<sup>-/-</sup> animals the gene Car9 is not removed but the enzymatic function is destroyed by a nonsense insertion into exon 1 (Gut et al., 2002). Therefore, it is thinkable that the CAIX epitopes are still present in CAIX<sup>-/-</sup> animals. But Gut et al. (2002) did not report any CAIX signals in western blot or immunohistochemistry experiments with CAIX<sup>-/-</sup> stomach samples. In addition, in the work by Scheibe et al. (2006) no signals were observed in CAIX<sup>-/-</sup> cardiomyocytes. Therefore, unspecific antibody binding in this work appears likely, even though

the observed staining pattern matches the reported CAIX distribution in the stomach, where the strongest signals were observed in the epithelium (Gut et al., 2002).

However, it remains unclear which CA isoform is responsible for the observed extracellular CA activity.

#### 4.1.2 MCTs in mouse cardiomyocytes

The lactate transport across the sarcolemma in cardiomyocytes is mediated by mono-carboxylate transporters (MCTs). Bonen (2001) found weak evidence of MCT4's presence in the human heart and MCT4 detection in rat heart remained negative. The MCT2 mRNA was not detected in the mouse heart (Jackson et al., 1997) whereas the results of Koehler-Stec et al. (1998) provided a very faint signal for MCT2 mRNA in the mouse heart (Koehler-Stec et al., 1998; Fig. 5). Pierre and Pellerin (2005) report that MCT2 was not detected in mouse heart samples with western blot, even though their results contain a faint signal for MCT2 in heart samples (Pierre and Pellerin, 2005; Fig. 1). However, there is only weak evidence for MCT2's presence in the mouse heart. The only isoform, whose presence in the heart has been confirmed by several authors is the MCT1 (Bonen, 2001; Koehler-Stec et al., 1998; Lin et al., 1998; Martinov et al., 2009; Pierre and Pellerin, 2005).

The  $K_m$  value for lactate uptake, determined in this work by lactate imaging is 2 mM. This value matches the values reported for MCT1 (3.5 mM; Bröer et al., 1998), when expressed in *Xenopus* oocytes. The  $K_m$  for the lactate-induced acidification, determined by  $H^+$  imaging from  $\Delta[H^+]_i / \Delta t$  is 17 mM and therefore suggests the presence of an additional lactate transporter with a higher  $K_m$ . The best candidate would be the MCT4 ( $K_m$ : 28 mM Fox et al., 2000), which was shown to be absent from mouse cardiomyocytes in this work. Hence, the cause for this high  $K_m$  must have other reasons.

When the buffer ratio was plotted against the basal  $[H^+]_i$  of individual cardiomyocytes, an exponential relation was observed. This means that the buffer ratio changes when  $[H^+]_i$  changes. Therefore, a doubled  $J_{A/B}$  would not lead to a doubled  $\Delta[H^+]_i / \Delta t$ , because the buffer ratio adapts during  $J_{A/B}$ . When lactate was applied to the cardiomyocytes at a concentration of

1 mM, the measured maximal  $\Delta[\text{H}^+]_i / \Delta t$  was 4.96 nM/min. If lactate was applied at a concentration of 10 mM,  $\Delta[\text{H}^+]_i / \Delta t$  was 36.31 nM/min. This means that the lactate-induced cytosolic  $\text{H}^+$  load is 7.3 times faster when the applied concentration is increased from 1 mM to 10 mM. The calculated  $J_{A/B}$  by the use of the adaptive buffer ratio was determined to be 0.48 mM/min when lactate was applied at a concentration of 1 mM and increased to 2.79 mM/min when the concentration of applied lactate was increased to 10 mM. This is a factor of 5.8. So, the measured  $\Delta[\text{H}^+]_i / \Delta t$  seems to provide a distorted picture of  $J_{A/B}$ . This is caused by the fact that the buffer ratio reduces with increasing  $[\text{H}^+]_i$ . Thus, the same amount of  $\text{H}^+$  entering the cell from a higher baseline but within the same time will cause a higher  $\Delta[\text{H}^+]_i / \Delta t$ . Consequently, the bigger  $J_{A/B}$ , the stronger  $\Delta[\text{H}^+]_i$  will be enhanced by the falling buffer ratio. This is probably the reason for the high  $K_m$  as determined from  $\Delta[\text{H}^+]_i / \Delta t$ . When the  $K_m$  was determined with  $J_{A/B}$  as calculated according to the adaptive buffer ratio, it was determined to be 7.6 mM. This is still a little bit higher than the 3.5 mM as reported by Bröer et al. (1998) or the 2 mM that were determined by lactate imaging, but it is in the same range. The reason for the slight mismatch of the  $K_m$  of 7.6 mM might be due to the small number of cells ( $n=49$ ) used for the determination of the buffer ratio, which might have caused the weak  $R^2$  of the fit for the adaptive buffer ratio ( $R^2 = 0.6$ ). Since the lactate imaging data show the real lactate flux, the  $K_m$  for lactate uptake into mouse cardiomyocytes, as determined by lactate imaging is more reliable. This view is supported by the finding that the determined  $K_m$  (2 mM) suits best the MCT1, which is the only MCT that was identified in mouse cardiomyocytes among MCT1, MCT2 and MCT4 in this work.

#### 4.1.3 NHE and NBC activity in mouse cardiomyocytes

The acid extruders NHE1 (Aiello et al., 1998; Ch'en et al., 2008; Choi et al., 2000; Garciarena et al., 2013; Khandoudi et al., 2001; Yamamoto et al., 2005) and NBCe1 (Ch'en et al., 2008; Yamamoto et al., 2005) are reported to be present in cardiomyocytes. In this work, the presence of NHE and NBC activity in ventricular mouse cardiomyocytes was observed.

In experiments in which mouse cardiomyocytes were acidified with  $\text{NH}_4\text{Cl}$ -prepulse in HEPES-only-buffered medium, in presence of the NHE inhibitor cariporide (30  $\mu\text{M}$ ; Ch'en et al., 2008; Orłowski and Grinstein, 2003), acid extrusion in  $\Delta[\text{H}^+]_i / \Delta t$  was reduced by 86% and  $J_{A/B}$  was



reduced by 78%. This points to NHE activity in mouse cardiomyocytes, unless cariporide has some unknown, unspecific side effects.

When  $\text{CO}_2/\text{HCO}_3^-$  was introduced to  $\text{NH}_4\text{Cl}$ -prepulse acidified cells, whose acid extrusion had been inhibited by cariporide, acid extrusion accelerated. This points to a  $\text{HCO}_3^-$ -dependent acid extruding mechanism. In sodium free,  $\text{CO}_2/\text{HCO}_3^-$ -buffered medium, acid extrusion in  $\Delta[\text{H}^+]_i / \Delta t$  was reduced by 63%,  $J_{\text{A/B}}$  was reduced by 76,7%. This indicates a partial sodium dependence of the  $\text{HCO}_3^-$ -dependent acid extruding mechanism. Therefore, the presence of a NBC isoform is likely. Ch'en et al. (2008) and Yamamoto et al. (2005) reported the electrogenic NBCe1 in rat cardiomyocytes. In this work, depolarisation of ventricular mouse cardiomyocytes with high extracellular potassium concentrations (40 mM) did not alter acid extrusion. In addition, western blot experiments confirmed the absence of NBCe1 from the mouse heart. Therefore, mouse cardiomyocytes might contain an electroneutral NBC.

Choi et al. (2000) detected the NBCn1 on the RNA level in the rat heart. Ch'en et al. (2008) reported that acid extrusion from rat cardiomyocytes in  $\text{CO}_2/\text{HCO}_3^-$ -buffered medium was completely abolished when the NHE and NBC activity were inhibited with cariporide and the NBC inhibitor S0859. Therefore it can be concluded that S0859 inhibits the NBCe1 and the NBCn1. In this work, application of S0859 (30  $\mu\text{M}$ ) in the presence of cariporide (30  $\mu\text{M}$ ) partially inhibited acid extrusion. In 24% of the measured cardiomyocytes, S0859 caused a reduction in acid extrusion ( $\Delta[\text{H}^+]_i / \Delta t$ ) of 90% or more. 22.6% of the cardiomyocytes show inhibition of 50% or more. 33.9 % of the cells showed less than 10% inhibition and are therefore considered as S0859-insensitive. Hence, an additional, S0859-insensitive,  $\text{HCO}_3^-$ -dependent acid extruding mechanism must be active in ventricular mouse cardiomyocytes. This mechanism is most likely coupled to sodium because acid extrusion in cells insensitive to S0859 was reduced when extracellular sodium was absent. In addition, in 20% of the cells, acid extrusion in absence of extracellular sodium was reduced by less than 10%. In total,  $J_{\text{A/B}}$  was reduced by 94% in HEPES-only-buffered conditions, whereas in  $\text{CO}_2/\text{HCO}_3^-$  buffer,  $J_{\text{A/B}}$  was just reduced by 76.7% if extracellular sodium was absent. This may indicate a third acid extruding mechanism, which is independent of sodium but depends on  $\text{CO}_2/\text{HCO}_3^-$  buffer. The S0859-insensitive and  $\text{Na}^+$ -independent mechanism are not described in the literature so far and may therefore provide an option for future research.

The absence of electrogenic NBC activity from cardiomyocytes appears logical in view of their excitability. Cytosolic acidification would activate the electrogenic NBC, which would hyperpolarize the cell. This would reduce excitability, which would be in contrast to the findings by Garciarena et al. (2013), who reported that cardiomyocytes compensate reduced contractility during acid load by elevated cytosolic  $\text{Ca}^{2+}$  levels. Therefore cardiomyocytes' strategy while facing  $\text{H}^+$  load seems to be the maintenance of contractility rather than its reduction. In addition, an electrogenic NBC would get active when the cell contracts. Especially in cardiomyocytes, which possess a comparatively long phase of depolarisation in comparison to neurons (Schmidt et al., 2005), an electrogenic NBC would inhibit the sodium/calcium-exchanger, as reported by Garciarena et al. (2013) via cytosolic  $\text{Na}^+$  load. But these speculations are contradictory to the detection of NBCe1 activity in the rat, rabbit and guinea-pig cardiomyocytes (Yamamoto et al., 2005). Obviously, in those species the potential disadvantages of electrogenic NBC activity do not affect heart activity. Why, and if electrogenic NBC activity might even be beneficial in those species cannot be answered here.

No matter which NBC or NBC-like isoform is present in mouse cardiomyocytes, its activity strongly depends on the activity of extracellular CA. When the maximal acid extruding  $J_{\text{A/B}}$  after  $\text{NH}_4\text{Cl}$  induced acid load was calculated based on the adaptive buffer ratio, a reduction of 78.4% was observed when CA was inhibited with EZA. Since no intracellular CA activity had been observed during this work, the EZA effect must be caused by inhibition of extracellular CA. Thus it can be concluded that in ventricular mouse cardiomyocytes the activity of extracellular CA is of crucial importance for the NBC function.

#### 4.1.3.3 NHE vs. NBC activity in mouse cardiomyocytes

In  $\text{CO}_2/\text{HCO}_3^-$  buffer, the  $\text{Na}^+$ -dependent but cariporide insensitive acid extruding mechanism contributes 53.8% of mouse cardiomyocytes total acid extruding  $J_{\text{A/B}}$ . This fraction is most likely related to electroneutral NBC activity and is composed of a S0859 sensitive and a S0859 insensitive isoform. 22.9% of acid extrusion is cariporide sensitive and is therefore considered to be contributed by NHE. 23.2% of acid extruding  $J_{\text{A/B}}$  are neither  $\text{Na}^+$  nor cariporide-sensitive. Therefore, an acid extruding mechanism in addition to NHE and NBC must be present in ventricular mouse cardiomyocytes.

## 4.2 Buffer capacity vs. fixed and adaptive buffer ratio

The classic measure for the cellular H<sup>+</sup> buffering ability is the buffer capacity (Vaughan-Jones et al., 2002; Leem et al., 1999; Zamboni et al. 2003). The intrinsic buffer capacity in guinea-pig cardiomyocytes was reported to increase when the pH drops and was determined to be approximately 25 mM at pH 7.2 (Leem et al., 1999). This is in line with the intrinsic buffer capacity as determined by Zamboni et al. (2003) for rat, rabbit and guinea-pig cardiomyocytes. The CO<sub>2</sub>/HCO<sub>3</sub><sup>-</sup>-dependent buffer capacity was reported to increase with the cytosolic pH and was determined to be approximately 25 mM at pH 7.2 (Leem et al., 1999). The total buffer capacity  $\beta_{\text{tot}}$  as the sum of  $\beta_i$  and  $\beta_{\text{CO}_2}$  was found to increase with the cytosolic pH and was determined to be 50 mM at pH 7.2.

In this work, the buffer capacity of ventricular mouse cardiomyocytes was determined to be 8.8 mM at pH 7.18 in HEPES-only-buffered and 30.24 mM at pH 7.22 in CO<sub>2</sub>/HCO<sub>3</sub><sup>-</sup>-buffered conditions. Here, the buffer capacity as determined in HEPES-only-buffered conditions might be considered as  $\beta_i$ . But the cellular respiration might have produced enough CO<sub>2</sub> to provide significant CO<sub>2</sub>/HCO<sub>3</sub><sup>-</sup> buffering. This was not tested during this work but the experiments for lactate uptake in N<sub>2</sub>- and O<sub>2</sub>-gassed condition provide evidence for a contribution of endogenous CO<sub>2</sub> formation to the buffering. To be on the safe side, the common terms  $\beta_i$  and  $\beta_{\text{CO}_2}$  are not used in this work. However, the values for the buffer capacity as determined in this work are a bit smaller than those reported by Leem et al. (1999) for guinea-pig cardiomyocytes but they are in the same range. When the CA was inhibited with EZA, the buffer capacity was determined to be 13.1 mM. This is a reduction of the buffer capacity by 56.7%, which means that more than half of the buffer capacity in CO<sub>2</sub>/HCO<sub>3</sub><sup>-</sup>-buffered conditions is dependent on the activity of extracellular CA. This can be explained by extracellular CA's effect on the NBC activity. Theparambil et al. (2014) could show that in cortical astrocytes, the NBCe1 is defining the CO<sub>2</sub>/HCO<sub>3</sub><sup>-</sup>-dependent buffer capacity. Therefore, also other NBC isoforms might contribute to the cellular buffer capacity.

Another way to describe the cellular H<sup>+</sup> buffering properties is the so called buffer ratio  $\rho$  (Michael Dietrich, unpublished). The difference between  $\beta$  and  $\rho$  is:  $\beta = \Delta[B^-]_i / \Delta\text{pH}_i$  whereas  $\rho = \Delta[B^-]_i / \Delta[H^+]_i$ . It appears to be more intuitional to consider the  $\Delta[H^+]_i$  than  $\Delta\text{pH}_i$  because of the

logarithmic nature of pH. This means that if the pH changes from 7.0 to 6.0 or 8.0,  $\Delta\text{pH}_i$  is 1. But if the same pH change is considered as  $[\text{H}^+]_i$ , pH 7.0 is a  $[\text{H}^+]_i$  of 100 nM, pH 6.0 is a  $[\text{H}^+]_i$  of 1000 nM and pH 8.0 is a  $[\text{H}^+]_i$  of 10 nM. Hence,  $\Delta[\text{H}^+]_i$  from pH 7.0 to 6.0 is 900 nM whereas  $\Delta[\text{H}^+]_i$  from pH 7.0 to 8.0 is 90 nM, so 10 times less. Thus, if the intracellular concentration of free  $\text{H}^+$  is measured in  $\Delta\text{pH}_i$ , acidifications are smaller and alkalinisations are bigger than in  $\Delta[\text{H}^+]_i$ .

However, the use of  $\beta$  and  $\rho_{\text{fixed}}$  in this work is the calculation of  $J_{A/B}$ . For this, the measured  $\Delta\text{pH}_i/\Delta t$  was multiplied with  $\beta$  and the measured  $\Delta[\text{H}^+]_i/\Delta t$  was multiplied with  $\rho_{\text{fixed}}$ . This was done for the lactate-induced acidification in HEPES-only-,  $\text{CO}_2/\text{HCO}_3^-$ - and  $\text{CO}_2/\text{HCO}_3^-$ -buffered conditions in the presence of EZA (30  $\mu\text{M}$ ). The  $J_{A/B}$  derived from  $\Delta\text{pH}_i/\Delta t$  and  $\beta$  shows a similar behaviour as the lactate flux measured with lactate imaging. The  $J_{A/B}$  derived from  $\Delta[\text{H}^+]_i/\Delta t$  and  $\rho_{\text{fixed}}$  shows a similar behaviour as the lactate flux in HEPES and  $\text{CO}_2/\text{HCO}_3^-$  conditions, but the effect caused by EZA is less prominent than in the lactate flux. In lactate imaging experiments, the reduction of lactate influx by inhibition of CA was 27%, the reduction of  $J_{A/B}$  derived from  $\Delta\text{pH}_i/\Delta t$  and  $\beta$  was 48.9% and the reduction of  $J_{A/B}$  derived from  $\Delta[\text{H}^+]_i/\Delta t$  and  $\rho_{\text{fixed}}$  was 19.2%.

The determined  $\beta$  and  $\rho$  were plotted against the basal pH and  $[\text{H}^+]_i$ , respectively.  $\beta$  showed a broad scattering and no clear correlation with the basal pH. In contrast, for  $\rho$  an exponential correlation with the basal  $[\text{H}^+]_i$  was obvious, even though the  $R^2$  for  $\text{CO}_2/\text{HCO}_3^-$  conditions was weak. This might have been due to a small n number. However, the buffer ratio increases when  $[\text{H}^+]_i$  drops. Hence, a fixed, averaged value for  $\rho$  must cause an error in the calculated  $J_{A/B}$  as individual cells possess individual basal  $[\text{H}^+]_i$  and because  $\rho$  will change during  $J_{A/B}$ . The equation of the fit describing the correlation was used to convert the SNARF recordings, that had been calibrated to  $[\text{H}^+]_i$ , to  $\rho/t$ . So, a trace showing the buffer ratio at each moment of the measurement was produced. This buffer ratio will take into account individual variations of the basal  $[\text{H}^+]_i$  and corrects the changes of  $\rho$  during  $J_{A/B}$ . This buffer ratio was named adaptive buffer ratio  $\rho_{\text{adap}}$ .

When the  $J_{A/B}$  was determined with  $\rho_{\text{adap}}$ , application of EZA caused a reduction of 42.8% s. This is quite close to the effect determined with  $\beta$ . But the EZA effect observed with  $\rho_{\text{adap}}$  and  $\beta$  is much stronger than the effect observed with lactate imaging. The effect observed with  $\rho_{\text{fixed}}$  is much closer to the effect observed with lactate imaging. Thus, additional evidence for the advantage of  $\rho_{\text{adap}}$  and  $\beta$  over  $\rho_{\text{fixed}}$  is needed. This evidence is derived from the determination

of the  $K_m$  for lactate induced  $J_{A/B}$  in mouse cardiomyocytes. For the  $\rho_{\text{fixed}}$  calculated  $J_{A/B}$  a  $K_m$  of 15 mM was determined, whereas  $\beta$  calculated  $J_{A/B}$  provides a  $K_m$  10 mM. The  $\rho_{\text{adap}}$  calculated  $J_{A/B}$  reveals a  $K_m$  of 7.6 mM. This is much closer to the  $K_m$  of 2 mM as determined by lactate imaging. Since the MCT1 is the only MCT that was detected in the mouse heart and since its  $K_m$  was determined to be 3.5 mM in *Xenopus* oocytes (Bröer et al., 1998), the true  $K_m$  should be found in the range below 10 mM. Thus, based on the  $K_m$  determination,  $\rho_{\text{adap}}$  is the most reliable measure for the cellular  $H^+$  buffering ability.

#### 4.3 Lactate transport and physiological implementation

The heart is a highly oxidative tissue (Ventura-Clapier et al., 2003). Glucose, fatty acids and lactate are reported to be utilised to meet cardiomyocytes' energy needs (Baker et al., 1998; Bergman et al., 2009; Gertz et al., 1988; Gladden, 2007; Johannson et al., 2001; Kemppainen et al., 2002; Wahl et al., 2009). Consequently, it produces  $CO_2$ . As  $CO_2$  equilibrates in water with  $HCO_3^-$  and  $H^+$ , its release potentially acidifies the cell. Therefore it appears plausible to minimize the residence time in the cytosol.  $CO_2$  diffuses as fast as  $1.85\text{-}1.89 \times 10^5 \text{ cm}^2/\text{s}$  at  $25^\circ\text{C}$  in water (Unver and Himmelblau, 1964 Maharajh and Walkley, 1972), so it may quickly reach the membrane and leave the cell if it is not hindered. Intracellular CA activity would slow down the  $CO_2$  efflux, because  $HCO_3^-$  is reported to have a diffusion coefficient in water of  $1.185 \times 10^{-5} \text{ cm}^2/\text{s}$  (Vanysek, 2000) and was calculated to be even slower in the cytosol ( $77 \times 10^{-7} \text{ cm}^2/\text{s}$ , Swietach et al., 2003).  $H^+$  diffuse, as previously mentioned, slow inside cardiomyocytes ( $8\text{-}12 \times 10^{-7} \text{ cm}^2/\text{s}$  Zamboni et al., 2003). Thus, the intracellular conversion of  $CO_2$  does not only cause intracellular  $H^+$  load, but also slows down the efflux of  $CO_2$ . Hence, the absence of cytosolic CA activity might be beneficial for the release of  $CO_2$  from mouse cardiomyocytes. In contrast, extracellular CA might convert cell derived  $CO_2$  to  $HCO_3^-$  and  $H^+$  and thereby keeps the  $CO_2$  gradient steep. In addition,  $HCO_3^-$  and  $H^+$  could not arbitrarily diffuse across the tissue but their movement would rely on buffering and  $HCO_3^-$  transporting mechanisms, so it can be regulated. Heming et al. (1994) reported that just extracellular CA activity is contributing to  $CO_2$  equilibration across alveolar capillaries which might be similar in cardiomyocytes. Vandenberg et al. (1996) refer the original idea of a beneficial effect of missing cytosolic CA activity on the  $CO_2$  venting to Roughton (1935), thus it is not a very recent hypothesis. Vandenberg et al.

(1996) could show that extracellular but not intracellular CA activity supports CO<sub>2</sub> venting in the ferret heart. In this work, extracellular but not intracellular CA activity was observed, which allows the speculation that in the mouse heart CO<sub>2</sub> venting depends on extracellular CA activity, too. The extracellular conversion of CO<sub>2</sub> to HCO<sub>3</sub><sup>-</sup> and H<sup>+</sup> might support the uptake of lactate via MCT as it provides H<sup>+</sup>. At the same time, the extracellular formation of HCO<sub>3</sub><sup>-</sup> might support the cellular HCO<sub>3</sub><sup>-</sup> uptake via NBC. If the NBC was more active, HCO<sub>3</sub><sup>-</sup> influx would increase and thereby support intracellular H<sup>+</sup> buffering. Consequently, the intracellular H<sup>+</sup> load, caused by MCT, would reduce and allow faster lactate influx. The functional interaction of MCT and NBC has been shown by Becker et al. (2004) in *Xenopus* oocytes and the functional interaction of NBC and extracellular CA has been observed as well (Alvarez et al., 2003; Morgan et al., 2007; Orłowski et al., 2012). Wetzell et al. (2001) showed that the lactate uptake into skeletal muscle depends on the activity of extracellular CA. This might indicate a functional interaction of MCT and extracellular CA but, according to the mentioned interactions CA/NBC and NBC/MCT, it is also thinkable that the observed effect is due to an indirect interaction of extracellular CA and MCT via NBC (CA→NBC→MCT).

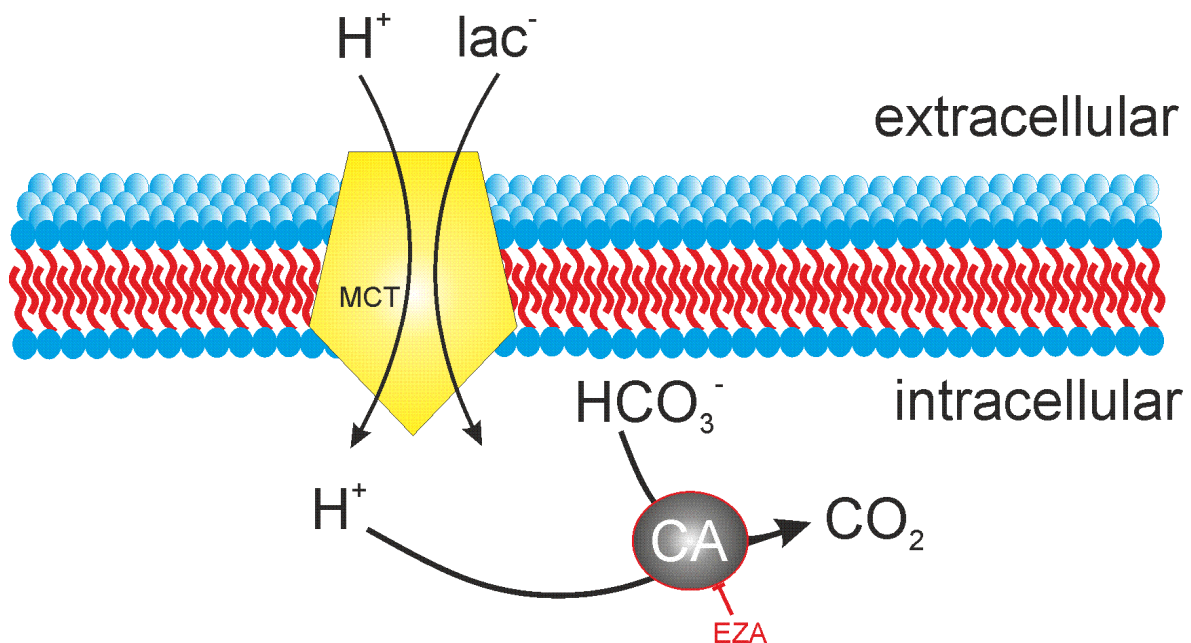


**Figure 50** Model of potential catalytic interaction of MCT and intracellular CA

The catalytic activity of cytosolic carbonic anhydrase (CA) might slow down the cytosolic acidification, caused by lactate uptake via MCT. In this case, the inhibition of CA with EZA would lead to faster cytosolic acidification when lactate is applied to the cells.

In this work, no intracellular CA activity was observed but inhibition of CA activity with EZA did speed up the lactate-induced cytosolic H<sup>+</sup> load. In Figure 50, the mechanism of a potential speed up of lactate-induced cytosolic H<sup>+</sup> load as caused by inhibition of a theoretical intracellular CA is shown. In contrast, an extracellular CA activity might provide H<sup>+</sup> for the MCT but could not slow down the hereby caused cytosolic H<sup>+</sup> load at the same time, unless an additional interaction comes into play (Figure 51). If the extracellular CA would support the NBC, it could slow down the cytosolic H<sup>+</sup> load, caused by MCT (Figure 53).

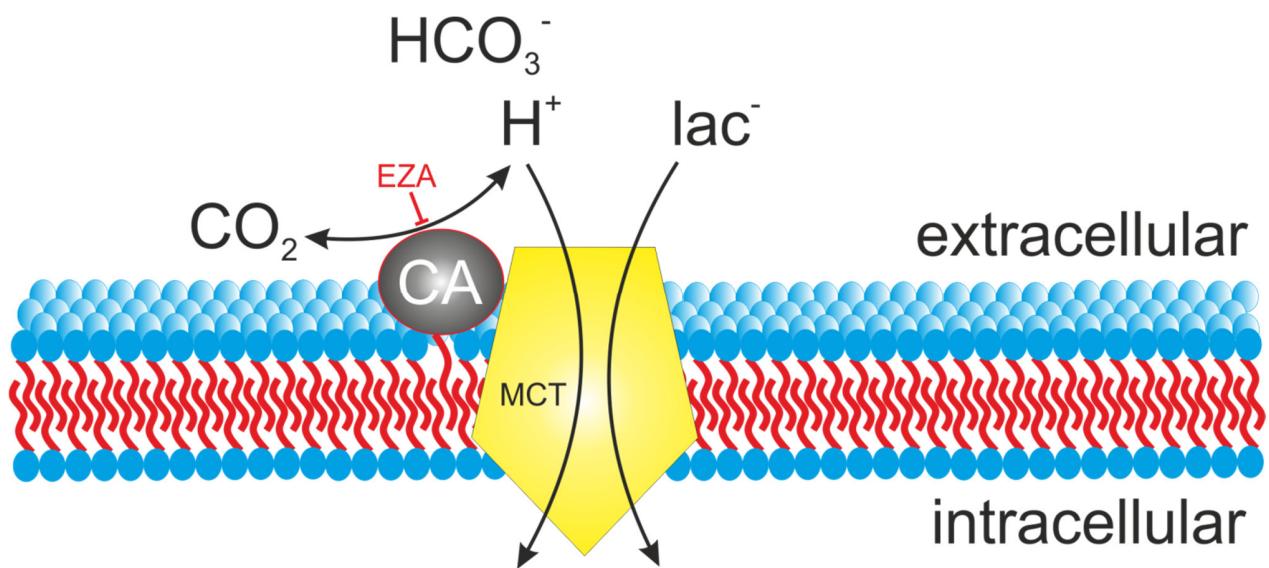


**Figure 51** Model of potential catalytic interaction of MCT and extracellular CA

The catalytic activity of extracellular carbonic anhydrase (CA) might speed up the lactate uptake via MCT. In this case, the inhibition of CA with EZA would lead to slower cytosolic acidification when lactate is applied to the cells.

In this work, the acid extruding-, cariporide insensitive-, CO<sub>2</sub>/HCO<sub>3</sub><sup>-</sup>- and Na<sup>+</sup>-dependent J<sub>A/B</sub> is expected to be mediated by NBC. This activity is reduced from 2.6 mM/min to 0.56 mM/min when CA is inhibited, which is a reduction of 78.4%. Consequently it can be concluded that NBC activity in mouse cardiomyocytes is highly dependent on extracellular CA activity. The lactate-induced J<sub>A/B</sub> and the lactate influx, as determined by SNARF and *Laconic* imaging, were reduced by 42% and 27%, respectively, when CA was inhibited with EZA. To test if lactate uptake depends on NBC activity, the inhibitor S0859 was used. Ch'en et al. (2008) reported that S0859 completely inhibits CO<sub>2</sub>/HCO<sub>3</sub><sup>-</sup>-dependent acid extrusion in rat cardiomyocytes when applied at a concentration of 30 μM. In this work it is shown that S0859 only partially

inhibited  $\text{CO}_2/\text{HCO}_3^-$ -dependent acid extrusion from mouse cardiomyocytes. In addition, it was found that it reduces lactate induced acidification, which cannot be due to inhibition of NBC (Figure 52). Since another commonly used NBC inhibitor, DIDS (4,4'-diisothiocyanostilbene-2,2'-disulfonic acid Chen et al., 2012; Grichtchenko et al., 2001), is known to inhibit the MCT1 (Wilson et al., 2009), it is possible to assume the same for S0859. Ch'en et al. (2008) described this inhibitor as specific for NBC and they could rule out a side effect on the acid/base transporters NHE, AE1, AE2 and CHE. An effect on MCTs was not tested in that publication, even though the authors explicitly mention this possibility. Experiments by Sina Ibne Noor with *Xenopus* oocytes expressing MCT4 (unpublished data) revealed an inhibiting effect of S0859 on MCT. Therefore, the effect of NBC on MCT has not been ultimately proven in this work.

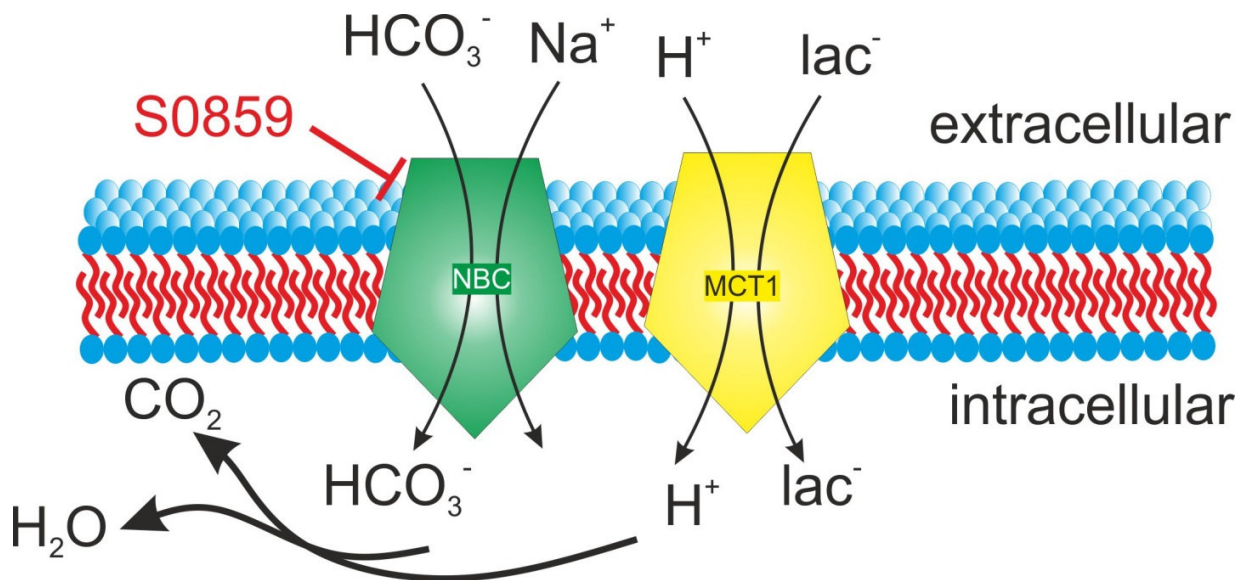


**Figure 52** Scheme of S0859 effect on lactate-induced acidification

The NBC inhibitor S0859 is reported to completely block NBC activity in rat cardiomyocytes by Ch'en et al. (2008) at a concentration of 30  $\mu\text{M}$ . As NBCs are meant to counteract cytosolic  $\text{H}^+$  load, its activity is supposed to slow down lactate induced acidification. Consequently, its inhibition must result in faster lactate induced acidification.

In the introduction, it was mentioned that MCT and NHE might be co-localised in intercalated disks (Garciaarena et al., 2013; Halestrap et al., 1997). Since interaction between NHE and CAII has been reported (Li et al., 2002; Orłowsky and Grinstein, 2004), it was thinkable that the observed effect of EZA on the lactate influx might be due to a functional interaction of NHE and extracellular CA. The main argument against an interaction of MCT and NHE was the  $[\text{H}^+]_i$



threshold of NHE that had been reported to be approximately pH 6.9 in guinea-pig cardiomyocytes (Leem et al., 1999). In this work, during application of extracellular lactate at a concentration of 3 mM, the cytosolic pH dropped in average to a minimum of pH 7.06 in HEPES-only and  $\text{CO}_2/\text{HCO}_3^-$ -buffered conditions. The acid extrusion in HEPES-only-buffered conditions was calculated to stop at pH 6.82, whereas in  $\text{CO}_2/\text{HCO}_3^-$ -buffered conditions acid extrusion was calculated to persist until pH 7.0. This threshold in HEPES-only-buffered conditions is most likely due to NHE inactivation. Therefore, the threshold for NHE in mouse cardiomyocytes is considered to be pH 6.82. Thus, application of lactate at a concentration of 3 mM could not have activated the NHE. This was confirmed with lactate imaging, where inhibition of NHE with cariporide (30  $\mu\text{M}$ ) did not have any effect on the lactate influx. Hence, the NHE can be excluded from the observed effect by EZA.

However, a coupling of cellular  $\text{CO}_2$  release and lactate uptake is likely. Since oxidative lactate consumption leads to cellular  $\text{CO}_2$  release, the interplay of extracellular CA, NBC and MCT might be a feedback mechanism by which increased cellular respiration stimulates the uptake of monocarboxylates (Figure 53).

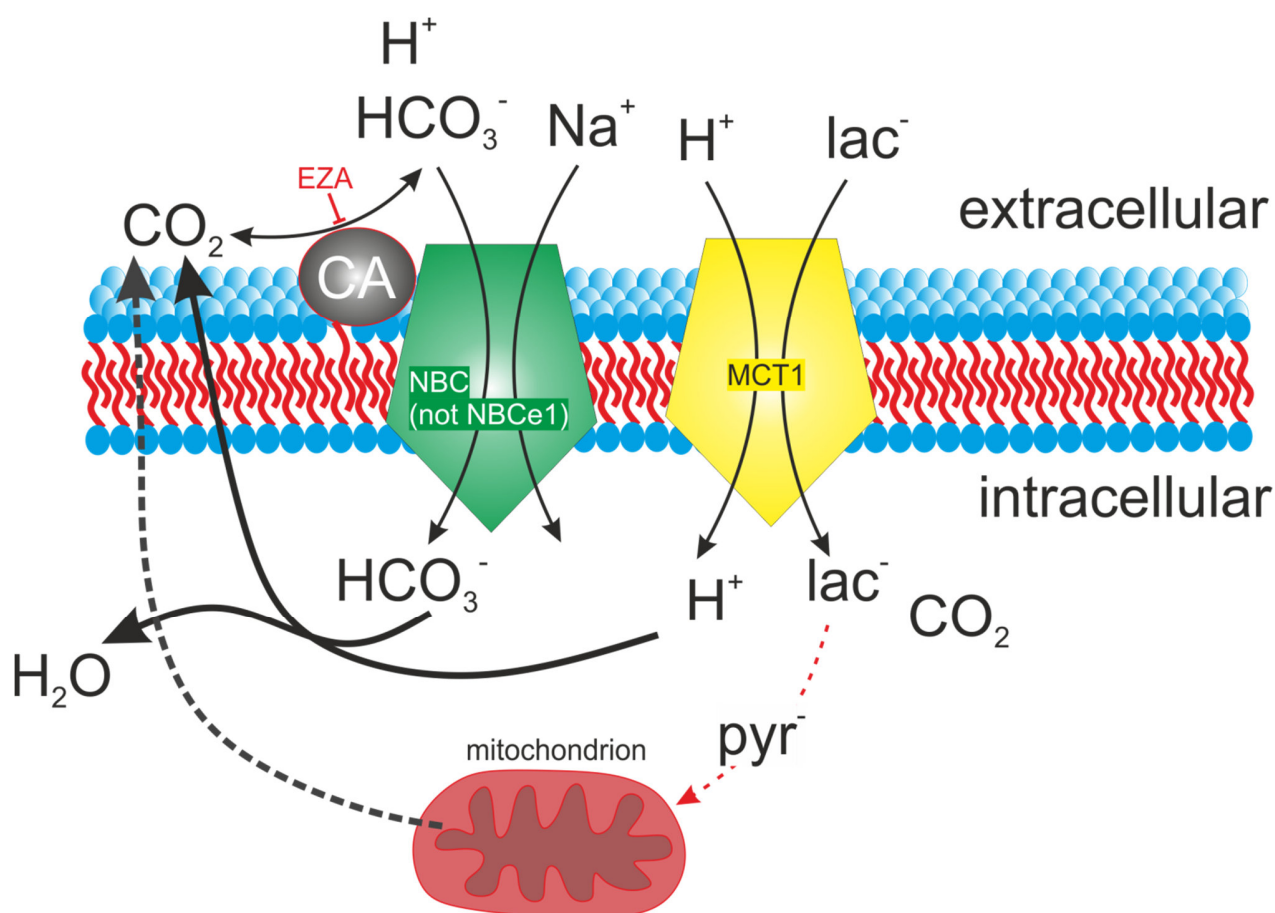


**Figure 53** Model of NBC, CA and MCT1 interaction

As no cytosolic carbonic anhydrase activity was observed, the effects of EZA on lactate induced acidification and lactate influx must be caused by inhibition of extracellular CA. But inhibition of extracellular CA cannot speed up the cytosolic, lactate induced acidification, unless it interacts with another acid/base regulator like NBC.

This idea was further investigated by the extracellular application of lactate in HEPES-only-buffered solution, either gassed with 100%  $\text{O}_2$  or 100%  $\text{N}_2$  (Figure 54). When the solution was gassed with 100%  $\text{N}_2$  it was assumed that the TCA cycle would stop due to NADH accumulation and consequently  $\text{CO}_2$  release would stop as well. In contrast, the solution gassed with 100%  $\text{O}_2$  was assumed to allow respiration and  $\text{CO}_2$  formation. In addition, the gassing with 100%  $\text{O}_2$  or 100%  $\text{N}_2$  shall drive out all other gasses, so that those solutions might be considered as  $\text{CO}_2$  free.

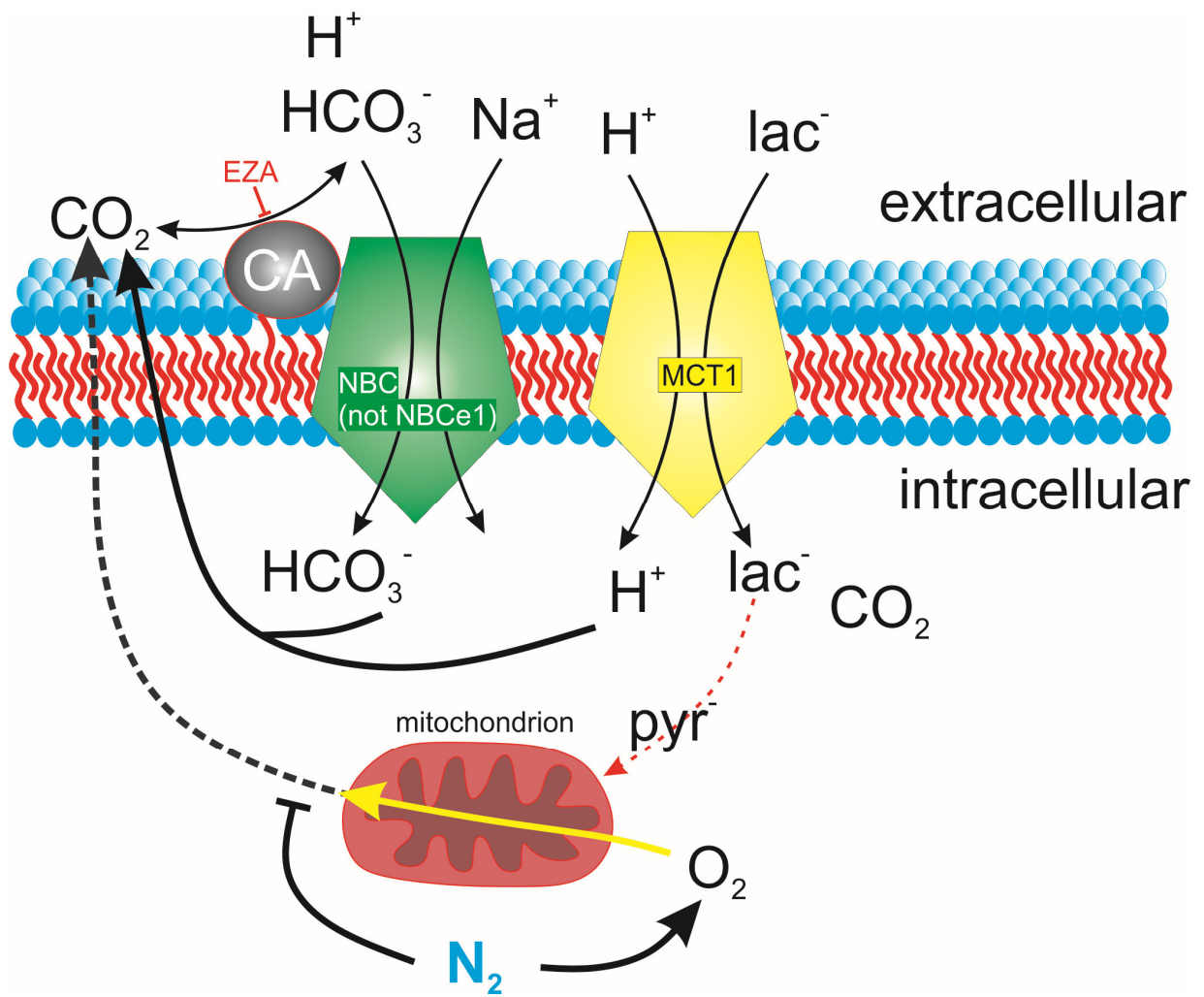


**Figure 54** Potential interaction of respiration and lactate uptake

If the cells are kept in HEPES-only-buffered solution, gassed with 100% N<sub>2</sub> all residual O<sub>2</sub> should be driven out of the cells and mitochondrial CO<sub>2</sub> formation should stop.

The lactate-induced acidification was 12.6% faster in N<sub>2</sub> than in O<sub>2</sub> gassed solution. When the CA was inhibited with EZA in O<sub>2</sub> gassed solution, lactate-induced acidification did speed up by 8%. This is interpreted as the effect of cell-derived CO<sub>2</sub> on the lactate-induced acidification. The CO<sub>2</sub> is thought to leave the cell and to be converted at the extracellular cell surface to HCO<sub>3</sub><sup>-</sup> and H<sup>+</sup>. The HCO<sub>3</sub><sup>-</sup> may then be reimported into the cell and support the CO<sub>2</sub>/HCO<sub>3</sub><sup>-</sup>-dependent H<sup>+</sup> buffering.

Several authors described the heart's ability to consume lactate. Baker et al. (1998) could show that red muscle (soleus) and the heart take up lactate. This uptake increases with training and is mediated by MCT1 (in rat). Gertz et al. (1988) found that the human heart takes up lactate

with a rate of 35  $\mu\text{mol}/\text{min}$  at rest. This rate increases during exercise to 120.4  $\mu\text{mol}/\text{min}$ . Lactate labelled with  $^{14}\text{C}$  revealed that the lactate that had been taken up was completely converted to  $\text{CO}_2$ . In contrast, just 26% of the glucose that had been taken up by the heart was converted to  $\text{CO}_2$  at rest. During exercise, the oxidative glucose turnover increased to 52.6%. 12.3% of the glucose, taken up from the blood was converted to lactate (5.7  $\mu\text{mol}/\text{min}$ ) and 60% entered glycogen stores. The heart was found to take up lactate with a rate of 120.4  $\mu\text{mol}/\text{min}$  from the blood and to release lactate with a rate of 16.2  $\mu\text{mol}/\text{min}$  during exercise. These findings are in line with the more recent results by Bergman et al. (2009), who also report myocardial lactate uptake and release at the same time. According to them, the myocardial lactate release increases from approximately 25  $\mu\text{mol}/\text{min}$  at rest to 75  $\mu\text{mol}$  during exercise. The myocardial lactate consumption increased from approximately 80  $\mu\text{mol}/\text{min}$  at rest to 200  $\mu\text{mol}/\text{min}$  during exercise. Kempainen et al. (2002) reported that the myocardial glucose uptake increased from rest to 30%  $V_{\text{O}_2,\text{max}}$ , was stable at 55% and reduced at 75%.

In this work, the consumption of lactate via conversion to pyruvate by cardiomyocytes was confirmed on the single cell level with lactate imaging. When lactate was applied to the cells in presence of glucose (1 mM), the cytosolic lactate concentration rose. Then the MCT inhibitor AR C155858 was applied to the cells at a concentration of 300 nM (Ovens et al., 2010). This caused a drop in cytosolic lactate and was interpreted as lactate consumption. The measured lactate consumption was 10 times slower than the lactate influx when lactate was applied at a concentration of 0.5 mM to the cells. This means that the reported blood lactate concentration of approximately 1 mM at resting conditions (Bergman et al., 2009; Kempainen et al., 2002) would be sufficient to meet the cardiomyocytes lactate demand.

Inhibition of the respiratory chain with  $\text{NaN}_3$  (5 mM) in the presence of the MCT inhibitor AR C155858, resulted in an immediate increase of the intracellular lactate concentration. To relate the lactate consumption to the overall energy metabolism of mouse cardiomyocytes, the following assumptions were made:

- (1) Since, under those conditions, no lactate can leave the cell or get consumed, the speed of lactate formation reflects the speed of glycolysis.
- (2) This speed of glycolysis reflects the cellular ATP demand.

- (3) Each lactate consumed for oxidative phosphorylation converts its potential energy to 14-15 molecules ATP.

Hence, the rate of lactate consumption must be multiplied with 14-15 to compare its contribution to the cellular ATP supply with the contribution by glycolysis. Like this, the ATP provided by lactate consumption is calculated to be 106%-114% of the ATP provided by glycolysis, if the oxidative phosphorylation is inhibited. This would mean that the blood lactate concentration in resting conditions would be sufficient to meet the cardiomyocytes ATP demand. The logical consequence of this would be that cardiomyocytes stop ATP production from glucose if an adequate amount of lactate is provided. However, the energy demand of cardiomyocytes in the used system may not reflect the *in vivo* situation because the cells were quiescent by the absence of extracellular calcium, the application of contraction inhibitor and the lack of pacemaker stimulation.

When the MCT was inhibited in the absence of extracellular lactate, the cytosolic lactate concentration rose. Compared with the lactate formation in the presence of  $\text{NaN}_3$  (5 mM) and the MCT inhibitor AR C155858, the steady state lactate formation contributes to the total ATP production with 5.7%. Gertz et al. (1988) measured a myocardial lactate uptake of 34.9  $\mu\text{mol}/\text{min}$  at resting conditions. This lactate was completely converted to  $\text{CO}_2$ . The myocardial glucose uptake was determined to be 28.33  $\mu\text{mol}/\text{min}$ . 12.3% of this glucose was converted via glycolysis to lactate and 26% percent were converted to  $\text{CO}_2$ . It is assumed that out of 1 molecule glucose 30-32 molecules ATP are generated (Schmidt et al, 2005; Pfeiffer et al., 2001) if converted to  $\text{CO}_2$ . The conversion of glucose to lactate generates 2 molecules of ATP. Thus, according to the data reported by Gertz et al., (1988), the oxidative consumption of lactate and glucose generates ATP with a rate of 506  $\mu\text{mol}/\text{min}$  and 228  $\mu\text{mol}/\text{min}$ , respectively. The conversion of glucose to lactate generates additional ATP with a rate of 7  $\mu\text{mol}/\text{min}$ . Thus, the total rate of human myocardial ATP formation under the assumed conditions is 741  $\mu\text{mol}/\text{min}$ . The fraction of glycolysis that exceeds the speed of oxidative phosphorylation contributes with 0.94% to the total ATP formation. This is less than the 5.7% as assumed for isolated mouse cardiomyocytes in this work, but it lies within a similar range. The difference might be due to the fact that Gertz et al. (1988) just considered the lactate formation from exogenous glucose and could not take into account the lactate formation from glycogen stores, whereas in this work the total lactate formation is considered. Anyway, since the compared systems are very

different, a difference in this value must be expected. Thus, it can be concluded that in the steady state of the used system, glycolysis slightly exceeds the oxidative phosphorylation, which results in slow cytosolic lactate formation.

The release of lactate and its net consumption at the same time are contradictory, unless cardiomyocytes undergo a metabolic switch in the presence of lactate. This will be discussed in the next section.

#### 4.4 Final conclusion, model & further speculations

During this work it was shown that mouse cardiomyocytes

- (1) possess NHE activity
- (2) possess electro-neutral NBC or NBC-like activity
- (3) mediate lactate uptake via MCT1
- (4) lack cytosolic CA activity
- (5) possess extracellular CA activity
- (6) import lactate faster if the extracellular CA is active
- (7) consume and produce lactate
- (8) produce pyruvate out of lactate

Furthermore this work provides evidence for

- (9) different  $\text{HCO}_3^-$ -dependent acid extruding mechanism that include a S0859-sensitive, a S0859-insensitive and a  $\text{Na}^+$ -independent fraction
- (10) impact of cellular respiration on cytosolic  $\text{H}^+$  buffering
- (11) unspecific inhibition of the MCT1 by S0859. This was further confirmed in *Xenopus* oocytes expressing the MCT4 by Sina Ibne Noor (unpublished data).

The findings of this work are summarized in Figure 55. The CO<sub>2</sub> released from the cells during oxidative metabolism may support further uptake of MCT1 substrates, such as lactate. In turn, further consumption of lactate in the citric acid cycle will go along with CO<sub>2</sub> release. Therefore, an auto regulation of lactate uptake by cellular respiration is postulated. When lactate was applied to the cells in HEPES-only-buffered solution gassed with 100% N<sub>2</sub>, the  $\Delta [H^+]_i/\Delta t$  was 12.6% faster compared to lactate application in medium gassed with 100% O<sub>2</sub>. But for different reasons, this effect might be under estimated due to the used system:

- (1) The cells were isolated and because of continuous perfusion, the artificial extracellular space became non-finite. Consequently, CO<sub>2</sub> leaving the cell might be converted by extracellular CAs but the resulting HCO<sub>3</sub><sup>-</sup> would be partially washed away, thus less can be reimported by NBC.
- (2) The cells were quiescent and experiments were performed at room temperature so that the overall cell energy turnover most likely had dropped. This can be assumed based on the finding that cardiomyocytes show hibernation if they are exposed to severe energy stress (Cadenas et al., 2010; Casey and Arthur, 2000), hence, the forced inhibition of contractile activity should work the other way around and save energy. Therefore, the cells may not have provided the rate of CO<sub>2</sub> release that might occur in the intact and active heart. Especially when the heart rate increases, the release of CO<sub>2</sub> may rise and thereby stimulate further uptake of energy substrates.
- (3) The inhibition of oxidative phosphorylation will result in a rapid lactate formation which might inhibit further lactate uptake.
- (4) The myoglobin will provide an oxygen buffer whose extend has not been determined during this work.

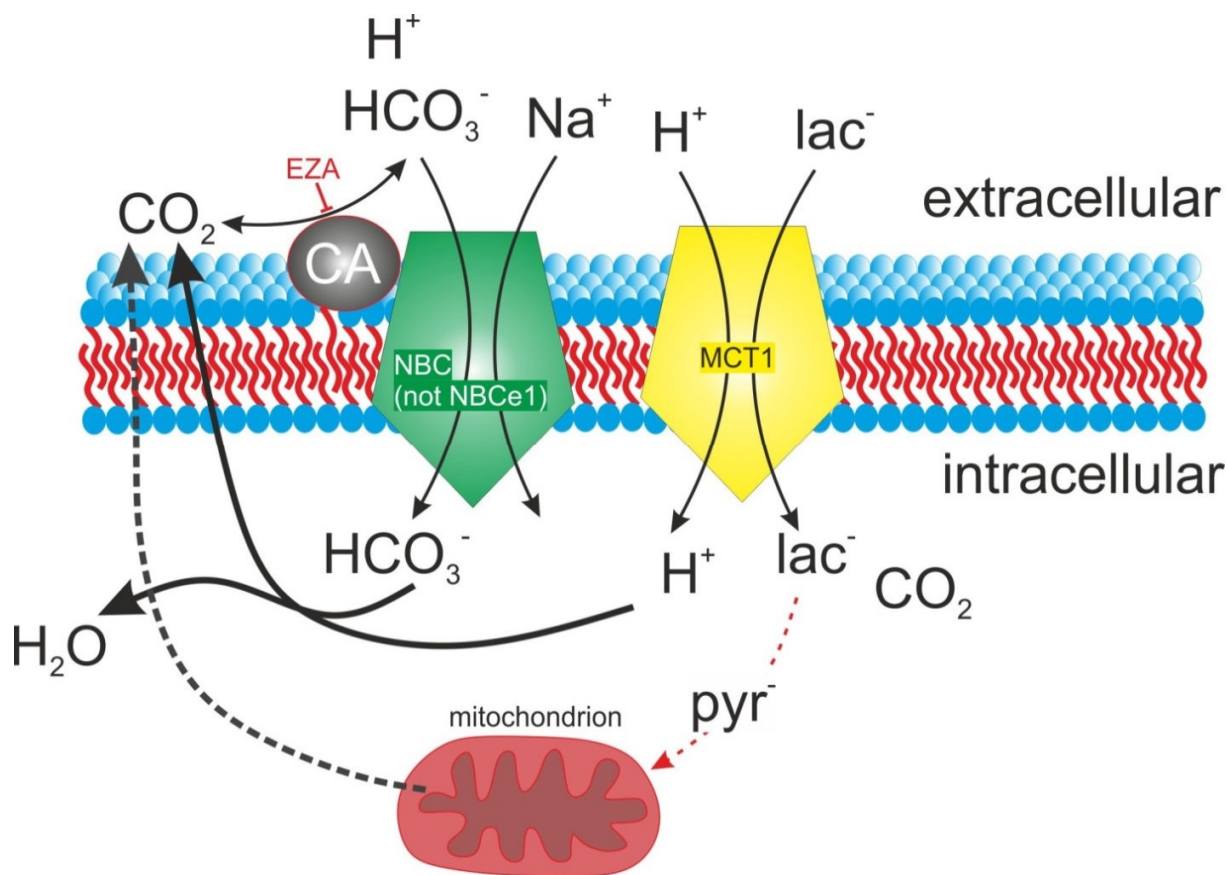


**Figure 55** Final model of CA, NBC, MCT and mitochondrion interaction

The lactate is taken up into the cell by the MCT1 and is converted to pyruvate in the cytosol. This fuels mitochondria. The rise in cytosolic pyruvate might stimulate mitochondrial CO<sub>2</sub> release, which in turn would reduce the lactate-induced acidification. This reduction is abolished when the extracellular carbonic anhydrase (CA) is inhibited. Consequently, the extracellular CA must provide a catalytic support to an acid/base regulator that reduces the cytosolic acidification. Since it is shown that this is not the NHE, the remaining candidates are NBCs or NBC-like acid/base regulators. In this work it was not achieved to figure out which of those is present in mouse cardiomyocytes.

Thus, *in vivo* the effect of cellular CO<sub>2</sub> release on the lactate transport might be much more significant than *in vitro*.

Gertz et al. (1988) and Bergman et al. (2009) reported the controversial behaviour of the human heart to consume and release lactate at the same time, which results in a net uptake. According to Bergman et al. (2009), this lactate uptake contributes with 4.9% at rest and 15% during exercise to the overall body lactate disposal. In this work, this contrariness was scaled down to the single cardiomyocytes. On the one hand they were shown to consume lactate if applied, but on the other hand they were shown to produce lactate if absent in the extracellular space.



According to the previously mentioned assumptions for the energy metabolism, cardiomyocytes completely meet their ATP demand from lactate if applied (in the used conditions). In this work it was shown that extracellular lactate application leads to enhanced cytosolic pyruvate formation, thus glycolysis might be hindered if cells take up lactate. Based on the previously made assumptions, glycolytic ATP generation contributes with 11.25% (5.7% lactate forming glycolysis, 5.5% glycolysis driving TCA) to the total ATP generation, if glucose is the only energy substrate. It appears unlikely that the consumption of lactate is just a compensation for the lost ATP production due to cytosolic lactate load, because the assumed ATP production from lactate consumption (122%) exceeds the 11.25% by far. A more complex explanation might be similar to theories about the astrocyte-neuron-lactate shuttle (Chih and Roberts, 2003): if lactate or fatty acids are used for energy generation, glucose may be saved for the pentose phosphate way, which is needed for the glutathione reduction (Takahashi et al., 2012).

The ROS in cardiomyocytes are produced in big parts in the respiratory chain at complex III (Ghosh et al., 2005), so the activity of the oxidative metabolism is directly linked to ROS formation. Therefore, stimulation of the respiratory chain, either by hyperglycemia or by increased energy needs, may raise the mitochondrial ROS production. ROS formation may lead to muscle fatigue via reduced  $\text{Ca}^{2+}$  sensitivity (Reid, 2008 review). This means that ROS formation during strong respiratory activity would, in addition to being toxic anyway, decrease the myocardial endurance as well. Therefore cardiomyocytes must be protected from ROS.

So glucose is needed to compensate the ROS formation via pentose phosphate way and glutathione reduction. But if big amounts of glucose get available to cardiomyocytes, like under diabetic conditions, this may have the opposite effect and cause ROS formation as shown by Fiordaliso et al. (2004) and Ye et al. (2003). This might be due to excessive demand of the respiratory chain as shown by Nishikawa et al. (2007) in cultured aortic endothelial cells. Therefore the cellular glucose must be “guided” to the pentose phosphate way.

Jain et al. (2003) could show that the glucose-6-phosphate dehydrogenase, the rate limiting enzyme of the pentose phosphate pathway, is stimulated by ROS in rat cardiomyocytes. In addition, Leite et al. (2011) could find direct inhibition of the phosphofructokinase by lactate. Herrero-Mendez et al. (2009) could show that artificial stimulation of neuronal glycolysis via phosphofructokinase activation inhibits the pentose phosphate way. So inhibition of the

phosphofructokinase with lactate, as reported by Leite et al. (2011) might just work the other way around and stimulate the pentose phosphate pathway.

If this is considered all together, strong physical activity might stimulate the pentose phosphate way by glucose-6-phosphate dehydrogenase stimulation with ROS on the one hand and with lactate uptake, inhibiting the phosphofructokinase, on the other hand (Figure 56 and Figure 57).

Especially during strong physical activity where the blood lactate level was measured to reach up to 10 mM in humans (Kemppainen et al., 2002) it appears plausible, that oxidative tissues such as the myocardium increase the lactate consumption to meet their energy needs. Lactate may be converted to the glycolytic end product pyruvate, which was confirmed in this work by pyruvate imaging. In addition to the direct inhibition of the glycolysis via phosphofructokinase inhibition by lactate, the increased cytosolic pyruvate and consequently decreased NAD<sup>+</sup> levels (since conversion of lactate to pyruvate produces NADH out of NAD<sup>+</sup>) following lactate uptake must inhibit the glycolysis additionally. The hereby crotched glucose might be used for NADPH production in the pentose phosphate way, which is needed in turn to reduce glutathione (Herrero-Mendez et al., 2009; Takahashi et al., 2012, see the model here in Figure 57).

This hypothesis is further supported by the findings of Kemppainen et al. (2002). They could show that human myocardial glucose uptake during exercise is elevated at 30% and 55%  $V_{O_{2max}}$  compared to resting conditions but reduces when the training intensity is increased to 75%  $V_{O_{2max}}$ . This is in contrast to the glucose uptake in skeletal muscle, where it increases with increased workload, also at 75%  $V_{O_{2max}}$  exercise. In addition they could measure an increase in plasma lactate concentration from approximately 1 mM at resting conditions to approximately 9.5 mM at 75%  $V_{O_{2max}}$  exercise, whereas the blood glucose level remained between 5 and 6.5 mM. Thus, the main myocardial ATP metabolism might have switched from respiratory glucose to lactate consumption. The physiological meaning of this might be the myocardial protection from ROS (Figure 56 and Figure 57).

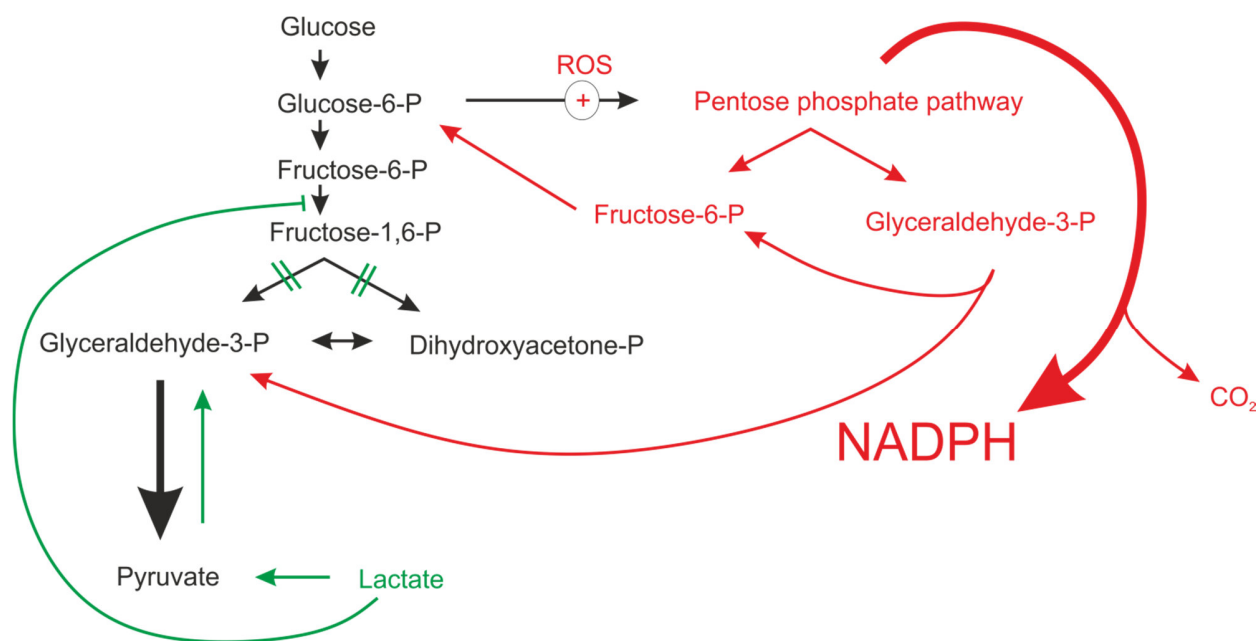


**Figure 56** Potential stimulation of pentose phosphate pathway by lactate and ROS

The glycolysis is shown in **black**, the pentose phosphate way in **red** and the potential impact of lactate in **green**.

The uptake of lactate leads to an increase in cytosolic pyruvate. As pyruvate is the end product of the glycolysis, this increase in cytosolic pyruvate must slow down the glycolysis. In addition, Leite et al. (2011) could show that lactate inhibits the phosphofructokinase. Since, according to this hypothesis, the glycolysis gets inhibited by the uptake of lactate, more glucose-6-phosphate is available for the pentose phosphate way. Jain et al. (2003) could show that ROS may stimulate the glucose-6-phosphate dehydrogenase, which is the rate limiting enzyme of the pentose phosphate way. Both, the increase in ROS formation and the increased lactate uptake can be expected to occur during strong physical activity. Therefore, the consumption of lactate by cardiomyocytes might serve as protection from ROS.

During this work, it was not possible to measure the cytosolic glucose in mouse cardiomyocytes. Therefore, a glucose saving effect by lactate consumption remains speculative. Tsai et al. (2005) could show that cytosolic presence of another mitochondrial energy substrate, D-3-hydroxybutyrate, in rat cardiomyocytes decreases the glucose consumption. Since the blood glucose level remains constant between 5 mM and 6.5 mM (Kempainen et al., 2002), cardiomyocytes should be able to keep the cytosolic glucose concentration constant as well. Still, lactate consumption might save glycogen stores for other cellular processes than ATP production. A correlation between lactate consumption and ROS formation remains to be tested.

As this idea is still at the level of a hypothesis, it contains some minor gaps in line of argumentation. The major one of those is caused by the findings of Kempainen et al. (2002) and Tsai et al. (2005), who show that either heavy work load or application of alternative energy substrates (D-3-hydroxybutyrate) lead to reduced glucose uptake into the heart. If the use of this hypothetical metabolic switch would be that glucose gets saved for the pentose phosphate way, the cellular glucose uptake should remain the same, since it would still be needed, just in a different pathway.

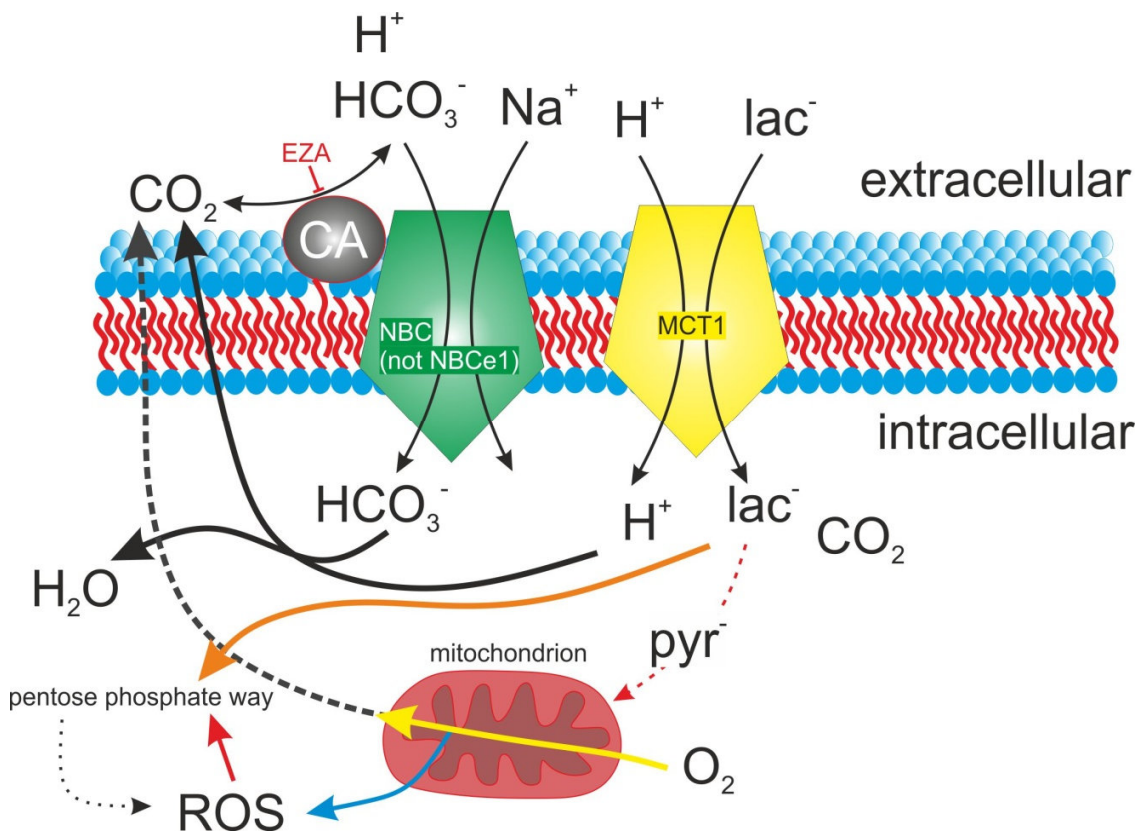


**Figure 57** Final model with hypothetical ROS protection by lactate

According to this model, increased respiratory activity is followed by increased  $\text{CO}_2$  release. This stimulates lactate uptake. The lactate is converted to pyruvate, which is being consumed in the mitochondria. As the elevated cytosolic lactate levels lead to an elevated pyruvate level, the glycolysis most likely slows down. In addition, lactate might directly inhibit the phosphofructokinase and hereby slow down glycolysis (Leite et al., 2011). At the same time, increased ROS levels may stimulate the pentose phosphate way (Jain et al., 2003).

EZA: CA inhibitor, ROS: reactive oxygen species, pyr: pyruvate

But if this postulated regulation would be a bit more elaborated than just inhibition of a biochemical process by elevated product concentrations, the total cellular glucose utilization could drop down if the cell faces cytosolic lactate load. Such regulation would include the above mentioned mechanisms of phosphofructokinase inhibition and glucose-6-phosphate dehydrogenase activation and maybe some further more. If the extreme case of an oxidative pentose phosphate pathway is assumed, where the end-products fructose-6-P and glyceraldehyde-3-P are continuously reused for glucose-6-P generation, much less glucose would be needed to meet the cellular NADPH needs. This might explain the observed drop in myocardial glucose consumption at heavy work load as observed by Kemppainen et al. (2002).

If the model shown in Figure 57 is scaled down to transient, regional effects within the heart tissue, it would not be controversial to the findings by Gertz et al. (1988) and Bergman et al. (2009), who reported that the human heart possesses continuous lactate release and uptake. According to Pfeiffer et al. (2001), the ATP production via fermentation is beneficial if ATP is needed fast. Thus, at rest or during moderate exercise, lactate formation might occur in cardiomyocytes during contraction. Oxidative phosphorylation might consume all pyruvate provided by glycolysis and lactate conversion in the intermediate phases of relaxation. During strong exercise (75 %  $V_{O_{2max}}$ ) the elevated blood lactate level might counteract myocardial lactate formation and according to the metabolic model in Figure 56 and Figure 57, the utilisation of glucose might be favoured by the pentose phosphate pathway due to ROS formation.

#### 4.5 Potential MCT / NHE interaction

As mentioned in the introduction, the reported co-localisation of MCT and NHE at the intercalated discs of cardiomyocytes opens the possibility of an interaction. Even though in this work no effect of NHE on the lactate uptake was observed, the used conditions differ from the *in vivo* situation. The NHE is reported to be regulated by many stimuli so that its threshold and overall activity might differ according to metabolic state and myocardial activity. For example  $\text{Ca}^{2+}$  is reported to stimulate the NHE activity (Bertrand et al., 1994; Vaughan-Jones et al., 2008; Wakabayashi et al., 1997), so that the transporter might get activated in the same rhythm as the cell contracts, since each contraction follows a cytosolic rise in  $\text{Ca}^{2+}$ . So, the NHE might stimulate lactate uptake each time the cell contracts. In addition, ROS are reported to stimulate NHE activity (Vaughan-Jones et al., 2008), which would fit very well to the hypothesis that lactate uptake and consumption might serve as ROS protection. In this case, the NHE might get active when the ROS production becomes critical and stimulate the MCT activity. As consequence, in accordance to the above mentioned hypothesis, the pentose phosphate pathway would get stimulated.

#### 4.6 Non-catalytic interaction of extracellular CA and MCT

In this work, a non-catalytic interaction of MCT1 and the extracellular CAs CAIV, CAIX or CAXIV was not observed in mouse cardiomyocytes. This might be due to different reasons. First of all, the presence of CAIV and CAIX on mouse cardiomyocytes, as reported by Scheibe et al. (2006), was not confirmed in this work. Second, if a non-catalytic interaction between MCT1 and any CA in mouse cardiomyocytes would have a significant impact on the cellular physiology, it is very likely that its loss in a knockout animal is compensated. For example, the MCT1 or other CA isoforms might get upregulated in the knock out animal, so that no difference between WT and KO animal could be observed. This was not tested during this work because it would just explain why the non-catalytic interaction cannot be observed but it would not prove its existence. To avoid compensatory regulations, it might be necessary to disrupt the potential non-catalytic interaction during a live cell imaging experiment. This might be done with an antibody that prevents the CAIX and/or CAXIV from getting into close proximity to the MCT1. Before this could be done in cardiomyocytes, this technic should be tested first in *Xenopus* oocytes that contain MCT1 and CAIX and/or CAXIV.

## 5. LITERATURE

---

- Aguilera et al. (2008) Dual Role of LldR in Regulation of the *lldPRD* Operon, involved in L-Lactate Metabolism in *Escherichia coli*. *JOURNAL OF BACTERIOLOGY* 190: 2997-3005
- Ai HW et al. (2006) Directed evolution of a monomeric, bright and photostable version of Clavularia cyan fluorescent protein: structural characterization and applications in fluorescence imaging. *The Biochemical journal* 400:531-40
- Alvarez BV et al. (2007) Carbonic anhydrase inhibition prevents and reverts cardiomyocyte hypertrophy. *The Journal of physiology* 579:127-45.
- Alvarez BV et al. (2003) Direct extracellular interaction between carbonic anhydrase IV and the human NBC1 sodium/bicarbonate co-transporter. *Biochemistry* 42:12321-9.
- Alvarez BV et al. (2013) Quantification of carbonic anhydrase gene expression in ventricle of hypertrophic and failing human heart *BMC Cardiovascular Disorders* 13:2
- Baker SK et al. (1998) Training intensity-dependent and tissue-specific increases in lactate uptake and MCT-1 in heart and muscle. *Journal of applied physiology* 84:987-94.
- Banerjee I et al. (2007) Determination of cell types and numbers during cardiac development in the neonatal and adult rat and mouse. *American journal of physiology Heart and circulatory physiology* 293:H1883-91.
- Becker HM, Deitmer JW (2004) Voltage dependence of H<sup>+</sup> buffering mediated by sodium bicarbonate cotransport expressed in *Xenopus* oocytes. *The Journal of biological chemistry* 279:28057-62.
- Becker HM et al. (2005) Transport activity of MCT1 expressed in *Xenopus* oocytes is increased by interaction with carbonic anhydrase. *The Journal of biological chemistry* 280:39882-9.
- Becker HM et al. (2011) Intramolecular proton shuttle supports not only catalytic but also noncatalytic function of carbonic anhydrase II. *Proceedings of the National Academy of Sciences of the United States of America* 108:3071-6.
- Bell PB et al. (1987) Formaldehyde sensitivity of a GFAP epitope, removed by extraction of the cytoskeleton with high salt. *Journal of Histochemistry & Cytochemistry* 35:1375-1380.
- Beltrami AP et al. (2001) Evidence that human cardiac myocytes divide after myocardial infarction. *The New England Journal of Medicine* 344: 1750-1757
- Bergman BC et al. (1999) Muscle net glucose uptake and glucose kinetics after endurance training in men Muscle net glucose uptake and glucose kinetics after endurance training in men. *American Journal of Physiology Endocrinology and Metabolism* 277: 81-92.
- Bergman BC et al. (2009) Myocardial glucose and lactate metabolism during rest and atrial pacing in humans. *The Journal of physiology* 587:2087-99.
- Roussel G et al. (1979) Demonstration of a specific localisation of carbonic anhydrase C in the glial cells of rat CNS by an immunohistochemical method. *Brain Research* 160:47-55.
- Bonen A (2001) The expression of lactate transporters (MCT1 and MCT4) in heart and muscle. *European Journal of Applied Physiology*:6-11.
- Borlak J, Zwadlo C (2004) The myosin ATPase inhibitor 2,3-butanedione monoxime dictates transcriptional activation of ion channels and Ca<sup>2+</sup>-handling proteins. *Molecular pharmacology* 66:708-17.

- Bröer S et al. (1998) Characterization of the monocarboxylate transporter 1 expressed in *Xenopus laevis* oocytes by changes in cytosolic pH *Biochemical Journal* 333:167-174.
- Brzozowski Z et al. (2010) Carbonic anhydrase inhibitors. Regioselective synthesis of novel 1-substituted 1,4-dihydro-4-oxo-3-pyridinesulfonamides and their inhibition of the human cytosolic isozymes I and II and transmembrane cancer-associated isozymes IX and XII. *European journal of medicinal chemistry* 45:3656-61.
- Cadenas S et al. (2010) Mitochondrial reprogramming through cardiac oxygen sensors in ischaemic heart disease. *Cardiovascular research* 88:219-28.
- Casey JR et al. (2010) Sensors and regulators of intracellular pH. *Nature reviews Molecular cell biology* 11:50-61.
- Casey TM, Arthur PG (2000) Hibernation in Noncontracting Mammalian Cardiomyocytes. *Circulation* 102:3124-3129.
- Ch'en FF-T et al. (2003) Temperature dependence of Na<sup>+</sup>-H<sup>+</sup> exchange, Na<sup>+</sup>-HCO<sub>3</sub><sup>-</sup> cotransport, intracellular buffering and intracellular pH in guinea-pig ventricular myocytes. *Journal of Physiology* 552:3: 715-726
- Ch'en FF-T et al. (2008) S0859, an N-cyanosulphonamide inhibitor of sodium-bicarbonate cotransport in the heart. *British journal of pharmacology* 153:972-82.
- Chen M et al. (2012) The electro neutral Na<sup>+</sup>:HCO<sub>3</sub><sup>-</sup> cotransporter NBCn1 is a major pH<sub>i</sub> regulator in murine duodenum. *The Journal of physiology* 590:3317-33.
- Chen Q et al. (2003) Production of reactive oxygen species by mitochondria: central role of complex III. *The Journal of biological chemistry* 278:36027-31.
- Chih C-P, Roberts Jr EL (2003) Energy substrates for neurons during neural activity: a critical review of the astrocyte-neuron lactate shuttle hypothesis. *Journal of cerebral blood flow and metabolism : official journal of the International Society of Cerebral Blood Flow and Metabolism* 23:1263-81.
- Chin ER, Allen DG (1998) The contribution of pH-dependent mechanisms to fatigue at different intensities in mammalian single muscle fibres. *Journal of Physiology* 512.3:831-840
- Choi I et al. (2000) An electroneutral sodium/bicarbonate cotransporter NBCn1 and associated sodium channel. *Nature* 405:571-5.
- Choi I et al. (1999) Cloning and characterization of a human electrogenic Na<sup>+</sup>-HCO<sub>3</sub><sup>-</sup> cotransporter isoform (hhNBC). *The American journal of physiology* 276:C576-84.
- Dart C, Vaughan-Jones RD (1992) Na<sup>+</sup>-HCO<sub>3</sub><sup>-</sup> symport in the sheep cardiac purkinje fibre. *Journal of Physiology* 451:365-385.
- Dawson DM et al. (1963) Lactic Dehydrogenases : Functions of the Two Types.
- De Giusti VC et al. (2011) Antibodies against the cardiac sodium/bicarbonate co-transporter (NBCe1) as pharmacological tools. *British journal of pharmacology* 164:1976-89.
- Deitmer JW (1991) Electrogenic sodium-dependent bicarbonate secretion by glial cells of the leech central nervous system. *Journal of General Physiology* 98, 637-655.
- Deitmer JW, Chesler M (2009) Neuron-Glia pH Regulation. *Encyclopedia of Neuroscience* 739-747
- Dimmer K et al. (2000) The low-affinity monocarboxylate transporter MCT4 is adapted to the export of lactate in highly glycolytic cells. *The Biochemical journal* 350:219-27.



- Du L et al. (2004) Differential myocardial gene delivery by recombinant serotype-specific adeno-associated viral vectors. *Molecular therapy : the journal of the American Society of Gene Therapy* 10:604-8.
- Endeward V, Gros G (2009) Extra- and intracellular unstirred layer effects in measurements of CO<sub>2</sub> diffusion across membranes - a novel approach applied to the mass spectrometric <sup>18</sup>O technique for red blood cells. *The Journal of physiology* 587:1153-67.
- Evans RK et al. (2003) Effect of myocardial volume overload and heart failure on lactate transport into isolated cardiac myocytes. *Journal of applied physiology* 94:1169-76.
- Fiordaliso F et al. (2004) Antioxidant treatment attenuates hyperglycemia-induced cardiomyocyte death in rats. *Journal of molecular and cellular cardiology* 37:959-68.
- Fishbein WN et al. (2002) Relative distribution of three major lactate transporters in frozen human tissues and their localization in unfixed skeletal muscle. *Muscle & nerve* 26:101-12.
- Forster RE, Crandall ED (1975) Time course of exchanges between red cells and extracellular fluid during CO<sub>2</sub> uptake. *Journal of applied physiology* 38: 710-18.
- Garcia CK et al. (1994) Molecular characterization of a membrane transporter for lactate, pyruvate, and other monocarboxylates: implications for the Cori cycle. *Cell* 76:865-73.
- Garcia et al. (1995) cDNA Cloning of MCT2, second Monocarboxylate Transporter Expressed in different Cells than MCT1. *The Journal of Biological Chemistry* 270: 1843-1849
- Garcia-Dorado D et al. (2009) Myocardial protection against reperfusion injury: The cGMP pathway. *Thrombosis and Haemostasis* 101:635-642.
- Garcia-Dorado et al. (1997) Gap Junction Uncoupler Heptanol Prevents Cell-to-Cell Progression of Hypercontracture and Limits Necrosis During Myocyrdial Reperfusion. *Circulation* 96:3579-3586
- Garciarena CD et al. (2013) Sarcolemmal localisation of Na<sup>+</sup>/H<sup>+</sup> exchange and Na<sup>+</sup>-HCO<sub>3</sub><sup>-</sup> co-transport influences the spatial regulation of intracellular pH in rat ventricular myocytes. *The Journal of physiology* 591:2287-306.
- Gawenis LR et al. (2007) Colonic anion secretory defects and metabolic acidosis in mice lacking the NBC1 Na<sup>+</sup>/HCO<sub>3</sub><sup>-</sup> cotransporter. *The Journal of biological chemistry* 282:9042-52.
- Geers C, Gros G (2000) Carbon dioxide transport and carbonic anhydrase in blood and muscle. *Physiological reviews* 80:681-715.
- Geers C et al. (1992) Carbonic anhydrase in skeletal and cardiac muscle from rabbit and rat. *The Biochemical journal* 282:165-71.
- Gertz EW et al. (1988) Myocardial substrate utilization during exercise in humans. Dual carbon-labeled carbohydrate isotope experiments. *The Journal of clinical investigation* 82:2017-25.
- Gevers W (1977) Generation of protons by metabolic processes in heart cells. *Journal of Molecular and Cellular Cardiology* 9:867-874
- Ghosh S et al. (2005) Cardiomyocyte apoptosis induced by short-term diabetes requires mitochondrial GSH depletion. *American journal of physiology Heart and circulatory physiology* 289:H768-76.
- Gilmour KM (2010) Perspectives on carbonic anhydrase. *Comparative biochemistry and physiology Part A, Molecular & integrative physiology* 157:193-7.
- Gladden LB (2008) A lactatic perspective on metabolism. *Medicine and science in sports and exercise* 40:477-85.

- Gopal E et al. (2004) Expression of slc5a8 in kidney and its role in Na<sup>+</sup>-coupled transport of lactate. *The Journal of biological chemistry* 279:44522-32.
- Grichtchenko II et al. (2001) Cloning, characterization, and chromosomal mapping of a human electroneutral Na<sup>+</sup>-driven Cl-HCO<sub>3</sub> exchanger. *The Journal of biological chemistry* 276:8358-63.
- Gut MO et al. (2002) Gastric hyperplasia in mice with targeted disruption of the carbonic anhydrase gene Car9. *Gastroenterology* 123: 1889-1903
- Gwathmey JK et al. (1991) Contractile deactivation and uncoupling of crossbridges. Effects of 2,3-butanedione monoxime on mammalian myocardium. *Circulation research* 69:1280-92.
- Halestrap AP et al. (1997) Lactate transport in heart in relation to myocardial ischemia. *The American journal of cardiology* 80:17A-25A.
- Halestrap AP, Meredith D (2004) The SLC16 gene family-from monocarboxylate transporters (MCTs) to aromatic amino acid transporters and beyond. *European journal of physiology* 447:619-28.
- Hanu R et al. (2009) Monocarboxylic acid transporters , MCT1 and MCT2 , in cortical astrocytes in vitro and in vivo. *American Journal of Physiology Cell Physiology* 278:921-930.
- Heming TA et al. (1994) Roles of intra- and extracellular carbonic anhydrase in alveolar-capillary CO<sub>2</sub> equilibration. *American Physiological Society* 77:697-705
- Herrero-Mendez A et al. (2009) The bioenergetic and antioxidant status of neurons is controlled by continuous degradation of a key glycolytic enzyme by APC/C-Cdh1. *Nature cell biology* 11:747-52.
- Hill TL, Inesi G (1982) Equilibrium cooperative binding of calcium and protons by sarcoplasmic reticulum ATPase. *PNAS* 79: 3978-3982
- Hille C et al. (2008) Time-domain fluorescence lifetime imaging for intracellular pH sensing in living tissues. *Analytical and bioanalytical chemistry* 391:1871-9.
- Hilvo M et al. (2004) Expression of carbonic anhydrase IX in mouse tissues. *The journal of histochemistry and cytochemistry* 52:1313-21.
- Hilvo M et al. (2005) Characterization of CA XV, a new GPI-anchored form of carbonic anhydrase. *The Biochemical journal* 392:83-92.
- Huxtable R, Bressler R (1973) Isolation of sarcoplasmic reticulum fraction Assays : *Reactions* 323:573-583.
- Ivanov SV et al. (1998) Down-regulation of transmembrane carbonic anhydrases in renal cell carcinoma cell lines by wild-type von Hippel-Lindau transgenes. *Proceedings of the National Academy of Sciences of the United States of America* 95:12596-601.
- Jain M et al. (2003) Glucose-6-phosphate dehydrogenase modulates cytosolic redox status and contractile phenotype in adult cardiomyocytes. *Circulation research* 93:e9-16.
- Johannsson E et al. (2001) Upregulation of the Cardiac Monocarboxylate Transporter MCT1 in a Rat Model of Congestive Heart Failure. *Circulation* 104:729-734.
- Kabaeva Z et al. (2008) Blebbistatin extends culture life of adult mouse cardiac myocytes and allows efficient and stable transgene expression. *American journal of physiology Heart and circulatory physiology* 294:H1667-74.
- Kemppainen J et al. (2002) Myocardial and skeletal muscle glucose uptake during exercise in humans. *The Journal of Physiology* 542:403-412.

- Khandoudi N et al. (2001) Inhibition of the cardiac electrogenic sodium bicarbonate cotransporter reduces ischemic injury. *Cardiovascular research* 52:387-96.
- Kim G et al. (2004) Carbonic Anhydrase III Is Not Required in the Mouse for Normal Growth , Development , and Life Span Carbonic Anhydrase III Is Not Required in the Mouse for Normal Growth, Development, and Life Span. *Molecular and Cellular Biology*. 24: 9942-47
- Kitakaze M et al. (1988) Acidosis during early reperfusion prevents myocardial stunning in perfused ferret hearts. *The Journal of clinical investigation* 82:920-7.
- Klier M et al. (2013) Intracellular and Extracellular Carbonic Anhydrases Cooperate Non-Enzymatically to Enhance Activity of Monocarboxylate Transporters. *The Journal of biological chemistry*.
- Koehler-Stec EM et al. (1998) Monocarboxylate transporter expression in mouse brain. *American Journal of Physiology Endocrinology and Metabolism* 275: 516-524.
- Kroemer G, Poussegur J (2008) Tumor Cell Metabolism: Cancer's Achilles' Heel. *Cancer Cell* 13:472-482
- Lakshmi Devi S, Anuradha CV (2010) Mitochondrial damage, cytotoxicity and apoptosis in iron-potentiated alcoholic liver fibrosis: amelioration by taurine. *Amino acids* 38:869-79.
- Leem CH et al. (1999) Characterization of intracellular pH regulation in the guinea-pig ventricular myocyte. *The Journal of physiology* 517 :159-80.
- Leite TC et al. (2011) Lactate downregulates the glycolytic enzymes hexokinase and phosphofructokinase in diverse tissues from mice. *FEBS letters* 585:92-8.
- Lewis SE et al. (1988) N-ethyl-N-nitrosourea-induced null mutation at the mouse Car-2 locus: an animal model for human carbonic anhydrase II deficiency syndrome. *Proceedings of the National Academy of Sciences of the United States of America* 85:1962-6.
- Li X et al. (2002) Carbonic anhydrase II binds to and enhances activity of the Na<sup>+</sup>/H<sup>+</sup> exchanger. *The Journal of biological chemistry* 277:36085-91.
- Li Z et al. (2003) Adenovirus-mediated gene transfer to adult mouse cardiomyocytes is selectively influenced by culture medium. *The journal of gene medicine* 5:765-72.
- Lin RY et al. (1998) Human monocarboxylate transporter 2 (MCT2) is a high affinity pyruvate transporter. *The Journal of biological chemistry* 273:28959-65.
- Loiselle FB et al. (2004) Regulation of the human NBC3 Na<sup>+</sup>/HCO<sub>3</sub><sup>-</sup> cotransporter by carbonic anhydrase II and PKA. *American journal of physiology Cell physiology* 286:C1423-33.
- Louch WE et al. (2011) Methods in cardiomyocyte isolation, culture, and gene transfer. *Journal of molecular and cellular cardiology* 51:288-298.
- Lucas-Lopez C et al. (2005) Absolute Stereochemical Assignment and Fluorescence Tuning of the Small Molecule Tool, (-)-Blebbistatin. *European Journal of Organic Chemistry* 2005:1736-1740.
- Lundgren E et al. (1985) Extracellular matrix components influence the survival of adult cardiac myocytes in vitro. *Experimental cell research* 158:371-81.
- Maharajh DM, Alkley J (1972) The Temperature Dependence of the Diffusion Coefficients of Ar, CO<sub>2</sub>, CH<sub>4</sub>, CH<sub>3</sub>Cl, CH<sub>3</sub>Br, and CH<sub>2</sub>Br<sub>2</sub> in Water. *Canadian Journal of Chemistry* 51: 944-952
- Manning Fox JE et al. (2000) Characterisation of human monocarboxylate transporter 4 substantiates its role in lactic acid efflux from skeletal muscle. *The Journal of physiology* 529: 285-93.

- Margolis DS et al. (2008) Phenotypic characteristics of bone in carbonic anhydrase II-deficient mice. *Calcified tissue international* 82:66-76.
- Markandeya YS et al. (2011) Caveolin-3 regulates protein kinase A modulation of the Cav3.2 ( $\alpha_{1H}$ ) T-type  $Ca^{2+}$  channels. *The Journal of biological chemistry* 286:2433-44.
- Martin PM et al. (2006) Identity of SMCT1 (SLC5A8) as a neuron-specific  $Na^+$ -coupled transporter for active uptake of L-lactate and ketone bodies in the brain. *Journal of neurochemistry* 98:279-88.
- Martinov V et al. (2009) Increased expression of monocarboxylate transporter 1 after acute ischemia of isolated, perfused mouse hearts. *Life sciences* 85:379-85.
- Matsuyama D, Kawahara K (2008) Maintenance and characterization of spontaneous contraction rhythm in cultured cardiac myocytes fused with cardiac fibroblasts. *Bio Systems* 92:226-32.
- Messonnier L et al. (2007) Importance of pH regulation and lactate/ $H^+$  transport capacity for work production during supramaximal exercise in humans. *Journal of applied physiology* 102:1936-44.
- Morgan PE et al. (2007) Interactions of transmembrane carbonic anhydrase, CAIX, with bicarbonate transporters. *American journal of physiology Cell physiology* 293:C738-48.
- Muir AR (1967) The effects of divalent cations on the ultrastructure of the perfused rat heart. *Journal of anatomy* 101:239-61.
- Newsholme P et al. (2007) Diabetes associated cell stress and dysfunction: role of mitochondrial and non-mitochondrial ROS production and activity. *The Journal of physiology* 583:9-24.
- Nishikawa T et al. (2007) Impact of mitochondrial ROS production on diabetic vascular complications. *Diabetes research and clinical practice* 77:41-5.
- O'Connell TD et al. (2003) Isolation and Culture of Adult Mouse Cardiac Myocytes for Signaling Studies. *Alliance for Cellular Signaling Research Reports* 1:1-9.
- Orlowski A et al. (2012) Binding of carbonic anhydrase IX to extracellular loop 4 of the NBCe1  $Na^+/HCO_3^-$  cotransporter enhances NBCe1-mediated  $HCO_3^-$  influx in the rat heart. *American journal of physiology Cell physiology* 303:C69-80.
- Orlowski J, Grinstein S (2004) Diversity of the mammalian sodium/proton exchanger SLC9 gene family. *Pflügers Archiv : European journal of physiology* 447:549-65.
- Ovens MJ et al. (2010) AR-C155858 is a potent inhibitor of monocarboxylate transporters MCT1 and MCT2 that binds to an intracellular site involving transmembrane helices 7-10. *The Biochemical journal* 425:523-30.
- Pan P et al. (2006) Carbonic anhydrase gene expression in CA II-deficient ( $Car2^{-/-}$ ) and CA IX-deficient ( $Car9^{-/-}$ ) mice. *The Journal of physiology* 571:319-27.
- Pan P et al. (2012) Brain phenotype of carbonic anhydrase IX-deficient mice. *Transgenic research* 21:163-76.
- Paradis M et al. (2010) The effects of nitric oxide-oxidase and putative glutathione-peroxidase activities of ceruloplasmin on the viability of cardiomyocytes exposed to hydrogen peroxide. *Free radical biology & medicine* 49:2019-27.
- Paroder V et al. (2006)  $Na^+$ /monocarboxylate transport (SMCT) protein expression correlates with survival in colon cancer: molecular characterization of SMCT. *Proceedings of the National Academy of Sciences of the United States of America* 103:7270-5.

- Pastorekova S et al. (2004) Carbonic anhydrase inhibitors: the first selective, membrane-impermeant inhibitors targeting the tumor-associated isozyme IX. *Bioorganic & medicinal chemistry letters* 14:869-73.
- Pfeiffer T et al. (2001) Cooperation and Competition in the Evolution of ATP-Producing Pathways. *Science* 292:504-507
- Pierre K, Pellerin L (2005) Monocarboxylate transporters in the central nervous system: distribution, regulation and function. *Journal of Neurochemistry* 94: 1-14.
- Pierre K et al. (2002) MCT2 is a major neuronal monocarboxylate transporter in the adult mouse brain. *Journal of cerebral blood flow and metabolism* 22:586-95.
- Pilegaard H et al. (1999) Distribution of the lactate/H<sup>+</sup> transporter isoforms MCT1 and MCT4 in human skeletal muscle. *The American journal of physiology* 276: 843-8.
- Poole RC, Halestrap AP (1994) N-terminal protein sequence analysis of the rabbit erythrocyte lactate transporter suggests identity with the cloned monocarboxylate transport protein MCT1. *The Biochemical journal* 303: 755-9.
- Poolman RA et al. (1998) Cell cycle profiles and expressions of p21 CIP1 and p27 KIP1 during myocyte development. *International Journal of Cardiology* 67:133-142.
- Potter C, Harris AL (2004) Hypoxia Inducible Carbonic Anhydrase IX, Marker of Tumor Hypoxia, Survival Pathway and Therapy Target. *Cell Cycle*:164-167.
- Räisänen SR et al. (1999) Carbonic anhydrase III protects cells from hydrogen peroxide-induced apoptosis. *The FASEB journal : official publication of the Federation of American Societies for Experimental Biology* 13:513-22.
- Reid MB (2008) Free radicals and muscle fatigue: Of ROS, canaries, and the IOC. *Free radical biology & medicine* 44:169-79.
- Robergs RA, Ghiasvand F, Parker D (2004) Biochemistry of exercise-induced metabolic acidosis. *American journal of physiology Regulatory, integrative and comparative physiology* 287:R502-16.
- Robertson N et al. (2004) Role of Carbonic Anhydrase IX in Human Tumor Cell Growth , Survival , and Invasion. *Cancer Research*: 6160-6165.
- Rodgers LS et al. (2009) An improved protocol for the isolation and cultivation of embryonic mouse myocytes. *Cytotechnology* 59:93-102.
- Roos A, Boron WF (1981) Intracellular pH. *Physiological reviews* 62:296-434
- Roughton (1935) RECENT WORK ON CARBON DIOXIDE TRANSPORT BY THE BLOOD  
*Physiological Reviews* 15: 241-296
- Roy P et al. (2010) Enhanced sensitivity to hydrogen peroxide-induced apoptosis in Evi1 transformed Rat1 fibroblasts due to repression of carbonic anhydrase III. *The FEBS journal* 277:441-52.
- Ruiz-Meana M, García-dorado D (2009) Pathophysiology of Ischemia-Reperfusion Injury : New Therapeutic Options for Acute Myocardial Infarction. *Revista Española de Cardiología* 62:199-209.
- Ruiz-Meana M et al. (1999) Propagation of Cardiomyocyte Hypercontracture by Passage of Na<sup>+</sup> Through Gap Junctions. *Circulation Research* 85: 280-287
- Sambrano GR et al. (2002) Navigating the signalling network in mouse cardiac myocytes. *Nature* 420:712-714.

- San Martín A et al. (2013) A Genetically Encoded FRET Lactate Sensor and Its Use To Detect the Warburg Effect in Single Cancer Cells. *PLoS ONE* 8:e57712.
- San Martín A et al. (2014) Imaging Mitochondrial Flux in Single Cells with a FRET Sensor for Pyruvate. *PLoS ONE* 9:e85780.
- Schäfer C et al. (2011) Importance of bicarbonate transport for protection of cardiomyocytes against reoxygenation injury. *American Journal of Physiology Heart and Circulatory Physiology*. 278: 1457-1463
- Scheibe RJ et al. (2006) Expression of membrane-bound carbonic anhydrases IV, IX, and XIV in the mouse heart. *The journal of histochemistry and cytochemistry* 54:1379-91.
- Scheuermann BW et al. (2000) Carbonic anhydrase inhibition delays plasma lactate appearance with no effect on ventilatory threshold. *Journal of Applied Physiology* 88:713-721.
- Schlüter K-D, Piper HM (2005) Isolation and Culture of Adult Ventricular Cardiomyocytes. *Practical Methods in Cardiovascular Research* 557-567.
- Schmidt RF et al. (2005) Physiologie des Menschen.- *Springer Medizin Verlag*, 29. Auflage
- Schneider H-P et al. (2013) GPI-anchored carbonic anhydrase IV displays both intra- and extracellular activity in cRNA-injected oocytes and in mouse neurons. *PNAS* 110: 1494-1499.
- Schroeder MA et al. (2010) Measuring intracellular pH in the heart using hyperpolarized carbon dioxide and bicarbonate: a <sup>13</sup>C and <sup>31</sup>P magnetic resonance spectroscopy study. *Cardiovascular research* 86:82-91.
- Schroeder MA et al. (2013) Extramitochondrial domain rich in carbonic anhydrase activity improves myocardial energetics. *PNAS* 110:E958-E967
- Schueler C et al. (2011) Transport activity of the sodium bicarbonate cotransporter NBCe1 is enhanced by different isoforms of carbonic anhydrase. *PloS one* 6:e27167.
- Sender S et al. (1998) Localization of Carbonic Anhydrase IV in Rat and Human Heart Muscle. *Journal of Histochemistry & Cytochemistry* 46:855-861.
- Sender S et al. (1994) Immunohistochemical localization of carbonic anhydrase IV in capillaries of rat and human skeletal muscle. *Journal of Histochemistry & Cytochemistry* 42:1229-1236.
- Shah GN et al. (2005) Carbonic anhydrase IV and XIV knockout mice: roles of the respective carbonic anhydrases in buffering the extracellular space in brain. *Proceedings of the National Academy of Sciences of the United States of America* 102:16771-6.
- Shiels A, Jeffery S, Wilson C, Carter N (1984) Radioimmunoassay of carbonic anhydrase III in rat tissues. *The Biochemical journal* 218:281-4.
- Shiels A et al. (1982) Synthesis of rat muscle carbonic anhydrase III in a cell-free translation system. *FEBS letters* 148:122-5.
- Silverman N (1988) The Catalytic Mechanism of Carbonic Anhydrase: Implications of a Rate-Limiting Protolysis of Water. *Accounts of Chemical Research* 21: 30-36.
- Sjöblom et al., (2009) Duodenal acidity “sensing” but not epithelial HCO<sub>3</sub><sup>-</sup> supply is critically dependent on carbonic anhydrase II expression. *PNAS* 106(31): 13094–13099
- Sly SS, Hu PY (1995) HUMAN CARBONIC ANHYDRASES AND CARBONIC ANHYDRASE DEFICIENCIES. *Annu.Rev.Biochem.*64:375-401
- Souders CA et al. (2009) Cardiac fibroblast: the renaissance cell. *Circulation research* 105:1164-76.

- Spicer SS (1979) The Immunohistochemical localization of Carbonic Anhydrase in Rodent Tissues. *Journal of Histochemistry and Cytochemistry* 27: 820-831.
- Spicer SS et al. (1990) Comparative distribution of carbonic anhydrase isozymes III and II in rodent tissues. *The American journal of anatomy* 187:55-64.
- Spicer SS (1993) Advantages of histochemistry for the study of cell biology. *The Histochemical journal* 25:531-47.
- Spitzer et al. (2002) Facilitation of intracellular H<sup>+</sup> ion mobility by CO<sub>2</sub>/HCO<sub>3</sub><sup>-</sup> in rabbit ventricular myocytes is regulated by carbonic anhydrase. *Journal of Physiology* 541.1:159–167
- Srinivas SR et al. (2005) Cloning and functional identification of slc5a12 as a sodium-coupled low-affinity transporter for monocarboxylates (SMCT2). *The Biochemical journal* 392:655-64.
- Stock C, Schwab A (2009) Protons make tumor cells move like clockwork. *Pflügers Archiv - European Journal of Physiology* 458:981-992.
- Stridh MH et al. (2012) Lactate flux in astrocytes is enhanced by a non-catalytic action of carbonic anhydrase II. *The Journal of physiology* 590:2333-51.
- Supuran CT (2008) Carbonic anhydrases: novel therapeutic applications for inhibitors and activators. *Nature reviews Drug discovery* 7:168-81.
- Sutherland FJ et al. (2003) MOUSE ISOLATED PERFUSED HEART : CHARACTERISTICS AND CAUTIONS. *Clinical and Experimental Pharmacology and Physiology* 30: 867-878.
- Swietach P, et al. (2003) Modelling intracellular H<sup>+</sup> ion diffusion. *Progress in Biophysics & Molecular Biology* 83:69–100
- Takahashi S et al. (2012) Astroglial pentose phosphate pathway rates in response to high-glucose environments. *ASN neuro* 4:71-88.
- Terracio L et al. (1991) Expression of collagen binding integrins during cardiac development and hypertrophy. *Circulation Research* 68:734-744.
- Theparambil SM et al. (2014) The Electrogenic Sodium Bicarbonate Cotransporter NBCe1 is a High-Affinity Bicarbonate Carrier in Cortical Astrocytes. *The Journal of Neuroscience* 34:1148-1157
- Thomas RC et al. (1991) Homeostatic muffling. *Nature* 350:564
- Tsai Y-C et al. (2006) Stereoselective effects of 3-hydroxybutyrate on glucose utilization of rat cardiomyocytes. *Life sciences* 78:1385-91.
- Tweedie S, Edwards Y (1989) Mouse carbonic anhydrase III: nucleotide sequence and expression studies. *Biochemical genetics* 27:17-30.
- Unver AA, Himmelblau DM (1964) Diffusion Coefficients of CO<sub>2</sub>, C<sub>2</sub>H<sub>4</sub>, C<sub>3</sub>H<sub>6</sub> and C<sub>4</sub>H<sub>8</sub> in Water from 6° to 65° C. *Journal of Chemical and Engineering Data* 9:428–431
- Vandenberg JI et al. (1996) Carbonic anhydrase and cardiac pH regulation. *The American journal of physiology* 271:1838-46.
- Vanysek P (2000) Ionic conductivity and diffusion at infinite dilution. *CRC Handbook of Chemistry and Physics*, 79th edition 93–95. CRC Press, London.
- Vaughan-Jones RD et al. (2002) Intrinsic H<sup>+</sup> ion mobility in the rabbit ventricular myocyte. *The Journal of Physiology* 541:139-158.
- Vaughan-Jones RD et al. (2006) Spatial aspects of intracellular pH regulation in heart muscle. *Progress in Biophysics and Molecular biology* 90:207-224

- Vaughan-Jones RD et al. (2009) Intracellular pH regulation in heart. *Journal of molecular and cellular cardiology* 46:318-31.
- Ventura-Clapier R et al. (2004) Energy metabolism in heart failure. *The Journal of physiology* 555:1-13.
- Ver Donck L, Borgers M (1991) Myocardial protection by R 56865: a new principle based on prevention of ion channel pathology. *The American journal of physiology* 261:H1828-35.
- Villafuerte et al. (2014) Facilitation by intracellular carbonic anhydrase of  $\text{Na}^+\text{-HCO}_3^-$  co-transport but not  $\text{Na}^+/\text{H}^+$  exchange activity in the mammalian ventricular myocyte. *The Journal of Physiology* 592.5:991–1007
- Vinnakota KC, Beard DA (2011) Kinetic analysis and design of experiments to identify the catalytic mechanism of the monocarboxylate transporter isoforms 4 and 1. *Biophysical journal* 100:369-80.
- Volz A et al. (1991) Longevity of Adult Ventricular Rat Heart Muscle Cells in Serum-free Primary Culture. *Journal of Molecular and Cellular Cardiology* 173:161-173.
- Vuillemin M, Pexieder T (1997) Carbonic anhydrase II expression pattern in mouse embryonic and foetal heart. *Anatomy and embryology* 195:267-77.
- Wahl P et al. (2009) Moderne Betrachtungsweisen des Laktats : Laktat ein überschätztes und zugleich unterschätztes Molekül. *Schweizerische Zeitschrift für «Sportmedizin und Sporttraumatologie»* 57: 100-107
- Wakabayashi S et al. (1997) Calmodulin-binding autoinhibitory domain controls “pH-sensing” in the  $\text{Na}^+/\text{H}^+$  exchanger NHE1 through sequence-specific interaction. *Biochemistry* 36:12854-61.
- Wakabayashi S et al. (1994) The  $\text{Na}^+/\text{H}^+$  Exchanger Isoform 1 (NHE1) Is a Novel Member of the Calmodulin-binding Proteins. *The Journal of Biological Chemistry* 269:13703-13709.
- Walter A, Gutknecht J (1984) Monocarboxylic acid permeation through lipid bilayer membranes. *The Journal of membrane biology* 77:255-64.
- Wandernoth PM et al. (2010) Role of carbonic anhydrase IV in the bicarbonate-mediated activation of murine and human sperm. *PloS one* 5:e15061.
- Wetzel P et al. (2001) Extracellular carbonic anhydrase activity facilitates lactic acid transport in rat skeletal muscle fibres. *The Journal of physiology* 531:743-56.
- Wilson MC et al. (1998) Lactic acid efflux from white skeletal muscle is catalyzed by the monocarboxylate transporter isoform MCT3. *The Journal of biological chemistry* 273:15920-6.
- Wilson MC et al. (2009) Studies on the DIDS-binding site of monocarboxylate transporter 1 suggest a homology model of the open conformation and a plausible translocation cycle. *The Journal of biological chemistry* 284:20011-21.
- Wykoff CC et al. (2000) Hypoxia-inducible expression of tumor-associated carbonic anhydrases. *Cancer research* 60:7075-83.
- Xiao XH, Allen DG (2000) Activity of the  $\text{Na}^+/\text{H}^+$  exchanger is critical to reperfusion damage and preconditioning in the isolated rat heart. *Cardiovascular research* 48:244-53.
- Yamamoto T et al. (2005) Functional diversity of electrogenic  $\text{Na}^+\text{-HCO}_3^-$  cotransport in ventricular myocytes from rat, rabbit and guinea pig. *The Journal of physiology* 562:455-75.
- Yanase H et al. (2008) Cellular expression of a sodium-dependent monocarboxylate transporter (Slc5a8) and the MCT family in the mouse kidney. *Histochemistry and cell biology* 130:957-66.



- Ye G et al. (2003) Metallothionein prevents diabetes-induced deficits in cardiomyocytes by inhibiting reactive oxygen species production. *Diabetes* 52:777-83.
- Zaniboni M et al. (2003) Proton permeation through the myocardial gap junction. *Circulation research* 93:726-35.
- Zhou YY et al. (2000) Culture and adenoviral infection of adult mouse cardiac myocytes: methods for cellular genetic physiology. *American journal of physiology Heart and circulatory physiology* 279:H429-36.
- Zobel C et al. (2003) Molecular dissection of the inward rectifier potassium current (IK1) in rabbit cardiomyocytes: evidence for heteromeric co-assembly of Kir2.1 and Kir2.2. *The Journal of physiology* 550:365-72.
-

# CURRICULUM VITAE

	Born in Buxtehude
1990-1994	elementary school (Wiegensen)
1994-2003	Gymnasium Süderelbe (Hamburg)
2003-2004	Civilian service
2004-2005	Studies in chemistry (University of Hamburg)
2005-2010	Studies in biology (TU Kaiserslautern)
June 2010	Diploma thesis ("Co-expression of the monocarboxylate transporter MCT1 and the carbonic anhydrases CAII and CIV in mouse tissues")
2010-2014	Dissertation in the department of Zoology/Membrane-transport